Identification of redox-linked structural changes in ribonucleotide reductase (RNR) by way of reaction-induced FT-IR spectroscopy

A Dissertation
Presented to
The Academic Faculty

by

Ryan Atlee Watson

In Partial Fulfillment
of the Requirements for the Degree
Doctor of Philosophy in the
School of Chemistry and Biochemistry

Georgia Institute of Technology
August 2018

IDENTIFICATION OF REDOX-LINKED STRUCTURAL CHANGES IN RIBONUCLEOTIDE REDUCTASE (RNR) BY WAY OF REACTION-INDUCED FT-IR SPECTROSCOPY

Approved by:

Dr. Bridgette A. Barry, Advisor
School of Chemistry and Biochemistry
Georgia Institute of Technology

Dr. Jake D. Soper
School of Chemistry and Biochemistry
Georgia Institute of Technology

Dr. Adegboyega K. Oyelere
School of Chemistry and Biochemistry
Georgia Institute of Technology

Dr. Francesca Storici
School of Biological Sciences
Georgia Institute of Technology

Dr. David Sherrill
School of Chemistry and Biochemistry
Georgia Institute of Technology

Date Approved: July 20th, 2018

To my Family and Friends

ACKNOWLEDGEMENTS

I want to start by expressing my sincerest gratitude to my mentor and advisor, Prof. Bridgette A. Barry, whose unwavering dedication and enthusiasm for science have forever shaped, not only the scientist, but the person I have become throughout my time at Georgia Tech. Bridgette's resolve, instinct for research, and devotion to her students serves as a benchmark that I will always carry with me. I can't thank her enough for sharing her deep expertise, patiently tolerating my constant questions, and always listening to each ramble.

I am grateful to Adegboyega K. Oyelere for being a wonderful thesis chair. As well as my other committee members. Their discussions, insight, and guidance have truly been invaluable. Within my first 2 years, I had taken a class, graciously been allowed to work in their lab, or been present for a collaborative meeting with each of my committee members.

There are so many Barry lab members that have contributed to this work. Firstly, Dr. Adam R. Offenbacher who trained me, worked beside me, and my office mate. I'd like to thank you for all of the science and non-science related conversations to get us through those rough 40-plus day stretches with RNR. I would also like to thank Dr. Cynthia V. Pagba whose light-hearted spirit and laugh always reminded me to never take anything too seriously. I don't know how to say in words what each Barry lab members has meant. I am unworthy and indebted by each of your unfailing kindness and commitment to each other.

There are many family members that I would like to thank starting with my Mom, Dad, John, Thomas, Cody, and Alexandria. The bedrock. I could never have gotten to this point or through the rough times without all of your love and support. In the same vein,

Tyler, Hillary, Terry, and Kylie, ninety-seven percent of my decisions are garbage, thank you for being the three percent. I thank my grandma, Janice, for loving me to pieces. To my grandpa, Robert, who always encouraged me to always keep going and whose faith never wavered. To my aunts and uncles, I would like to thank you for always asking "how school is going" even when every response was "please don't ask."

There is no point of level of education where I do not have someone to thank. I would like to thank every professor and friend that supported me at Berry College. There are too many people to thank and give the credit they deserve, to each of you, I am forever grateful.

TABLE OF CONTENTS

LIST OF TABLES

LIST OF FIGURES

LIST OF SYMBOLS AND ABBREVIATIONS

μ	reduced mass
3AP	triapine
υ	vibrational frequency
α2	large subunit of ribonucleotide reductase
β2	small subunit of ribonucleotide reductase
Å	angstrom
Abs	absorbance
Apo-β2	ribonucleotide reductase with no iron bound
ADP	adenosine diphosphate
ATP	adenosine triphosphate
AU	absorbance units
AzUDP	2′-azido-2′-deoxyuridine 5′-diphosphate
CDP	cytosine diphosphate
DFT	density functional theory
dATP	deoxyadenosine triphosphate
dGTP	deoxyguanosine triphosphate
DNA	deoxtribonucleic acid
dTTP	deoxythymidine triphosphate
K_D	dissociation constant
kDa	kilodalton
EPR	electron paramagnetic resonance

E. coli	*Escherichia coli*
ENDOR	electron nuclear double resonance
ET	electron transfer
ETPT	electron transfer, proton transfer
FTIR	Fourier transform infrared
HEPES	4-(2-hydroxyethyl)-1-piperazineethanesulfonic acid
HU	hydroxyurea
Met-β2	hydroxyurea-treated β2 subunit of ribonucleotide reductase
NDP	nucleotide diphosphate
NTP	nucleotide triphosphate
PCET	proton-coupled electron transfer
PDB	protein database
PELDOR	pulsed electron double resonance
pK_A	acid dissociation constant
RNA	ribonucleic acid
RNR	ribonucleotide reductase
ROS	reactive oxygen species
SDS-PAGE	sodium dodecyl sulfate polyacrylamide gel electrophoresis
TTP	thymidine triphosphate
UDP	uridine diphosphate
UV	ultraviolet
V	volt
Y•	tyrosyl radical

Additional abbreviations are explained in the text.

SUMMARY

Ribonucleotide reductase (RNR) catalyzes the production of deoxyribonucleotides in all cells. RNR is a multiple subunit enzyme responsible for supplying cellular deoxynucleotide triphosphate (dNTP) pools by using radical based chemistry to convert nucleotides to the corresponding deoxy forms, the only pathway for *de novo* synthesis of the building blocks for both DNA replication and DNA repair. In *E. coli* class Ia RNR, a transient α2β2 complex forms when a ribonucleotide substrate binds to the α2 subunit. A tyrosyl radical (Y122O•)-differic cofactor in β2 initiates substrate reduction in α2 via a long distance, proton-coupled electron transfer (PCET) process generating a thiol radical located an astonishing 35Å away in the active site of the functional α2β2 complex. In this work, I use reaction-induced FT-IR spectroscopy to describe the α2β2 structural landscapes associated with catalysis and inhibition by anti-cancer chemotherapeutics. *E. coli* α2 and β2 mixing was performed with a substrate, CDP/UDP, and the appropriate allosteric effector, ATP/TTP. Isotopic labeling was implemented to define subunit-specific structural changes. Mixing of α2 and β2 subunits to form the active complex yielded amide I (C=O) and II (CN/NH) bands indicative of structural rearrangements associated with catalysis. The distinctive inhibitor, AzUDP, lifts the veil of the conformational mask accompanying proton-coupled electron transfer (PCET) to generating a nitrogen radical that is moderately stable. AzUDP demonstrates backbone rearrangement associated with a redox-induced shift between Y122OH and D84 as well as conformational dynamics linked to radical generation in the α subunit. Inhibitor-mediated reduction of Y122O• was associated with structural changes in α2, as well as β2. To define the spectral contributions

of tyrosyl radical reduction in the quaternary complex, $^{2}H_4$ labeling of β2 tyrosines and HU-editing were performed. These spectra provide evidence for a conformational rearrangement at a second β2 tyrosine(s), Y_x, in the α2β2 complex. To develop new drugs, information concerning the mechanism is critical. To obtain information, a more specific comprehension of the radical's complete cycle must be achieved. FTIR spectroscopy allows for the detection of single amino acid changes that take place as a result of RNR inhibition due to radical quenching or trapping. The FTIR spectra highlight the distinction between substrates and effectors during active turnover, and the conformational impact of inhibition during active turnover of the QC.

CHAPTER 1. INTRODUCTION

1.1 Ribonucleotide reductase

Ribonucleotides are produced from simple building blocks that consist of amino acids, tetrahydrofolate derivatives, NH_4^+, CO_2 and 5-ribosyl-1-pyrophosphate. No additional pathway has evolved for the production of deoxyribonucleotides, and no separate *de novo* pathway exists to produce deoxyribonucleotides without ribonucleotide reductase (RNR).[1] RNR reduces all four of the ribonucleotides to the corresponding deoxyribonucleotides, it is an essential enzyme in cellular growth for DNA synthesis and repair. The reduction process of ribonucleotides to deoxyribonucleotides proceeds through a conserved PCET pathway.[2] For DNA synthesis and repair to occur in cells, deoxyribonucleotides must be made readily available. RNR is the only enzyme capable of synthesizing and maintaining nucleotide pools. The salvage pathway can recover the purine and pyrimidine bases from DNA degradations which can be used to reform their nucleotides by phosphoribosylation.[3] However, the salvage pathway is unable to produce the deoxynucleotides needed for DNA synthesis and repair which can only be accomplished by RNR.[3-4] RNR, seen in Figure 1.1, is categorized into three classes. Each class uses a free radical to reduce the nucleotide substrate.[1, 5] The free radical is formed on a conserved cysteine amino acid residue in the active site of the enzyme. The free radical abstracts a hydrogen at the ribose 3′-carbon of the nucleotide.[6-7] The 2′-hydroxyl group is eliminated as H_2O leading to the formation of a disulfide bond between two conserved active site cysteine residues (225 and 462, *E. coli*). This mechanism is discussed further in section 1.1.4. For rapid catalysis to proceed, reduction of the disulfide bond must be

completed by thioredoxin (TR) or glutaredoxin (GR).[8] These two small proteins reduce the disulfide bond formed during deoxynucleotide production to allow turnover to continue. Without TR/GR reducing these conserved cysteine residues, RNR can only perform reduction of four nucleotides reactions before conserved cysteines require reduction of the disulfide bonds by thioredoxin reductase (TRR) or glutaredoxin reductase (GRR).[9]

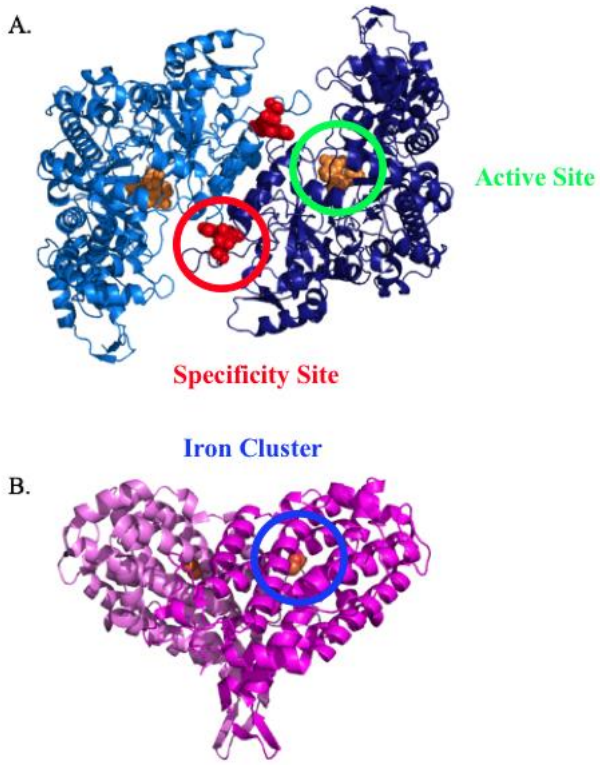

Figure 1.1 (A) 3.2 Å crystal structure α2 subunit with TTP effector (red) and GDP substrate (orange). The α2 subunit houses the active site for substrate turnover (PDB 4R1R). (B) 2.2 Å crystal structure (2XOF) β2 subunit with the diiron clusters responsible for radical generation shown in brown (iron) and red (oxygen). Substrate and effector binding sites are highlighted above: active site (green), specificity site (red), and iron cluster (blue).[10-12]

Ribonucleotide reduction retains a central role in the regulation of the cellular concentrations of the four dNTPs required for DNA synthesis. Maintenance of precise concentrations is essential for DNA synthesis fidelity.[13-14] These small dNTP pools suffice

in mammalian cells for only a few minutes of DNA replication and must therefore be renewed continuously during S-phase.[15] Cells not in S-phase are capable of synthesizing dNTPs *de novo*, albeit at a much slower rate due to decreased concentrations of RNR.[16] Due to the variable demands for dNTPs based on the given phase of the cell, the overall expression of RNRs is linked to the cycle of cell-division. Expression of the enzyme is increased during periods of cell growth while maintaining low levels of expression during cellular equilibrium.[17] Because RNR plays such a pivotal role in cell growth and division, it has remained a key target for pharmaceuticals that aim to inhibit its function.[18-19] Inhibition of the enzymatic function of RNR is attributed to its overexpression in rapidly multiplying cells and its association to tumor cells.[19-26]

RNR was the first protein discovered to house a stable radical.[27-30] The methodology by which ribonucleotide reduction occurs was unprecedented when first discovered.[31] Long-range proton-coupled electron transfer (PCET) system allows the radical hole to migrate 35 Å into the active site for nucleotide reduction.[30] Hypotheses detailing the mechanism of RNR remained clouded until high-resolution crystal structures of *E. coli* and mammalian class Ia RNR were solved.[10-12, 32-33] These crystal structures provided insight for researchers to explore the method of radical generation and subsequent propagation into the active site.[27, 34-36] They further provided physical evidence for theories based on allosteric regulatory effects concerning substrate reduction.[12, 37-41]

Free radicals are defined as any molecule with an uneven number of electrons in its valence shell.[42] Free radicals are highly reactive and can be generated *in vivo* as by-products of ordinary metabolism or from ecological factors.[43-44] For instance, the mitochondrial electron transport chain provides the primary source of ATP in the cell.[45]

During this process, electrons could exit the respiratory pathway preceding water formation and react with molecular oxygen resulting in the formation of superoxide (O_2^-), however, this is not normally expected.[45] Superoxide is toxic and has been associated with numerous disorders.[46] Overproduction of reactive oxygen species (ROS) accompanied with deficiencies in antioxidants leads to oxidative stress.[47] Radical cause oxidative stress by interacting with vital cellular components like DNA or cellular membranes, so they are highly destructive if not properly regulated.[48-49] The overall impact of ROS on cellular mechanisms is reliant on the period of exposure and the total oxidative strength of the radical species.[50] The cell contains an assortment of other safeguards when facing oxidative stress due to the likelihood of exposure.[51-52] Free radicals can be formed internally through natural processes or externally by radiation, medications, or pollution. Because it is not possible to measure free radicals in the body, the by-products are measured in response to oxidative stress.[53]

Antioxidants reduce cellular damage due to free radical reactivity by safely nullifying radical species before irreversible damage is triggered. The most widely studied antioxidant enzymes include superoxide dismutase (SOD) and glutathione reductase.[43, 54] Antioxidants are capable of destroying free radicals in one of two ways, either chain breaking or prevention.[54-55] Radical formation is accompanied by the less or gain of electron. In the second case, an additional radical was also formed. The formation of the highly reactive radical species will result in a chain reaction of unstable products. This process will proceed throughout the cell(s) until either the radicals are quenched by a chain breaking antioxidant (vitamin C, carotenoids, etc.) or by radical-radical reaction leading to radical termination.[56-57] Preventative antioxidants can avert the original chain reaction by

scavenging the initiating free radicals.[55] In either case, the antioxidant becomes oxidized and must be restored or new antioxidants must be produced. If a disproportion occurs between ROS and their antioxidant counters, irreparable damage can follow.[58] For example, a hydroxyl radical interacting with DNA can result in damage to the deoxyribose backbone and purine and pyrimidine bases.[42] The oxidative damage that results from this radical reaction leads to permanent modifications of the DNA sequence leading to mutagenesis and carcinogenesis in the system. When excessive concentrations of ROS are formed, they can have deleterious properties, however, free radicals are not merely associated with harmful consequences. At low/moderate levels, ROS can actually be advantageous and even necessary for certain biological activities. Phagocytes, for instance, target infecting microbes by means of radical species.[59] The radicals target and destabilize the cellular membrane acting as a biological defense mechanism.[60] Biological systems also utilize ROS in cellular signaling pathways such as nonphagocytic NADPH oxidase.[61] This enzyme is the key in regulating intracellular signaling cascades. Ribonucleotide reductase is one such enzyme that uses an organic free radical to catalyze the biosynthesis of deoxyribonucleotides for DNA synthesis.[6]

1.1.1 Classes of RNR based on metallo-cofactors

Ribonucleotide reductases can be assembled into three main classes as seen in Figure 1.2.[5, 37, 62-63] As is the case in each of these classes, all use radical-based chemistry for overall nucleotide reduction, but can be catalogued based on metallo-cofactors, aerobic vs. anaerobic, and catalytic state. Class I RNRs consist of two homodimeric proteins, α2, coded by the *nrdA* gene, and β2, coded by the *nrdB* gene. The α subunit contains the

catalytic site (or active site) and binding sites for allosteric effectors (the activity site and the specificity site). The β subunit contains an oxygen-linked diferric cluster and a stable tyrosyl free radical.[64] Class I RNR is further subcategorized based on the metallo-cofactor required for radical initiation.[7] Class Ia, Ib, and Ic consist of Fe^{3+}-O-Fe^{3+}, Mn^{3+}-O-Mn^{3+}, and Fe^{3+}-O-Mn^{4+} clusters, respectively. In class Ia and Ib, thiyl generation in the active site is induced by allosteric regulators binding to the α subunit that induces structural dynamics allowing the radical hole from the β subunit to be transferred.[33, 38-40, 65-67] However, class Ic uses a phenylalanine in the place of tyrosine and a Fe^{3+}-O-Mn^{4+} cluster to generate the radical.[62] Class Ia RNRs are found in mammals and *E. coli*, and has two sites of allosteric regulation, the specificity site and the activity site. Both sites are located in the α2 dimer.[5] Class Ib is restricted to only certain bacteria and only contains one site of allosteric regulation.[39] In class Ia, RNR is inhibited when dATP binds to the activity site in the N-terminal domain.[40] Class II uses a radical adenooxylcobalamine to initiate radical generation.[68] The anaerobic class III's α subunit is coded by *nrdD* and contains a stable oxygen-sensitive glycyl radical. The β subunit is coded by *nrdG*, and contains an iron-sulfur cluster that with *S*-adenosylmethionine can generate the glycyl radical needed for nucleotide reduction.[69]

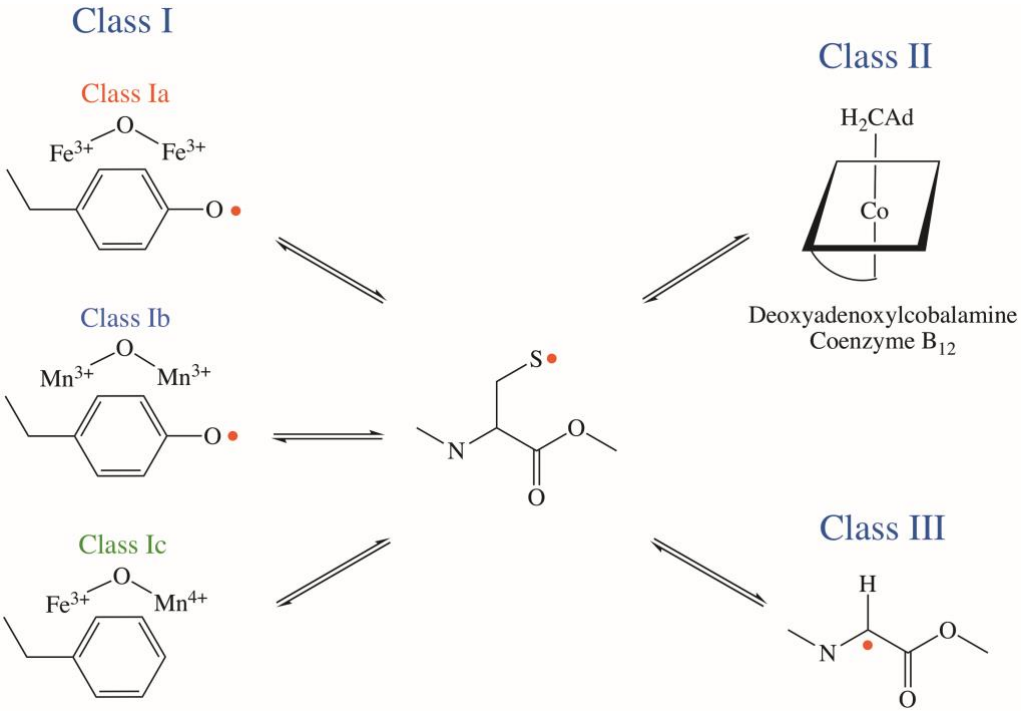

Figure 1.2 The three classes of RNR characterized by the mechanism they use for radical generation and on their structural differences. These classes are responsible for the generation of the cysteine radical in the α subunit active site.[19, 47]

To produce the fundamental tyrosyl radical in the class Ia *E. coli* β2 dimer, first the iron cluster must be constructed. The biosynthetic pathway for radical generation is limited by structural rearrangements and provides a method to control overall RNR activity.[70] The details of the metallo-cofactor formation are shown in Figure 1.3. The functional β2 enzyme is formed after the Fe^{2+}-β2 is oxidized by molecular oxygen (O_2) using amino acid residue tryptophan 48 as a reductant.[29] Four total electrons are necessary to fully reduce molecular oxygen. The two ferrous ions donate one electron each, with the third coming from Y122, and the fourth being provided from the aforementioned W48.[71-72] In *E. coli* β2, YfaE is a gene downstream of *nrdB* (encoding for β2) that codes for a putative ferrodoxin. It is hypothesized to be directly involved in the biosynthetic and maintenance pathways for

iron cluster formations. YfaE was isolated and reconstituted with 80% of its iron in $[2Fe2S]^{+}$ and the remaining 20% in $[4Fe4S]^{2+}$.[73] *In vitro* kinetic studies provide evidence that YfaE is kinetically proficient enough for reduction of the diferric cluster to the diferrous form, as well as deliver the required reducing agent in the biosynthetic pathway. When reductants are introduced to the active, radical containing β2, the tyrosyl radical can be scavenged forming the metβ2 state (diferric site and non-oxidized Y122). The reduced β2 can be formed when metβ2 is exposed to external reductants *in vivo*.[74-75]

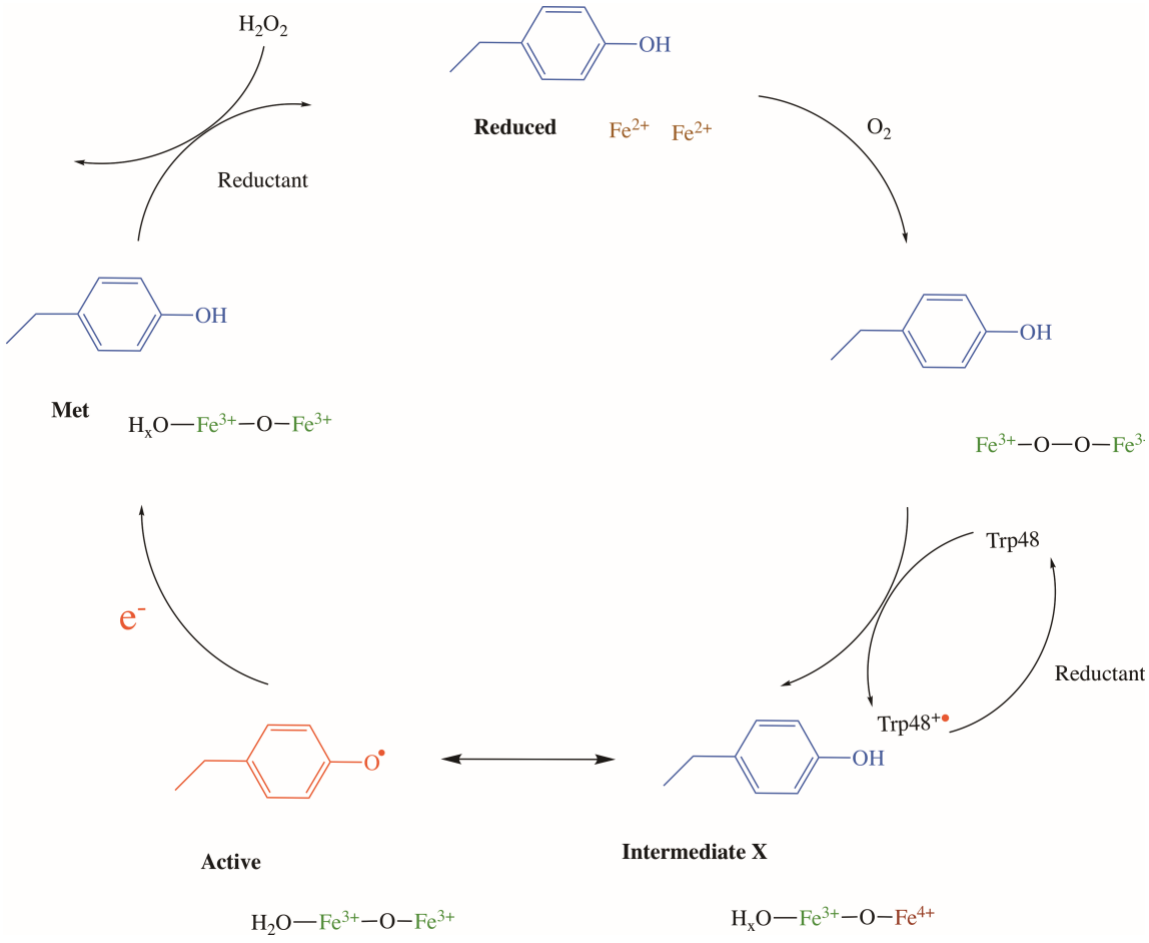

Figure 1.3 RNR Class Ia E. coli proposed biosynthetic and maintenance pathways for the diferric metallo-cofactor.[27-28, 36-37]

In assembling the diiron unit, the cluster and the environment surrounding the cluster, including metal bound ligands, go through various states during the lifecycle of RNR.[32, 76-77] Intermediate X shows this in Figure 1.3. Understanding the mechanism of oxygen activation requires knowledge of the reduced β2, and there is still much that remains unclear about the biosynthetic pathway of the diferric metallo-cofactor. One such example are the ligands that stabilize the metal cluster and the environments surrounding those ligands. Ser211 is a highly conserved amino acid located on the opposite side of the helix to Glu204. Mutation of the residue to alanine (S211A) was implemented as a probe to determine if a proposed interhelical hydrogen bond was vital for iron assembly and maintenance, while being so far displaced from the iron center. There was a noticeable conformational change from residues 208-215, and the diferric site has a much slower rate of reduction, while being more susceptible to radical scavenger hydroxyurea (HU) when compared to the wild type.[77-78]

A methodology was established using hydrogen peroxide to generate the tyrosyl radical in β2 crystals to observe potential conformational changes between the active and reduced states. This was characterized by electron paramagnetic resonance (EPR) spectroscopy and discussed in comparison with a 1.42 Å x-ray crystal structure of the metβ2.[79] The μ-oxo linked irons of the oxidized center are coordinated by four carboxylates and two histidine residues. The diferric cluster is proposed to undergo conformational changes during reduction of the β2 radical. These structural changes allow the iron center to be accessible to oxygen to allow the reformation of the active enzyme.[64] The reduced form of β2 and the apo-β2 have similar structures overall. Coordinating iron bound ligands have relatively small differences in position in the apo-β2 protein which sees the side

chains collapse in to occupy the space left by the dinuclear iron site.[76] These small modifications are attributed to minimizing the reorganization energy for iron reincorporation.

1.1.2 RNR class Ia E. coli subunits

The larger α subunit (86 kDa) is where nucleotide reduction occurs. The subunit encompasses the activity site, responsible for triggering the enzyme and starting radical transfer into the active site, the specificity site, which influences what substrate binding to the active site where nucleotide reduction takes place.[38-39, 66, 80-81] These two allosteric regulation sites (activity and specificity sites) allow the cell to maintain the proper ratio of deoxyribonucleotides available for DNA synthesis.[82-83] The monomer is composed of the N-terminal, predominantly helical domain (220 residues), a novel ten-stranded β/α barrel (480 residues), and a αβααβ domain (70 residues).[11-12, 76] The active site is where the transient cysteine radical is generated and is buried within the enzyme but remains close to the C-terminus of β2. Substrate analogs, such as AzidoUDP (AzUDP), were employed to trap the radical in the active site during substrate turnover to observe the active site radical. This resulted in the stoichiometric loss of Y122• content accompanying the formation of a substrate analog radical observed by 9 and 140 GHz EPR spectroscopy.[84-85] The pathway that the radical takes to the active site was also examined with the radical trap, 3-aminotyrosine ($Y_{731}NH_2Y$-α2 and $Y_{730}NH_2Y$-α2). This was the first direct evidence of a radical intermediate on the proposed radical pathway during turnover.[86] The two allosteric regulation sites in the α subunit were established in the crystallographic studies with adenosine-5′-(β,γ-imido) triphosphate (AMP-PNP), a non-hydrolyzable analogue of ATP

in the activity site and TTP in the specificity site.[39] Activity in RNR is cell cycle dependent in higher organisms where it is transcriptionally regulated and activity is subject to the binding of ATP and dATP for catalysis and inhibition, respectively.[17] The specificity site is located at the interface between the α monomers. This distance between the specificity site and the activity site is ~15 Å, so direct interaction seems unlikely. However, the effector, seen in Figures 1.1 and 1.4, stabilizes 3 highly flexible loops, referred to as Loops 1, 2, and 3, which facilitate communication with the substrate binding site. Loops 2 forms hydrophobic interactions with the base of the effector. These interactions influence the positions adopted by Loops 1 and 3 as a result.[39] Allosteric effectors have shown substantial control of RNR regulation which can modulate oligomerization based on regulation sites located 42 Å from the active site. These allosteric effectors demonstrate dramatic subunit rearrangements. Allosteric regulation of activity provides a mechanism to prevent the accumulation of cytotoxic levels of deoxyribonucleotides by communicating with the substrate-binding site. Structural evidence suggests the rearrangement of subunits based on binding by effectors.[87]

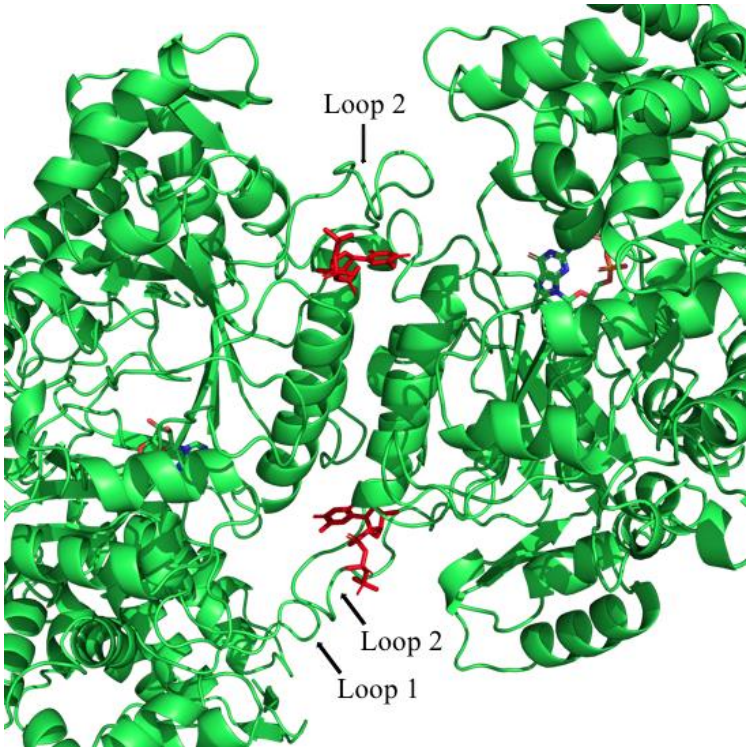

Figure 1.4 Crystal structure of the α2 subunit loop interactions with the effector bound TTP (red) to the specificity site. (PDB 4R1R).

In 1990, the work by Nordlund and coworkers presented a structure of class Ia RNR that provided information regarding the structure and function of the diiron cluster.[32] The smaller β subunit (45 kDa) houses the tyrosyl radical (Y122•) generated by the aforementioned metal cluster. Y122 was shown to be near the iron cluster, buried deep in a hydrophobic environment.[31] To date, several high-resolution crystal structures have been solved. These include different forms of class Ia *E. coli*,[10-12] mouse,[88] human,[89] and human p53[90] RNRs. The crystal structure of *E.coli* and murine RNR have similar coordination around their diferric cluster, but the murine RNR communicates with the solvent by a narrow hydrophobic channel and is less shielded than *E.coli* which would explain its higher susceptibility to cancer therapies.[91] Each β2 subunit is composed of 13 α-helices and 2 β-sheets. Due to its increased flexibility, the last 35 amino acid residues of the C-terminal tail

have not been resolved in the β2 crystal structure.[92] As it is located 35 Å from the catalytic site in the α subunit, Y122• is not directly participating in ribonucleotide reduction. Because of this vast distance between where the radical is produced and where the transient radical initiates substrate reduction, the process by which RNR completes this transfer was investigated. Early studies involved simple mutations of Y122 to a phenylalanine were performed in *E. coli* which resulted in the loss of all catalytic ability.[93] These findings are consistent with the understanding of radical introduction by the metallo-cofactor. Based on crystal structures, it was made clear that the diiron cluster needs Y122 to generate the radical required for substrate reduction. Accompanying site specific mutations were used in residues that were shown to be conserved in class Ia RNRs to determine the mechanism behind radical transfer. Mutation of Y356 was performed with the use of orthogonal tRNA synthases with 3-,4-dihydroxyphenylalanine (DOPA), a radical trap. The observed loss of Y122• was met with the formation of a new radical intermediate when DOPA356Y-β2 was mixed under catalytic conditions.[94] PELDOR spectroscopy was used to measure the distance between Y122• in one α:β pair and the proposed formation of DOPA356• in the neighboring α:β pair to compare with EPR spectroscopy and crystal structures. The relative position of this new radical supported the formation of DOPA356• under turnover conditions.[95]

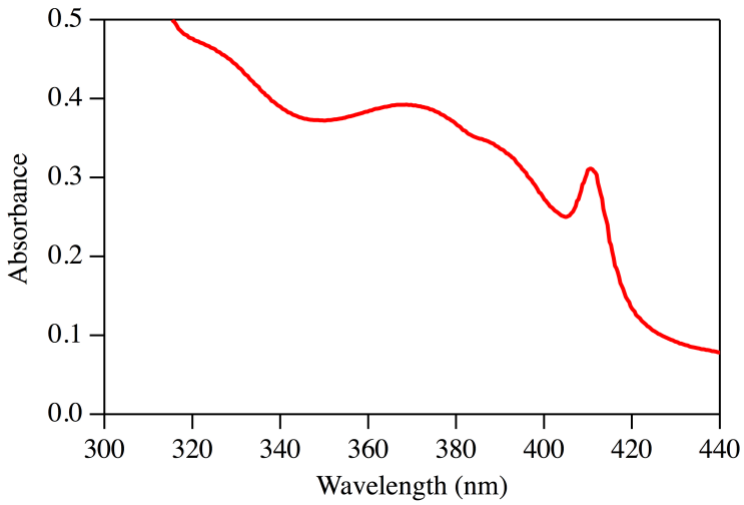

Figure 1.5 UV-Vis absorbance spectroscopy of E. coli β2. Y• is identified by a sharp peak at 410 nm with a shoulder at 390 nm. Iron contributions are detected at 325 and 375 nm.

Typically, free radicals are short lived due to their high reactivity.[96] This is not the case for Y122• that displays an unusually stable tyrosyl radical that can be stored until radical transfer is initiated by ATP binding to the activity site.[34] The increased stability is hypothesized to be linked to Y122 residing within a hydrophobic pocket 10 Å from the surface and is apparently inaccessible to solvent.[97] Mutations to small channels where Y122 is exposed to the protein surface has displayed an increased sensitivity to radical scavengers.[98] During β2 purification,[99] protein concentration is determined by UV-Vis spectroscopy at 280 nm. Determination of the tyrosyl radical concentration is more involved due to the nature of the radical spectrum in Figure 1.5. The tyrosyl radical peak (410 nm) has a sloping baseline, so to combat this, a baseline drop down method is used:[71]

$$[\mathrm{Y}\bullet] = \frac{A_{411nm} - \left[\frac{(3 \times A_{416nm}) + (2 \times A_{406nm})}{5}\right]}{1784\ M^{-1}cm^{-1}}$$

1.1.3 Regulation of RNR

As stated above, RNR turnover is regulated by the binding of dATP to the activity site so that when elevated levels of dATP are present in the cell, the enzyme becomes inactive.[78, 81] Another tool that the cell uses to regulate RNR functionality is the cell cycle. In mammals, RNR activity reaches its maximum during the S-phase.[100-101] As the cell exits the S-phase and enters G_2 phase, RNR is targeted by two ubiquitin ligases and the enzyme is degraded.[102] While small concentrations α and β subunits remain present during G_0/G_1 for DNA repair, transcription is minimal during these phases of the cell cycle.[103] Not only does the cell's ability to direct transcription and degradation allow for an additional means for regulatory control, but also the localization of RNR in the cell reinforces that strictness. RNR proteins are located predominantly in the cytoplasm where dNDPs are produced and diffuse into the nucleus during DNA synthesis.[104-105] Contrary to this, increasing studies have displayed α and β are translocated into the nucleus in response to DNA damage.[106-107] Understanding this process has just begun and innovative new studies will be needed to fully link RNR translocation into the nucleus.

1.1.4 Nucleotide reduction

Despite the divergent evolutionary pathways leading to the rise of multiple classes and subclasses of ribonucleotides reductase, this work focuses on class Ia and the mechanism of ribonucleotide reduction in it. The ribonucleotide reduction mechanism in Figure 1.6 was proposed based on mechanism-based inhibitors such as [3'-^{3}H]NDPs and 2'-halogenated ribo- and arabinonucleoside triphosphates demonstrated C-H bond cleavage and the importance of the 2'-group of the ribose.[108-110] This led to the theory that the

transient thiyl radical was removing the 3'-hydrogen of the nucleotide.[111] Deduction of further steps were based upon model reactions involving ethylene glycol dehydration.[112-113]

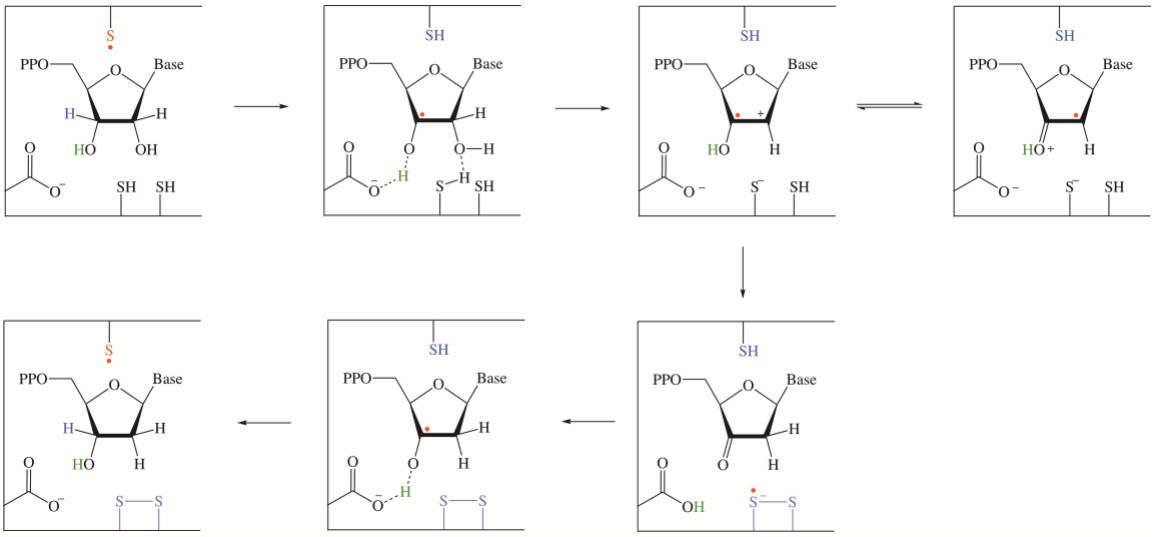

Figure 1.6 Proposed mechanism for nucleotide reduction of class Ia E. coli RNR.[2, 89]

Figure 1.6 illustrates the proposed mechanism for nucleotide reduction.[114] The overall reaction is initiated by binding of substrates and effectors to the α2 dimer. This leads to long-range PCET and transfer of the radical hole into the active site to generate C439•. The transient radical abstracts a hydrogen atom from the 3'-carbon and generates a substrate radical. The substrate radical facilitates the leaving of the protonated OH group at the 2'-carbon as H_2O. The redox-active cysteine pair (C225 and C462) reduce the substrate radical and briefly forms a cysteine radical at the newly formed disulfide bond. At this point, the hydrogen atom stored at C439 is returned to the 3'-carbon by regenerating the thiyl radical. For turnover to continue, conserved cysteine residues (C754 and C759) must reduce the disulfide bond formed in the active site during ribonucleotide reduction. After this is complete, the β subunit continue providing dNDPs for DNA replication.[115]

RNR requires small proteins, thioredoxin (TR) and glutaredoxin (GR) that contain redox-active thiols, to reduce disulfide bond formation that occurs during turnover. NADPH reduces the cysteines of the redoxins with specific thioredoxin reductase or glutathione and glutathione reductase.[8, 116]

1.2 The radical propagation pathway

1.2.1 Incorporation of unnatural amino acids

Multiple allosteric sites have been observed for *E. coli* β2.[38-39] These allosteric sites initiate substrate reduction and transfer of the radical hole into the active site. In the pursuit of a radical transportation pathway (Figure 1.7), initial experimentation involved mutation of conserved residues in the α:β subunits and the measuring of activity to determine key amino acid residues related to the function of RNR. A few of those mutations are: Y122F,[93] W48F,[117] Y356NO_2Y,[118] Y731F, and Y730F.[119] These mutations are at universally conserved residues and resulted in the loss of catalysis in the holoenzyme suggesting that these residues must play some role in nucleotide reduction or assembly of the diiron cofactor. The use of radical traps for these conserved tyrosine residues were used. DOPA356-β2, NH_2Y731-α2, and NH_2Y730-α2 mutants were monitored using stop-flow UV-VIS,[120] EPR,[86] and PELDOR spectroscopy.[86, 95] These experiments were the first direct evidence of radical formation in the proposed radical hopping pathway.

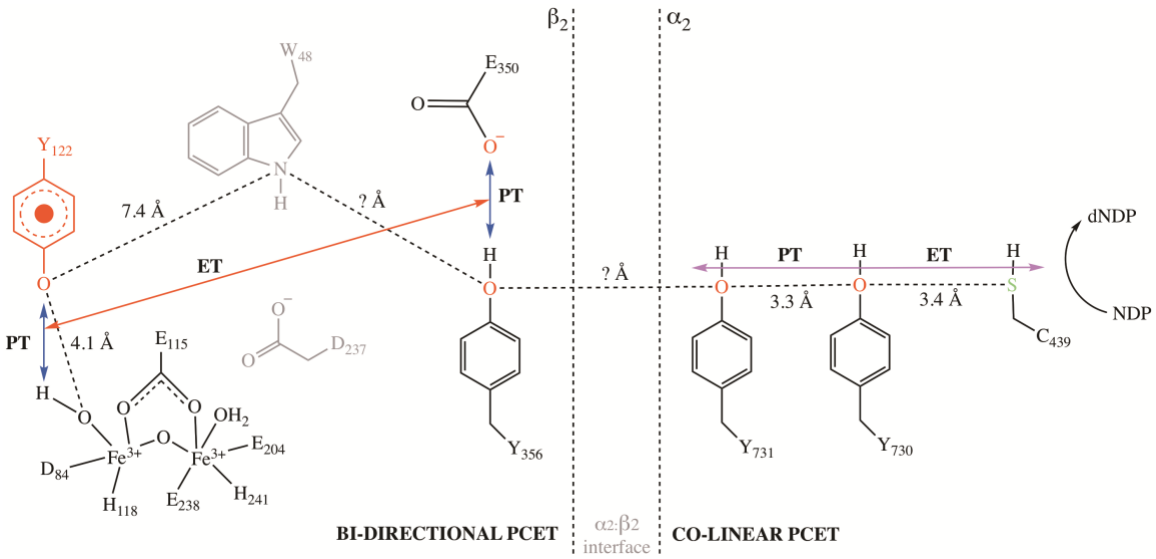

Figure 1.7 The proposed radical transfer pathway in E. coli RNR. Distances in the β2 subunit are from an oxidized crystal structure.23 Note that due to the disordered C-terminal tail in the β2 subunit, the position of Y356 is unknown.[61, 71-72, 89, 97-98]

The radical pathway was further manipulated using the perturbation of reduction potentials along the electron transfer pathway to accumulate the radical state outside of the normal Y122. Mutation of Y122 to a NO_2-Y122 was previously shown to retain activity catalyzing the formation of 0.6 equivalents of dCDP and 0.6 equivalents of a newly formed radical species.[121] Retention in activity is expected as the mutation remove the phenol group like previous mutations with phenylalanine. However, the reduction potential is significantly higher than the native Y122. Meaning that once the nucleotide (CDP) is reduced (dCDP), the radical is unable to regenerate Y122• and the radical accumulates in the lowest energy state.

1.2.2 Hydrogen bond formation between Y356 in E. coli β2 and water molecules from the interface

Tyrosine-356 is the last proposed aromatic amino acid in the radical transfer pathway within the β2 subunit and it is the only proposed residue that cannot be observed structurally.[122] Mutation of Y122 to NO_2Y122 disables functioning catalysis by dramatically raising the reduction potential by +200 mV at Y122. This site-directed mutant prohibits the reformation of Y122• and synthesis of deoxyribonucleotides is unable to proceed until the radical is regenerated at Y122. PELDOR spectroscopy experiments reveal 85-90% of the radical had accumulated at Y356 in β2 and the remaining 10-15% was delocalized over Y731 and Y730 in α2 as a result of increased reduction potential at Y122 not allowing reformation of the radical resting state.[123] These results confirm the radical species generation previously reported along the radical pathway. For nucleotide reduction to occur, the α2 subunit and the β2 subunit must associate with one another in the presence of substrates and effectors and the radical must pass between the α:β interface. This interface is highly sensitive and can be influenced by single point mutations.[65] Efforts have been made to understand the radical chemistry happening across the interface. In Figure 1.7, substitution at Y356 of the β subunit interface with 2,3,5-fluorotyrosine and the ensuing interactions with wt-α2, Y731F-α2, and Y730F-α2 using high field (263 GHz) EPR and ENDOR revealed hydrogen bonding to Y356•.[124] Two water molecules from the interface were observed coordinating to the tyrosyl radical. Y730F-α2 mutations revealed that Y731 is able to form one hydrogen bond with the interface and the formation of this hydrogen bond leads to a change in the electrostatic environment of Y356. Based on these results, there seems to be evidence that Y356 and Y731 are able to communicate across the subunit interface through hydrogen bonding interactions.[125]

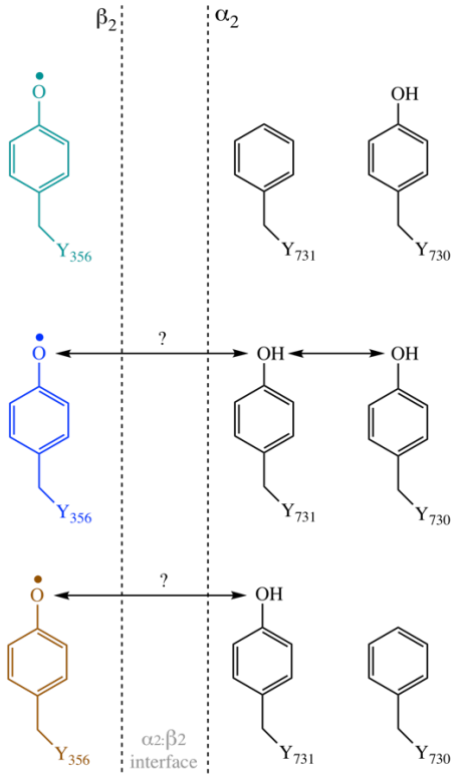

Figure 1.8 α and β communication across the α:β interface via hydrogen bonding interactions.

1.2.3 Hydrogen bonding network in E. coli α2

For catalysis to occur, a transient cysteine radical must be formed in the α2 active site.[1] The use of photo-active peptides has further elucidated electron transfer (ET) between Y356 and the mechanism by which the radical takes to the active site in the α2.[126] These peptides mimic the final 20 amino acids residues of the β2 C-terminal tail where a photo trigger is located directly adjacent to Y356. Radical initiation is promoted by Xe lamp irradiation ($\lambda \geq 300$ nm) and association of the peptide to the α2 dimer with ^{14}C-CDP and, allosteric effector, ATP display turnover via Y731, Y730, and C439.[127-128] Development of photoRNRs have replaced the conserved Y356 residue with tryptophan. This substitution yields a 3-fold increase in radical content. Typically, substitution of Y356 has

resulted in little to no enzymatic activity.[129] The use of this Y356W photo-oxidant maintains 20% of turnover capabilities relative to wt-β2.[130] Further analysis was focused on the specific interactions along the radical propagation pathway in the α subunit. 3-aminotyrosines were site-specifically incorporated at Y730 and Y731. ENDOR, DFT calculations and multi-frequency EPR data reports the detection of a single strong hydrogen bond with $NH_2Y731\bullet$ and one strong and one moderate hydrogen bond identified with $NH_2Y730\bullet$.[131-132] In Figure 1.8, alteration of the pathway using amino acid residues that have been shown to inactive the pathway, Y731F and Y730F,[119] resulting in the loss of the strong hydrogen bond interaction in both tyrosines. The data suggests that the strong hydrogen bond is a result of these two tyrosines hydrogen bonding to one another and that the proton between the tyrosines is transferred by collinear proton-coupled electron transfer. DFT calculations report that C439 is within hydrogen bonding distance to Y730. Mutation of the active site cysteine to alanine, C439A, result in loss of the second moderate hydrogen bond reports with $NH_2Y730\bullet$. Despite these findings, it remains entirely possible that water acts as the moderate hydrogen bond and that mutation of the cysteine results in disruption of the water network. X-ray structures of the NH_2Y-α reveal that the hydrogen bonding network remains unperturbed in comparison to the wild-type.

Furthermore, ruthenium complexes have been established to study long-range electron transfer reactions in functioning enzymes.[133-135] The photophysical characteristics of ruthenium has been advantageous in the catalytic capabilities of metalloenzymes in particular. Ruthenium complexes are proficient in flash photolysis to catalyze redox reactions. To study a tyrosyl radical in a natural protein environment, a ruthenium complex was designed to generate a tyrosyl radical by flash photolysis to study intramolecular

electron transfer.[136] Ruthenium photosensitizers are able to initiate electron transfer in complex enzymes containing site specific mutations. This permits for the direct analysis of electron transfer rates. A similar complex was designed by the Stubbe group, where they site-specifically incorporated a rhenium complex directly adjacent to Y356 in the β2 subunit.[137] With the Re-complex, direct observation of proton and electron transfer across the α/β interface was observed. By removing Y122 from the equation direct ET and PT transfer can be detected along the PCET pathway in the individual subunit, as well as, between the two subunits.

1.2.4 Thermodynamic landscape of radical pathway

Other classes of RNR initiate radical reduction and hydrogen atom abstraction from the ribonucleotide using their cofactors to generate the radical species.[1, 138] By doing so, these other classes avoid long-range radical transfer. Evolution has driven class Ia RNR to develop this mechanism, but what overall benefit does it provide? Implementation of NO_2Y122• acts as a thermodynamic block and in place of Y122• is 200 mV more oxidizing.[118] Radical traps further deviate typical reduction potentials in conserved residues to expose exquisite kinetic control over radical initiation. Amino acid derivatives allow for the exploitation of their properties with redox potentials that range from -50 to +270 mV and pK_As from 5.6 to 7.8 relative to that of tyrosine. By adjusting the redox potentials, radical transfer becomes the rate limiting step so that other activity regimes can be observed. This data provides support for the proposed involvement of redox active sites.[94] In Figure 1.9 A, reduction potentials of pathway moieties are organized to examine the role that reduction potentials play in radical transfer. From Figure 1.9 A, the process of

initiating the radical in the active site is observed to be ~200 mV uphill. Reduction potentials were measured using $\Delta E° = \frac{RT \ln K_{eq}}{nF}$, where K_{eq} = [Y356•]/[F_3Y122•], R is the ideal gas constant, T is the temperature, n is the number of electrons being transferred, and F is Faraday's constant.[139-140] Figure 1.9 B are the unnatural amino acids involved in the elucidation of this pathway.

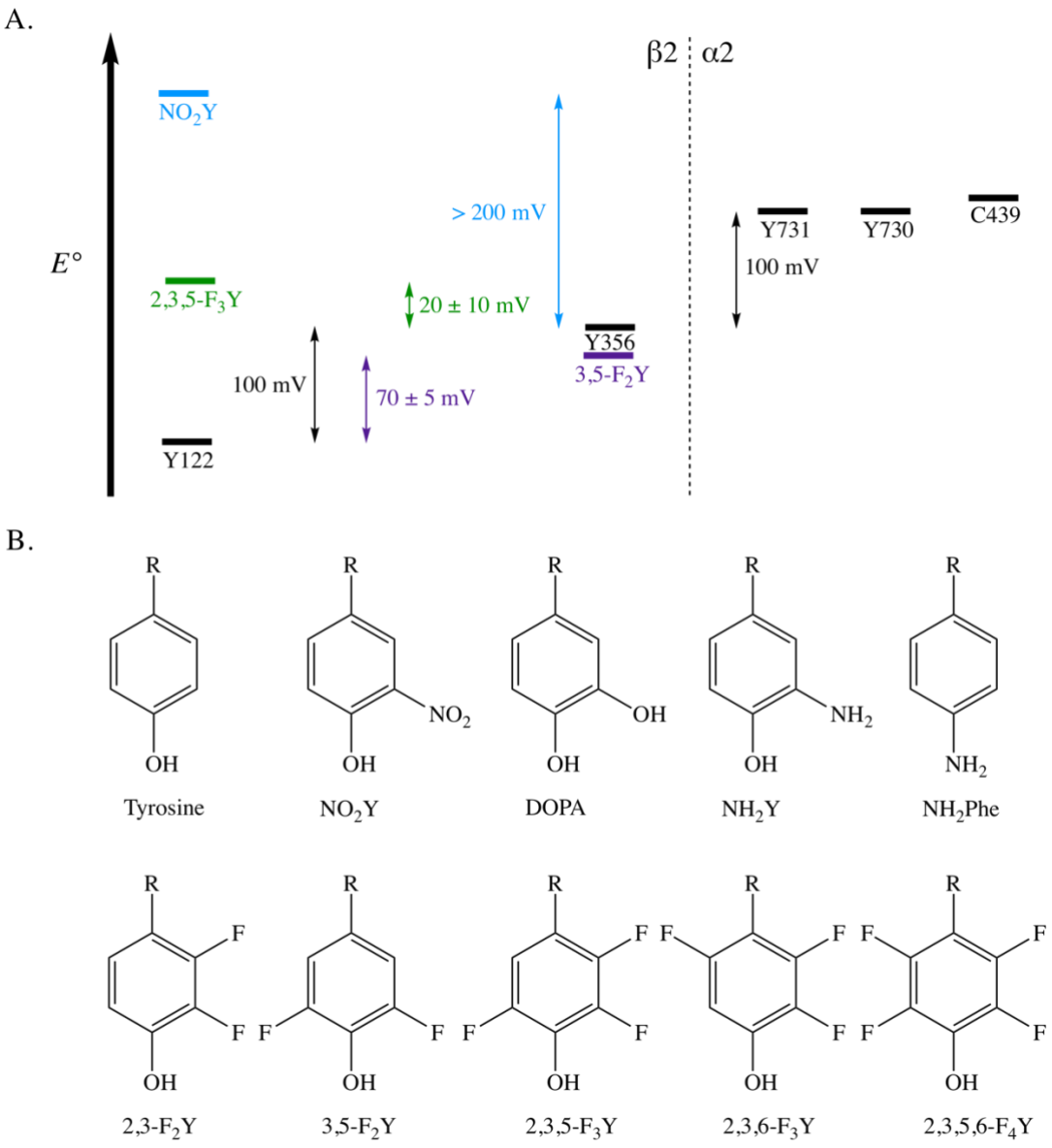

Figure 1.9 Unnatural amino acid incorporation into universally conserved amino acids in RNR. (A) Thermodynamic landscape of RNR radical pathway. (B) List of unnatural amino acids used to date that have been substituted into α2 or β2 to determine radical transport into the active site.[86, 94-95, 118, 120, 141-142]

1.3 Inhibition

In Figure 1.7, there are a sequence of conserved amino acid residues that have been proposed to be part of an electron transfer hopping pathway.[1, 15] This pathway has been

supported by the incorporation of unnatural amino acids at conserved residues in the passageway that has resulted in complete inactivation of the RNR enzyme or accumulation and detection of newly formed radical species outside of Y122 as discussed previously.[86, 127] In the pursuit of revealing the complicated mechanism surrounding RNR, we set out to explore the pharmaceutical implications on RNR. The main focus of this work will be the examination of inhibitors that target the $\alpha 2\beta 2$ active quaternary complex (QC) to prevent nucleotide reduction by radical scavengers quenching the tyrosyl radical and using substrate analogs to trap the radical in the active site in the aim to uncover new information concerning therapeutic inhibition.

1.3.1 Hydroxyurea

Hydroxyurea (HU) is commonly used for the treatment of myelogenous leukemia and has been supported as a cancer therapy for decades due to its direct quenching of the tyrosyl radical in RNR.[143-144] In fact, HU is the only inhibitor that is used to clinically neutralize RNR activity. HU was first synthesized in 1896,[145] buts its clinical use was not discovered until the 1960s.[37, 146-147] The method of hydroxyurea reduction of the tyrosyl radical could be feasible by direct interaction. Another possible method is, HU, being a small molecule, is able to gain access through small channels leading to the site of radical generation. Another potential route would be long-range electron transfer from the surface of the enzyme.[148] A group of three conserved cysteines provide a means of electron transfer from the surface of $\beta 2$ to the radical resting state to allow for indirect radical quenching from the surface. However, the effectiveness of HU is limited by its low affinity for RNR,

the cells ability to develop resistance, short half-life, small molecular size, and very high hydrophilicity.[37, 149-152]

1.3.2 Triapine

Triapine has shown promising results in actively targeting RNR and quenching the tyrosyl radical in a similar mechanism to HU, but is vastly more potent.[153-155] Triapine can significantly inhibit overall RNR activity in leukemia, non-small cell lung cancer, renal cancer, and increase radiation-mediated cytotoxicity in cervical cancer and colon cancer.[154, 156-160] Triapine has shown the most promise as an inhibitor of RNR activity from a group of thiosemicarbazones derivatives whose competency was tested via deoxyribonucleotide triphosphate concentrations and analysis of cell count as a function of time.[161] The mode of inhibition of Triapine has been greatly debated. It was proposed that Triapine chelates iron directly from the diiron cluster in β2 while another suggested that the iron was chelated from intracellular pools, drastically lowering iron concentrations, which inhibited the formations of the metallo cofactor.[162-163] The current model in the literature attributes Fe(II)-3AP as the active form *in vitro* and is active against HU resistant tumor cells by quenching the tyrosyl radical.[37] Introduction of Fe(II)-3AP to cancerous cells have exhibited increased cell death when used in combination with therapeutics like cisplatin or gemcitabine by making them more sensitive to drug specific interactions.[164] Its increased potency, which is 1000x more potent than HU,[165] could be linked to a potential binding site at β2.[166] Despite its clear clinical use and studies suggesting the active form during inhibition, in-depth molecular studies have not been performed to gain a clear picture of the method of inhibition by Triapine. Understanding the intricacies of inhibitor

interactions with their target enzymes will direct future drug engineering to design more potent therapies that can potentially mimic Triapine.

1.3.3 AzidoUDP

After the discovery of 3′-azido-3′-deoxythymidine (AZT) for the treatment of the human immunodeficiency virus (HIV),[167] there was a drastic increase in the study of new azido compounds to develop new treatment options. An RNR inhibitor that differentiates itself from the radical scavengers is 2´-azido-2´-deoxyuridine-5´-diphosphate (AzUDP). AzUDP mimics the substrate and binds in the active site. When bound it initiates radical transfer but ultimately forms a moderately stable nitrogen radical and traps the radical from returning to Y122. EPR identified the newly formed radical species was localized to the substrate being reduced in the active site.[85, 168] While not clinically relevant, as there is no direct specificity to cancerous cells, AzidoUDP aids in controlling the reaction mechanism behind long-range PCET to monitor previously unobservable conformational enzymatic states in conjunction with measuring the distances between radical initiation site in a β subunit and the substrate turnover site in the α subunit.[169]

1.4 FT-IR Spectroscopy

1.4.1 General introduction

Fourier-transform infrared (FT-IR) spectroscopy uses an essential piece of optical hardware, the interferometer, to collect high-spectral-resolution data over a wide spectral range.[170] Infrared light is emitted by a source and is directed into the interferometer to a beam splitter. The beam splitter directs half of the beam to a fixed mirror over a distance

(L) where it reflects the beam to the beam splitter having travelled a distance of 2L. The other portion of the infrared beam is directed to a second mirror with no fixed position. This mirror is under precise direction where it is moved around L by a controlled distance of x. The beam is reflected back to the beam splitter having travelled a distance of 2L ± x. Once recombined at the beam splitter, the two beams display a path length difference of 2x and will interfere when they recombine. The beam then exits the interferometer where it passes through the sample compartment and focused on the detector. This measured quantity is the intensity, I (x), of the combined beams as a function of the displacement of the mirror by distance x. The resulting interferogram is converted into a spectrum by means of Fourier transformation. There are 3 advantages of FT-IR spectroscopy over scanning spectroscopy: Fellgett's, Jacquinot's, and Connes' advantage.[171-173] Fellgett's advantage states that it collects all waves simultaneously at a higher signal-to-noise ratio.[171] Jacquinot's advantage (throughput advantage) states that the monochromator restricts the light that passes through it. This removes extraneous sources of light from entering the interferometer where throughput is based solely upon the diameter of the collimated beam from the IR source.[172] Finally, there is Connes' advantage of using a laser with a known wavelength passing through the interferometer. This provides a more stable and precise determination of vibrational modes than dispersive techniques that rely upon diffraction gratings.[173] Covalent bonds are modelled as two masses connected by a spring of a particular force constant k. The basic model for a harmonic oscillator with its modification to account for anharmonicity is enough to determine the origin of characteristic frequencies that can be assigned to functional groups within a molecule. Hooke's law expresses the fundamental vibrational frequencies (υ) of a molecule by $\upsilon = \frac{1}{2\pi}\sqrt{\frac{k}{\mu}}$, where μ is the

reduced mass of the atom. The reduced mass is defined as $\mu = \frac{m_1 m_2}{m_1 + m_2}$, in which m_1 and m_2 represent the masses of the chemical bond.[174] When a polar bond vibrates, the oscillating dipole creates a varying electric field. The stronger the dipole moment of the oscillating band, the stronger the electric field. If the IR frequency matches the frequency of the oscillating electromagnetic (EM) field, then the light is absorbed. If they do not, then the light is transmitted. Position of absorbing bands are influenced by the relative size of the molecule. Generally speaking, atoms or proteins of lighter mass and stronger bonds will display higher energy oscillations. Vibrational modes can be localized over two atoms, but can also be a number of atom motions occurring simultaneously.[175] FT-IR spectroscopy is used for detection of functional groups by examining the interaction of the EM spectrum with actual bonds and probing the functionality of a molecule. Covalent molecules have numerous types of bonds with roughly the same energy (C-C, C-H, C=O, etc.). These bonds show up in similar regions in the IR spectrum and can be categorized. With the Born Oppenheimer approximation of nuclei and electrons, you get a formula which describes the degrees of freedoms with 3 rotational degrees of freedom related to the center of mass motion of a molecule independent of whether the molecule is linear or nonlinear. Nonlinear molecules contain 3 modes of translation and 3 modes of rotation allowing for 3N-6 degrees of freedom for a molecule with a given number of atoms, N. Linear molecules retain all 3 modes of translation, but the rotational mode around the line between the atoms does not represent a change in physical space, therefore, there are only 2 rotational modes and is describes as 3N-5. These models presume a polyatomic molecule of $N > 2$. Excluding the simplest of compounds, most molecules have a nonlinear structure. This typically implies high sets of absorption frequencies, however, a lower number of

vibrations are observed due to redundant or degenerate vibrational modes. Absorption bands increase proportionately given the frequency of appearance of a functional group in a molecule.

The FT-IR spectroscopy has several comparative strengths to other methods of biological measurements. Nuclear magnetic resonance (NMR) spectroscopy has been historically limited by protein size.[176] Membrane environments induce line broadening effects associated with motion restriction in NMR spectroscopy[177] and light scattering artifacts in circular dichroism (CD) spectroscopy.[178] FT-IR spectroscopy is not limited by environmental factors or the size of proteins. Amide absorbance bands were originally assigned using force field treatments of amide vibrational regions to assign the IR absorbance of protein secondary structure.[179] FT-IR assignment was expanded upon to incorporate dihedral angles. Dihedral angles determine the overall geometry associated with the bonds, and it can be inferred from this information the strength and length of the bonds associated with the geometry of the molecule. The inclusion of this information influences the predicted energies of proposed protein secondary structure and can fine tune amide absorbance bands to more accurately predict where these bands will appear in the spectrum.[180] Amide I frequencies (1695-1610 cm^{-1}) have been reported as follows: anti-parallel β-sheet (1695-1675 cm^{-1}), α-helix (1660-1648 cm^{-1}), disordered (1648-1640 cm^{-1}), β-sheet (1640-1625 cm^{-1}), and aggregated strands (1628-1610 cm^{-1}).[181-184] Amide II frequencies relating to predominantly α-helical proteins are higher energy compared to mainly β-sheet proteins having spectral ranges of 1551-1545 cm^{-1} and 1525-1521 cm^{-1}, respectively.[185-186]

1.4.2 Difference FT-IR spectroscopy

FT-IR spectroscopy is a powerful technique that is able to detect perturbations in hydrogen bonding by shifts in frequency in amide regions in as little as 0.002 Å. [187] The principle theory for difference spectroscopy is the subtraction of protein absorbance spectra collected in state A from the spectra in state B.[188] Any vibrational frequency that is unaffected between the two states is subtracted out, simplifying the overall spectrum. Assignment of functional groups can still remain complex given the fluidity and scope of conformational changes in large proteins. Site-directed mutagenesis causes shifts in frequency based on reduced mass that makes the assignment of complex spectra more manageable.[189] Heavier isotopes are able to drastically effect the vibrational frequencies. These techniques enable the detection of single amino acid changes in the 260 kDa RNR holoenzyme. In the work presented, absorbance spectra were collected for two minutes after which there is a six-minute incubation time between these two points to allow turnover or inhibition to occur followed by another two-minute collection. To assess the catalytic state of the active complex, inhibitor is not added to the reaction mixture. The experimental design in this thesis was designed to maximize catalysis and inhibition signal-to-noise while minimizing baseline drift using UV-VIS absorbance kinetics.

1.4.3 Site-directed mutagenesis in RNR FT-IR spectroscopy

Difference FT-IR spectra are shown in Figure 1.10. In these difference FT-IR spectroscopy experiments, isolated β2 was monitored. In Figure 1.10 A, no inhibitor was added to the solution of β2. In a control experiment, a spectrum of β2 was measured at t_1 and t_2. A difference spectrum was calculated from β2 at t_1 minus β2 at t_2. As is to be

expected, the average conformations of β2 at t_1 are no different than the average conformations of β2 at t_2, thus the difference spectrum measures no changes. However, in the case of Figure 1.10 B, radical scavenger HU was inoculated in the isolated β2 solution which quenched the tyrosyl radical.

Previous work in our lab has consisted of global isotopic labeling experiments of β2 residues which began with Y122.[190] Isotopic labeling not only shifts absorbance bands associated with the incorporation of labels due to changes in mass. Among 16 tyrosines in β2, Y122• is spectroscopically unique.[191] Global labelling tyrosine in β2 using $^{2}H_4$-Y identified spectral contributions at 1498 cm^{-1} and 1514 cm^{-1} were due to Y122• and Y122OH, respectively. FT-IR spectroscopy revealed a dramatic 76 cm^{-1} downshift of the negative 1514 cm^{-1} band to 1438 cm^{-1}. This band is assignable to the stretching vibration of the tyrosines ring. An isotope down shift of 80 cm^{-1} is predicted by density functional theory (DFT) calculations. A second peak was observed to downshift 18 cm^{-1} from 1498 cm^{-1} to 1480 cm^{-1}. This signal is attributable to the C-O stretching vibration of the radical at Y122, supported by a 20 cm^{-1} downshift predicted by DFT calculations. These results illustrated the coupling of electron transfer to and from Y122 to conformational changes observed in the β2 subunit.

In agreement with these finding, small perturbations at 1661 and 1652 cm^{-1} were observed. Amide I C=O have multiple contributions from 1695-1610 cm^{-1} supporting the claim that radical reduction is associated with conformational reorientation. Furthermore, the connection between Y122 and D84 upon radical reduction was examined using globally labelled ^{13}C- and 4-^{13}C-aspartate β2 isotopic labeling as well as hydroxyurea and

hydroxylamine to induce single electron reduction.[192] Upon radical reduction, the iron bound D84 to act as a probe for hydrogen bonding modifications at the metal cluster. The positive 1687 cm^{-1} and the negative 1675 cm^{-1} bands downshifted to 1644 and 1635 cm^{-1}, respectively. These shifts were in agreement with simulated data that predicted a 43 cm^{-1} downshift. These labels also observed downshifts associated with 1661 and 1653 cm^{-1} bands to 1621 and 1613 cm^{-1}.[192] These results not only marked that D84 was sensitive to electrostatic changes around the metal cofactor, but that hydrogen bonding interactions were altered due to radical reduction at Y122. These findings were expanded upon difference spectroscopy using ^{13}C global labelling of the C_1 tyrosine carbon and DFT calculations with Newman projects to specifically identify the chemistry surrounding the radical generation site. Comparison of experimental and simulated isotope-edited FT-IR spectroscopy identified Y122 undergoing a conformational change during radical reduction forming a hydrogen bond with the conserved D84 iron bound residue. Examination of solvent isotope effects and proton inventories agree with the findings as there are two rate limiting electron transfer reactions, a large isotope effect (11.9), and a small isotope effect (1.4). The large isotope effect is a consequence of the oxidation reaction of HU. The small isotope effect is believed to be due to small hydrogen bonding changes associated with D84 and the formation of a hydrogen bond between Y122 and D84 after radical reduction.[193] Isotope effects of < 3 have been observed in enzymes that use hydrogen bonds to stabilize catalysis.[194] The results of these studies have identified key structural bands associated with reaction-induced Fourier-transform infrared (RIFT-IR) spectroscopy seen in Figure 1.10, as well as elucidating the first step associated with radical

transfer. Each of these studies was conducted in isolated β2 and the work presented in this thesis expands to include the QC and allosteric regulation observed in the α subunit.

The work presented in this thesis aims to move beyond isolated β2. To incorporate the α subunit and to begin to investigate the structural characteristics of the active α2β2 complex. The investigation of this complex aims to better understand the conformational dynamics associated with the PCET pathway and gain a deeper understanding of the mechanism of nucleotide reduction. Furthermore, the interaction between inhibitor and the QC strives to determine the means of inhibition that occurs in RNR and to understand the interactions that lead to enzyme inactivity.

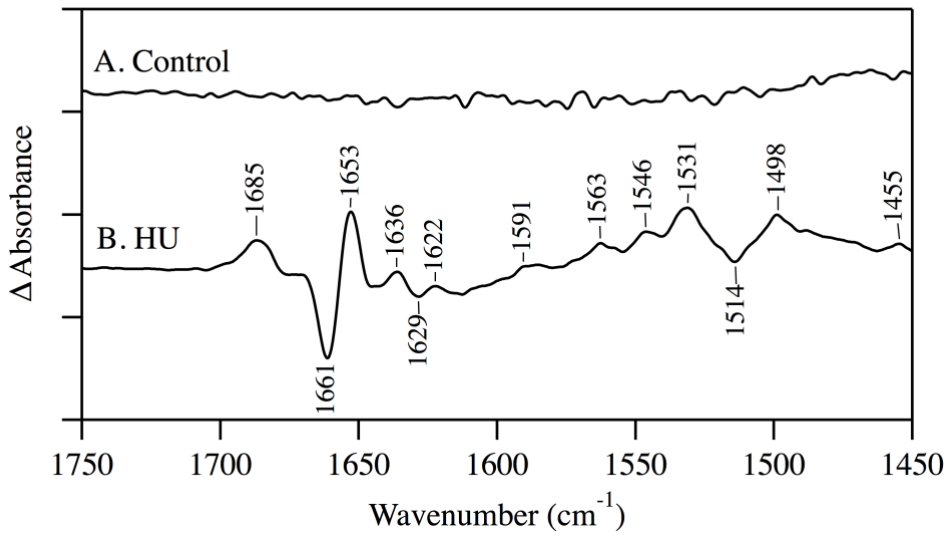

Figure 1.10 Reaction-induced FT-IR difference spectra. (A) 100 μM of isolated β2 with no inhibitors. (B) 100 μM of isolated β2 with 50 mM HU. Difference spectra were generated as detailed in the text.

1.5 References

1. Stubbe, J., Van der Donk, W. A. Protein radicals in enzyme catalysis. *Chemical Reviews* **1998,** *98*, 705-762.
2. Reece, S. Y., Hodgkiss, J. M., Stubbe, J., Nocera, D. G. Proton-coupled electron transfer: the mechanistic underpinning for radical transport and catalysis in biology. *Philosophical Transactions of the Royal Society B: Biological Sciences* **2006,** *361*, 1351-1364.
3. Geigenberger, P., Regierer, B., Nunes-Nesi, A., Leisse, A., Urbanczyk-Wochniak, E., Springer, F., van Dongen, J. T., Kossmann, J., Fernie, A. R. Inhibition of de novo pyrimidine synthesis in growing potato tubers leads to a compensatory stimulation of the pyrimidine salvage pathway and a subsequent increase in biosynthetic performance. *The Plant Cell* **2005,** *17*, 2077-2088.
4. Murray, A. W. The biological significance of purine salvage. *Annual review of biochemistry* **1971,** *40*, 811-826.
5. Jordan, A., Reichard, P. Ribonucleotide reductases. *Annual Reviews* **1998,** 67, 71-98.
6. Gon, S., Beckwith, J. Ribonucleotide reductases: influence of environment on synthesis and activity. *Antioxidants & redox signaling* **2006,** *8*, 773-780.
7. Nordlund, P., Reichard, P. Ribonucleotide reductases. *Annual Review of Biochemistry* **2006,** *75*, 681-706.
8. Prinz, W. A., Åslund, F., Holmgren, A., Beckwith, J. The role of the thioredoxin and glutaredoxin pathways in reducing protein disulfide bonds in the Escherichia coli cytoplasm. *Journal of Biological Chemistry* **1997,** *272*, 15661-15667.
9. Reichard, P., Thelander, L. Reduction of ribonucleotides. *Annual Review of Biochemistry Biochem* **1979,** *48*, 133-158.
10. Nordlund, P., Eklund, H. Structure and function of the Escherichia coli ribonucleotide reductase protein R2. *Journal of molecular biology* **1993,** *232*, 123-164.
11. Uhlin, U., Eklund, H. Structure of ribonucleotide reductase protein R1. *Nature* **1994,** *370*, 533.
12. Uhlin, U., Eklund, H. The ten-stranded β/α barrel in ribonucleotide reductase protein R1. *Journal of molecular biology* **1996,** *262*, 358-369.
13. Fan, H., Villegas, C., Wright, J. A. Ribonucleotide reductase R2 component is a novel malignancy determinant that cooperates with activated oncogenes to determine transformation and malignant potential. *Proceedings of the National Academy of Sciences* **1996,** *93*, 14036-14040.
14. Zhou, B. S., Tsai, P., Ker, R., Tsai, J., Ho, R., Yu, J., Shih, J., Yen, Y. Overexpression of transfected human ribonucleotide reductase M2 subunit in human cancer cells enhances their invasive potential. *Clinical & experimental metastasis* **1998,** *16*, 43-49.
15. Stubbe, J., Nocera, D. G., Yee, C. S., Chang, M. C. Radical initiation in the class I ribonucleotide reductase: long-range proton-coupled electron transfer? *Chemical reviews* **2003,** *103*, 2167-2202.
16. Bianchi, V., Borella, S., Rampazzo, C., Ferraro, P., Calderazzo, F., Bianchi, L. C., Skog, S., Reichard, P. Cell cycle-dependent metabolism of pyrimidine deoxynucleoside triphosphates in CEM cells. *Journal of Biological Chemistry* **1997,** *272*, 16118-16124.

17. Bjoerklund, S., Skog, S., Tribukait, B., Thelander, L. S-phase-specific expression of mammalian ribonucleotide reductase R1 and R2 subunit mRNAs. *Biochemistry* **1990,** *29*, 5452-5458.
18. Kwon, N. S., Stuehr, D. J., Nathan, C. F. Inhibition of tumor cell ribonucleotide reductase by macrophage-derived nitric oxide. *Journal of Experimental Medicine* **1991,** *174*, 761-767.
19. Nocentini, G. Ribonucleotide reductase inhibitors: new strategies for cancer chemotherapy. *Critical reviews in oncology/hematology* **1996,** *22*, 89-126.
20. Ehrenberg, A., Reichard, P. Electron spin resonance of the iron-containing protein B2 from ribonucleotide reductase. *Journal of Biological Chemistry* **1972,** *247*, 3485-3488.
21. Rosenkranz, H. S., Winshell, E. B., Mednis, A., Carr, H. S., Ellner, C. J. Studies with hydroxyurea. *Journal of Bacteriology* **1967,** *94*, 1025-1033.
22. Abratt, R. P. Summary. *Anti-Cancer Drugs* **1995,** *6*, 63-64.
23. Heinemann, V., Xu, Y. Z., Chubb, S., Sen, A., Hertel, L. W., Grindey, G., Plunkett, W. Inhibition of ribonucleotide reduction in CCRF-CEM cells by 2', 2'-difluorodeoxycytidine. *Molecular pharmacology* **1990,** *38*, 567-572.
24. Heinemann, V., Xu, Y. Z., Chubb, S., Sen, A., Hertel, L. W., Grindey, G. B., Plunkett, W. Cellular elimination of 2′, 2′-difluorodeoxycytidine 5′-triphosphate: a mechanism of self-potentiation. *Cancer research* **1992,** *52*, 533-539.
25. Cerqueira, N. M., Pereira, S., Fernandes, P. A., Ramos, M. J. Overview of ribonucleotide reductase inhibitors: an appealing target in anti-tumour therapy. *Current medicinal chemistry* **2005,** *12*, 1283-1294.
26. Sun, X., Eliasson, R., Pontis, E., Andersson, J., Buist, G., Sjöberg, B. M., Reichard, P. Generation of the glycyl radical of the anaerobic Escherichia coli ribonucleotide reductase requires a specific activating enzyme. *Journal of Biological Chemistry* **1995,** *270*, 2443-2446.
27. Bollinger Jr, J. M., Stubbe, J., Huynh, B. H., Edmondson, D. E. Novel diferric radical intermediate responsible for tyrosyl radical formation in assembly of the cofactor of ribonucleotide reductase. *Journal of the American Chemical Society* **1991,** *113*, 6289-6291.
28. Bollinger Jr, J. M., Tong, W. H., Ravi, N., Huynh, B. H., Edmonson, D. E., Stubbe, J. Mechanism of assembly of the tyrosyl radical-diiron (III) cofactor of E. coli ribonucleotide reductase. 2. Kinetics of the excess Fe2+ reaction by optical, EPR, and Mössbauer spectroscopies. *Journal of the American Chemical Society* **1994,** *116*, 8015-8023.
29. Stubbe, J., Van der Donk, W. Radicals with a controlled lifestyle. *Chemical Communication* **2003,** *2511*.
30. Licht, S., Gerfen, G. J., Stubbe, J. Thiyl radicals in ribonucleotide reductases. *Science* **1996,** *271*, 477-481.
31. Sjöberg, B., Reichard, P., Gräslund, A., Ehrenberg, A. The tyrosine free radical in ribonucleotide reductase from Escherichia coli. *Journal of Biological Chemistry* **1978,** *253*, 6863-6865.
32. Nordlund, P., Sjöberg, B. M., Eklund, H. Three-dimensional structure of the free radical protein of ribonucleotide reductase. *Nature* **1990,** *345*, 593.

33. Brignole, E. J., Tsai, K. L., Chittuluru, J., Li, H., Aye, Y., Penczek, P. A., Stubbe, J., Drennan, C. L., Asturias, F. 3.3-Å resolution cryo-EM structure of human ribonucleotide reductase with substrate and allosteric regulators bound. *eLife* **2018,** *7*, e31502.
34. Atkin, C. L., Thelander, L., Reichard, P., Lang, G. Iron and free radical in ribonucleotide reductase exchange of iron and mössbauer spectroscopy of the protein B2 subunit of the Escherichia coli enzyme. *Journal of Biological Chemistry* **1973,** *248*, 7464-7472.
35. Ayala, I., Range, K., York, D., Barry, B. A. Spectroscopic properties of tyrosyl radicals in dipeptides. *Journal of the American Chemical Society* **2002,** *124*, 5496-5505.
36. Bollinger, J., Edmondson, D., Huynh, B., Filley, J., Norton, Stubbe, J. Mechanism of assembly of the tyrosyl radical-dinuclear iron cluster cofactor of ribonucleotide reductase. *Science* **1991,** *253*, 292-298.
37. Aberg, A., Hahne, S., Karlsson, M., Larsson, A., Ormö, M., Ahgren, A., Sjöberg, B. Evidence for two different classes of redox-active cysteines in ribonucleotide reductase of Escherichia coli. *Journal of Biological Chemistry* **1989,** *264*, 12249-12252.
38. Eliasson, R., Pontis, E., Jordan, A., Reichard, P. Allosteric regulation of the third ribonucleotide reductase (NrdEF enzyme) from enterobacteriaceae. *Journal of Biological Chemistry* **1996,** *271*, 26582-26587.
39. Eriksson, M., Uhlin, U., Ramaswamy, S., Ekberg, M., Regnström, K., Sjöberg, B. M., Eklund, H. Binding of allosteric effectors to ribonucleotide reductase protein R1: reduction of active-site cysteines promotes substrate binding. *Structure* **1997,** *5*, 1077-1092.
40. Grinberg, I. R., Lundin, D., Hasan, M., Crona, M., Jonna, V. R., Loderer, C., Sahlin, M., Markova, N., Borovok, I., Berggren, G. Novel ATP-cone-driven allosteric regulation of ribonucleotide reductase via the radical-generating subunit. *Elife* **2018,** *7*, e31529.
41. Guarino, E., Salguero, I., Kearsey, S. E. Cellular regulation of ribonucleotide reductase in eukaryotes. *Seminars in Cell & Developmental Biology* **2014,** *30*, 97-103.
42. Halliwell, B., Gutteridge, J. M. Free radicals in biology and medicine. *Oxford University Press* **2015.**
43. Halliwell, B. Biochemistry of oxidative stress. *Portland Press* **2007.**
44. VanLoon, G. W., Duffy, S. J. Environmental chemistry: a global perspective. *Oxford university press* **2017.**
45. Cadenas, E., Sies, H. The lag phase. *Free radical research* **1998,** *28*, 601-609.
46. Kovacic, P., Pozos, R. S., Somanathan, R., Shangari, N., O'Brien, P. J. Mechanism of mitochondrial uncouplers, inhibitors, and toxins: focus on electron transfer, free radicals, and structure-activity relationships. *Current medicinal chemistry* **2005,** *12*, 2601-2623.
47. Valko, M., Morris, H., Mazur, M., Rapta, P., Bilton, R. F. Oxygen free radical generating mechanisms in the colon: do the semiquinones of vitamin K play a role in the aetiology of colon cancer? *Biochimica et Biophysica Acta* **2001,** *1527*, 161-166.
48. Adams, J. D., Odunze, I. N. Oxygen free radicals and Parkinson's disease. *Free Radical Biology and Medicine* **1991,** *10*, 161-169.
49. Dreher, D., Junod, A. F. Role of oxygen free radicals in cancer development. *European Journal of Cancer* **1996,** *32*, 30-38.

50. Myers Jr, L. Free radical damage of nucleic acids and their components: The direct absorption of energy. *Free radicals in biology* **1979,** *4*.
51. Jones, D. P. Redox potential of GSH/GSSG couple: Assay and biological significance. *Methods in enzymology* **2002,** 348, 93-112.
52. McCord, J. M., Fridovich, I. The reduction of cytochrome c by milk xanthine oxidase. *Journal of Biological Chemistry* **1968,** *243*, 5753-5760.
53. Robertson, J., Maughan, R., Duthie, G., Morrice, P. Increased blood antioxidant systems of runners in response to training load. *Clinical science* **1991,** *80*, 611-618.
54. Willcox, J. K., Ash, S. L., Catignani, G. L. Antioxidants and prevention of chronic disease. *Critical reviews in food science and nutrition* **2004,** *44*, 275-295.
55. Young, I., Woodside, J. Antioxidants in health and disease. *Journal of clinical pathology* **2001,** *54*, 176-186.
56. Burton, G. W. Antioxidant action of carotenoids. *The Journal of Nutrition* **1989,** *119*, 109-111.
57. Sato, K., Niki, E., Shimasaki, H. Free radical-mediated chain oxidation of low density lipoprotein and its synergistic inhibition by vitamin E and vitamin C. *Archives of Biochemistry and Biophysics* **1990,** *279*, 402-405.
58. Oberley, T., Oberley, L. Antioxidant enzyme levels in cancer. *Histology and histopathology* **1997,** *12*, 525-535.
59. Babior, B. M. Phagocytes and oxidative stress. *The American journal of medicine* **2000,** *109*, 33-44.
60. Droge, W. Free radicals in the physiological control of cell function. *Physiological reviews* **2002,** *82*, 47-95.
61. Lee, I. T., Yang, C. M. Role of NADPH oxidase/ROS in pro-inflammatory mediators-induced airway and pulmonary diseases. *Biochemical pharmacology* **2012,** *84*, 581-590.
62. Jiang, W., Yun, D., Saleh, L., Barr, E. W., Xing, G., Hoffart, L. M., Maslak, M. A., Krebs, C., Bollinger, J. M. A manganese (IV)/iron (III) cofactor in Chlamydia trachomatis ribonucleotide reductase. *Science* **2007,** *316*, 1188-1191.
63. Jordan, A., Pontis, E., Atta, M., Krook, M., Gibert, I., Barbe, J., Reichard, P. A second class I ribonucleotide reductase in Enterobacteriaceae: characterization of the Salmonella typhimurium enzyme. *Proceedings of the National Academy of Sciences* **1994,** *91*, 12892-12896.
64. Fontecave, M., Nordlund, P., Eklund, H., Reichard, P. The redox centers of ribonucleotide reductase of Escherichia coli. *Advances in enzymology and related areas of molecular biology* **1992**, 147-183.
65. Chen, P. Y. T., Funk, M. A., Brignole, E. J., Drennan, C. L. Disruption of an oligomeric interface prevents allosteric inhibition of Escherichia coli class Ia ribonucleotide reductase. *Journal of Biological Chemistry* **2018**, 10, 1074.
66. Ormö, M., Sjöberg, B. M. The Cys292→Ala substitution in protein R1 of class I ribonucleotide reductase from Escherichia coli has a global effect on nucleotide binding at the specificity-determining allosteric site. *European Journal of Biochemistry* **1996,** *241*, 363-367.
67. Zimanyi, C. M., Chen, P. Y. T., Kang, G., Funk, M. A., Drennan, C. L. Molecular basis for allosteric specificity regulation in class Ia ribonucleotide reductase from Escherichia coli. *Elife* **2016,** *5*, e07141.

68. Lammers, M., Follmann, H. The ribonucleotide reductases—a unique group of metalloenzymes essential for cell proliferation. *Inorganic Elements in Biochemistry* **1983,** 27-91.
69. Högbom, M., Stenmark, P., Voevodskaya, N., McClarty, G., Gräslund, A., Nordlund, P. The radical site in chlamydial ribonucleotide reductase defines a new R2 subclass. *Science* **2004,** *305*, 245-248.
70. Tong, W., Chen, S., Lloyd, S., Edmondson, D., Huynh, B., Stubbe, J. Mechanism of assembly of the diferric cluster tyrosyl radical cofactor of Escherichia coli ribonucleotide reductase from the diferrous form of the R2 subunit. *Journal of the American Chemical Society* **1996,** *118*, 2107-2108.
71. Bollinger, J., Edmondson, D., Huynh, B., Filley, J., Stubbe, J. Mechanism of assembly of the tyrosyl radical-dinuclear iron cluster cofactor of ribonucleotide reductase. *Science* **1991,** *253*, 292-298.
72. Ochiai, E., Mann, G., Gräslund, A., Thelander, L. Tyrosyl free radical formation in the small subunit of mouse ribonucleotide reductase. *Journal of Biological Chemistry* **1990,** *265*, 15758-15761.
73. Stubbe, J. Ribonucleotide reductases in the twenty-first century. *Proceedings of the National Academy of Sciences* **1998,** *95*, 2723-2724.
74. Fontecave, M., Gerez, C., Mansuy, D., Reichard, P. Reduction of the Fe (III)-tyrosyl radical center of Escherichia coli ribonucleotide reductase by dithiothreitol. *Journal of Biological Chemistry* **1990,** *265*, 10919-10924.
75. Sahlin, M., Graeslund, A., Petersson, L., Ehrenberg, A., Sjoeberg, B. M. Reduced forms of the iron-containing small subunit of ribonucleotide reductase from Escherichia coli. *Biochemistry* **1989,** *28*, 2618-2625.
76. Åberg, A., Nordlund, P., Eklund, H. Unusual clustering of carboxyl side chains in the core of iron-free ribonucleotide reductase. *Nature* **1993,** *361*, 276.
77. Logan, D. T., Su, X. D., Åberg, A., Regnström, K., Hajdu, J., Eklund, H., Nordlund, P. Crystal structure of reduced protein R2 of ribonucleotide reductase: the structural basis for oxygen activation at a dinuclear iron site. *Structure* **1996,** *4*, 1053-1064.
78. Rofougaran, R., Crona, M., Vodnala, M., Sjöberg, B. M., Hofer, A. Oligomerization status directs overall activity regulation of the Escherichia coli class Ia ribonucleotide reductase. *Journal of Biological Chemistry* **2008,** *283*, 35310-35318.
79. Högbom, M., Galander, M., Andersson, M., Kolberg, M., Hofbauer, W., Lassmann, G., Nordlund, P., Lendzian, F. Displacement of the tyrosyl radical cofactor in ribonucleotide reductase obtained by single-crystal high-field EPR and 1.4-Å x-ray data. *Proceedings of the National Academy of Sciences* **2003,** *100*, 3209-3214.
80. Ando, N., Brignole, E. J., Zimanyi, C. M., Funk, M. A., Yokoyama, K., Asturias, F. J., Stubbe, J., Drennan, C. L. Structural interconversions modulate activity of Escherichia coli ribonucleotide reductase. *Proceedings of the National Academy of Sciences* **2011,** *108*, 21046-21051.
81. Kashlan, O. B., Scott, C. P., Lear, J. D., Cooperman, B. S. A comprehensive model for the allosteric regulation of mammalian ribonucleotide reductase. Functional consequences of ATP-and dATP-induced oligomerization of the large subunit. *Biochemistry* **2002,** *41*, 462-474.

82. Kunz, B. A., Kohalmi, S. E., Kunkel, T. A., Mathews, C. K., McIntosh, E., Reidy, J. International commission for protection against environmental mutagens and carcinogens. Deoxyribonucleoside triphosphate levels: a critical factor in the maintenance of genetic stability. *Mutation research* **1994,** *318*, 1-64.
83. Von Döbeln, U., Reichard, P. Binding of substrates to Escherichia coli ribonucleotide reductase. *Journal of Biological Chemistry* **1976,** *251*, 3616-3622.
84. Ator, M. A., Salowe, S., Stubbe, J. 2'-Azido-2'-deoxynucleotideInteraction with E . coli Ribonucleotide Reductase: Generation of a New Radical Species. *Journal of the American Chemical Society* **1984,** *106*, 1886-1887.
85. Salowe, S., Bollinger, J. M., Ator, M. A., Stubbe, J. Alternative model for mechanism-based inhibition of Escherichia coli ribonucleotide reductase by 2'-azido-2/-deoxyuridine S'-diphosphate1. *Biochemistry* **1993,** *32*, 12749-12760.
86. Seyedsayamdost, M. R., Xie, J., Chan, C. T., Schultz, P. G., Stubbe, J. Site-specific insertion of 3-aminotyrosine into subunit α2 of E. coli ribonucleotide reductase: direct evidence for involvement of Y730 and Y731 in radical propagation. *Journal of the American Chemical Society* **2007,** *129*, 15060-15071.
87. Ando, N., Brignole, E. J., Zimanyi, C. M., Funk, M. A., Yokoyama, K., Asturias, F. J., Stubbe, J., Drennan, C. L. Structural interconversions modulate activity of Escherichia coli ribonucleotide reductase. *Proceedings of the National Academy of Sciences* **2011,** *108*, 21046-21051.
88. Strand, K. R., Karlsen, S., Kolberg, M., Røhr, Å. K., Görbitz, C. H., Andersson, K. K. Crystal structural studies of changes in the native dinuclear iron center of ribonucleotide reductase protein R2 from mouse. *Journal of Biological Chemistry* **2004,** *279*, 46794-46801.
89. Priya, P. L., Shanmughavel, P. A docking model of human ribonucleotide reductase with flavin and phenosafranine. *Bioinformation* **2009,** *4*, 123.
90. Smith, P., Zhou, B., Ho, N., Yuan, Y. C., Su, L., Tsai, S. C., Yen, Y. 2.6 Å X-ray crystal structure of human p53R2, a p53-inducible ribonucleotide reductase. *Biochemistry* **2009,** *48*, 11134-11141.
91. Kauppi, B., Nielsen, B. B., Ramaswamy, S., Larsen, I. K., Thelander, M., Thelander, L., Eklund, H. The three-dimensional structure of mammalian ribonucleotide reductase protein R2 reveals a more-accessible iron-radical site than Escherichia coli R2. *Journal of molecular biology* **1996,** *262*, 706-720.
92. Lycksell, P. O., Sahlin, M. Demonstration of segmental mobility in the functionally essential carboxyl terminal part of ribonucleotide reductase protein R2 from Escherichia coli. *FEBS letters* **1995,** *368*, 441-444.
93. Larsson, A., Sjöberg, B. Identification of the stable free radical tyrosine residue in ribonucleotide reductase. *The EMBO journal* **1986,** *5*, 2037-2040.
94. Seyedsayamdost, M. R., Yee, C. S., Reece, S. Y., Nocera, D. G., Stubbe, J. pH rate profiles of FnY356−R2s (n = 2, 3, 4) in Escherichia coli ribonucleotide reductase: Evidence that Y356 is a redox-active amino acid along the radical propagation pathway. *Journal of the American Chemical Society* **2006,** *128*, 1562-1568.
95. Seyedsayamdost, M. R., Chan, C. T. Y., Mugnaini, V., Stubbe, J., Bennati, M. PELDOR spectroscopy with DOPA-β2 and NH2Y-α2s: Distance measurements between residues involved in the radical propagation pathway of E. coli ribonucleotide reductase. *Journal of the American Chemical Society* **2007,** *129*, 15748-15749.

96. Ge, J., Yu, G., Ator, M. A., Stubbe, J. Pre-steady-state and steady-state kinetic analysis of E. coli class I ribonucleotide reductase. *Biochemistry* **2003,** *42*, 10071-10083.
97. Stehr, M., Schneider, G., Åslund, F., Holmgren, A., Lindqvist, Y. Structural basis for the thioredoxin-like activity profile of the glutaredoxin-like protein NrdH-redoxin from Escherichia coli. *Journal of Biological Chemistry* **2001**.
98. Gerez, C., Elleingand, E., Kauppi, B., Eklund, H., Fontecave, M. Reactivity of the tyrosyl radical of Escherichia coli ribonucleotide reductase. *The FEBS Journal* **1997,** *249*, 401-407.
99. Salowe, S., Stubbe, J. Cloning, overproduction, and purification of the B2 subunit of ribonucleoside-diphosphate reductase. *Journal of bacteriology* **1986,** *165*, 363-366.
100. Engström, Y., Eriksson, S., Jildevik, I., Skog, S., Thelander, L., Tribukait, B. Cell cycle-dependent expression of mammalian ribonucleotide reductase. Differential regulation of the two subunits. *Journal of Biological Chemistry* **1985,** *260*, 9114-9116.
101. Eriksson, S., Gräslund, A., Skog, S., Thelander, L., Tribukait, B. Cell cycle-dependent regulation of mammalian ribonucleotide reductase. The S phase-correlated increase in subunit M2 is regulated by de novo protein synthesis. *Journal of Biological Chemistry* **1984,** *259*, 11695-11700.
102. Liu, C., Powell, K. A., Mundt, K., Wu, L., Carr, A. M., Caspari, T. Cop9/signalosome subunits and Pcu4 regulate ribonucleotide reductase by both checkpoint-dependent and-independent mechanisms. *Genes & development* **2003,** *17*, 1130-1140.
103. Chabes, A. L., Björklund, S., Thelander, L. S Phase-specific transcription of the mouse ribonucleotide reductase R2 gene requires both a proximal repressive E2F-binding site and an upstream promoter activating region. *Journal of Biological Chemistry* **2004,** *279*, 10796-10807.
104. Engström, Y., Rozell, B. Immunocytochemical evidence for the cytoplasmic localization and differential expression during the cell cycle of the M1 and M2 subunits of mammalian ribonucleotide reductase. *The EMBO journal* **1988,** *7*, 1615-1620.
105. Pontarin, G., Fijolek, A., Pizzo, P., Ferraro, P., Rampazzo, C., Pozzan, T., Thelander, L., Reichard, P. A., Bianchi, V. Ribonucleotide reduction is a cytosolic process in mammalian cells independently of DNA damage. *Proceedings of the National Academy of Sciences* **2008,** *105*, 17801-17806.
106. Hu, C. M., Yeh, M. T., Tsao, N., Chen, C. W., Gao, Q. Z., Chang, C. Y., Lee, M.-H., Fang, J. M., Sheu, S. Y., Lin, C. J. Tumor cells require thymidylate kinase to prevent dUTP incorporation during DNA repair. *Cancer cell* **2012,** *22*, 36-50.
107. Niida, H., Katsuno, Y., Sengoku, M., Shimada, M., Yukawa, M., Ikura, M., Ikura, T., Kohno, K., Shima, H., Suzuki, H. Essential role of Tip60-dependent recruitment of ribonucleotide reductase at DNA damage sites in DNA repair during G1 phase. *Genes & development* **2010,** *24*, 333-338.
108. Stubbe, J., Ackles, D. On the mechanism of ribonucleoside diphosphate reductase from Escherichia coli. Evidence for 3'-C--H bond cleavage. *Journal of Biological Chemistry* **1980,** *255*, 8027-8030.
109. Stubbe, J., Ator, M., Krenitsky, T. Mechanism of ribonucleoside diphosphate reductase from Escherichia coli. Evidence for 3'-C--H bond cleavage. *Journal of Biological Chemistry* **1983,** *258*, 1625-1631.

110. Harris, G., Ashley, G. W., Robins, M. J., Tolman, R. L., Stubbe, J. 2'-deoxy-2'-halonucleotides as alternate substrates and mechanism-based inactivators of Lactobacillus leichmannii ribonucleotide reductase. *Biochemistry* **1987,** *26*, 1895-1902.
111. Mao, S., Holler, T., Yu, G., Bollinger Jr, J., Booker, S., Johnston, M., Stubbe, J. A model for the role of multiple cysteine residues involved in ribonucleotide reduction: amazing and still confusing. *Biochemistry* **1992,** *31*, 9733-9743.
112. Barton, D. Comprehensive natural products chemistry. *Newnes* **1999.**
113. Lenz, R., Giese, B. Studies on the mechanism of ribonucleotide reductases. *Journal of the American Chemical Society* **1997,** *119*, 2784-2794.
114. Uhlin, U., Eklund, H. Structure of ribonucleotide reductase protein R1. *Nature* **1994,** *370*, 533.
115. Lawrence, C. C., Bennati, M., Obias, H. V., Bar, G., Griffin, R. G., Stubbe, J. High-field EPR detection of a disulfide radical anion in the reduction of cytidine 5′-diphosphate by the E441Q R1 mutant of Escherichia coli ribonucleotide reductase. *Proceedings of the National Academy of Sciences* **1999,** *96*, 8979-8984.
116. Spyrou, G., Enmark, E., Miranda-Vizuete, A., Gustafsson, J. Å. Cloning and expression of a novel mammalian thioredoxin. *Journal of Biological Chemistry* **1997,** *272*, 2936-2941.
117. Bollinger Jr, J. M., Krebs, C., Stalking intermediates in oxygen activation by iron enzymes: Motivation and method. *Journal of inorganic biochemistry* **2006,** *100*, 586-605.
118. Yee, C. S., Seyedsayamdost, M. R., Chang, M. C., Nocera, D. G., Stubbe, J. Generation of the R2 subunit of ribonucleotide reductase by intein chemistry: insertion of 3-nitrotyrosine at residue 356 as a probe of the radical initiation process. *Biochemistry* **2003,** *42*, 14541-14552.
119. Ekberg, M., Sahlin, M., Eriksson, M., Sjöberg, B. M. Two conserved tyrosine residues in protein R1 participate in an intermolecular electron transfer in ribonucleotide reductase. *Journal of Biological Chemistry* **1996,** *271*, 20655-20659.
120. Seyedsayamdost, M. R., Stubbe, J. Site-Specific Replacement of Y356 with 3,4-dihydroxyphenylalanine in the β2 subunit of E. coli ribonucleotide reductase. *Journal of the American Chemical Society* **2006,** *128*, 2522-2523.
121. Yokoyama, K., Uhlin, U., Stubbe, J. A hot oxidant, 3-NO2Y122 radical, unmasks conformational gating in ribonucleotide reductase. *Journal of the American Chemical Society* **2010,** *132*, 15368-15379.
122. Eklund, H., Uhlin, U., Färnegårdh, M., Logan, D. T., Nordlund, P. Structure and function of the radical enzyme ribonucleotide reductase. *Progress in biophysics and molecular biology* **2001,** *77*, 177-268.
123. Yokoyama, K., Smith, A. A., Corzilius, B., Griffin, R. G., Stubbe, J. Equilibration of tyrosyl radicals (Y356•, Y731•, Y730•) in the radical propagation pathway of the Escherichia coli class Ia ribonucleotide reductase. *Journal of the American Chemical Society* **2011,** *133*, 18420-18432.
124. Ravichandran, K. R., Minnihan, E. C., Wei, Y., Nocera, D. G., Stubbe, J. Reverse electron transfer completes the catalytic cycle in a 2, 3, 5-trifluorotyrosine-substituted ribonucleotide reductase. *Journal of the American Chemical Society* **2015,** *137*, 14387-14395.

125. Nick, T. U., Ravichandran, K. R., Stubbe, J., Kasanmascheff, M. G., Bennati, M. Spectroscopic evidence for a H bond network at Y356 located at the subunit interface of active E. coli ribonucleotide reductase. *Biochemistry* **2017,** *56*, 3647-3656.
126. Pizano, A. A., Olshansky, L., Holder, P. G., Stubbe, J., Nocera, D. G. Modulation of Y356 photooxidation in E. coli class Ia ribonucleotide reductase by Y731 across the α2: β2 interface. *Journal of the American Chemical Society* **2013,** *135*, 13250-13253.
127. Reece, S. Y., Seyedsayamdost, M. R., Stubbe, J., Nocera, D. G. Direct observation of a transient tyrosine radical competent for initiating turnover in a photochemical ribonucleotide reductase. *Journal of the American Chemical Society* **2007,** *129*, 13828-13830.
128. Reece, S. Y., Seyedsayamdost, M. R., Stubbe, J., Nocera, D. G. Photoactive peptides for light-initiated tyrosyl radical generation and transport into ribonucleotide reductase. *Journal of the American Chemical Society* **2007,** *129*, 8500-8509.
129. Ekberg, M., Birgander, P., Sjöberg, B. M. In vivo assay for low-activity mutant forms of Escherichia coli ribonucleotide reductase. *Journal of bacteriology* **2003,** *185*, 1167-1173.
130. Olshansky, L., Greene, B. L., Finkbeiner, C., Stubbe, J., Nocera, D. G. Photochemical generation of a tryptophan radical within the subunit interface of ribonucleotide reductase. *Biochemistry* **2016,** *55*, 3234-3240.
131. Kasanmascheff, M., Lee, W., Nick, T. U., Stubbe, J., Bennati, M. Radical transfer in E. coli ribonucleotide reductase: a NH 2 Y 731/R 411 A-α mutant unmasks a new conformation of the pathway residue 731. *Chemical science* **2016,** *7*, 2170-2178.
132. Lee, W. Mechanistic studies of the radical transport pathway in aminotyrosine-substituted class Ia ribonucleotide reductase. *Massachusetts Institute of Technology* **2018.**
133. Winkler, J. R., Nocera, D. G., Yocom, K. M., Bordignon, E., Gray, H. B. Electron-transfer kinetics of pentaammineruthenium (III)(histidine-33)-ferricytochrome c. Measurement of the rate of intramolecular electron transfer between redox centers separated by 15 angstroms in a protein. *Journal of the American Chemical Society* **1982,** *104*, 5798-5800.
134. Winkler, J. R., Gray, H. B. Electron flow through metalloproteins. *Chemical reviews* **2013,** *114*, 3369-3380.
135. Winkler, J. R., Gray, H. B. Long-range electron tunneling. *Journal of the American Chemical Society* **2014,** *136*, 2930-2939.
136. Tebo, A. G., Quaranta, A., Herrero, C., Pecoraro, V. L., Aukauloo, A. Intramolecular photogeneration of a tyrosine radical in a designed protein. *ChemPhotoChem* **2017,** *1*, 89-92.
137. Olshansky, L., Stubbe, J., Nocera, D. G. Charge-transfer dynamics at the α/β subunit interface of a photochemical ribonucleotide reductase. *Journal of the American Chemical Society* **2016,** *138*, 1196-1205.
138. Mulliez, E., Fontecave, M., Gaillard, J., Reichard, P. An iron-sulfur center and a free radical in the active anaerobic ribonucleotide reductase of Escherichia coli. *Journal of Biological Chemistry* **1993,** *268*, 2296-2299.
139. Minnihan, E. C., Young, D. D., Schultz, P. G., Stubbe, J. Incorporation of fluorotyrosines into ribonucleotide reductase using an evolved, polyspecific aminoacyl-tRNA synthetase. *Journal of the American Chemical Society* **2011,** *133*, 15942-15945.

140. Ravichandran, K. R., Taguchi, A. T., Wei, Y., Tommos, C., Nocera, D. G., Stubbe, J. A> 200 meV uphill thermodynamic landscape for radical transport in Escherichia coli ribonucleotide reductase determined using fluorotyrosine-substituted enzymes. *Journal of the American Chemical Society* **2016,** *138*, 13706-13716.
141. Chang, M. C., Yee, C. S., Nocera, D. G., Stubbe, J. Site-specific replacement of a conserved tyrosine in ribonucleotide reductase with an aniline amino acid: a mechanistic probe for a redox-active tyrosine. *Journal of the American Chemical Society* **2004,** *126*, 16702-16703.
142. Ravichandran, K. R., Zong, A. B., Taguchi, A. T., Nocera, D. G., Stubbe, J., Tommos, C. Formal reduction potentials of difluorotyrosine and trifluorotyrosine protein residues: Defining the thermodynamics of multistep radical transfer. *Journal of the American Chemical Society* **2017,** *139*, 2994-3004.
143. Krakoff, I. H., Brown, N. C., Reichard, P. Inhibition of ribonucleoside diphosphate reductase by hydroxyurea. *Cancer Research* **1968,** *28*, 1559-1565.
144. Lassmann, G., Thelander, L., Gräslund, A. EPR stopped-flow studies of the reaction of the tyrosyl radical of protein R2 from ribonucleotide reductase with hydroxyurea. *Biochemical and biophysical research communications* **1992,** *188*, 879-887.
145. Dresler, W., Stein, R. Ueber den hydroxylharnstoff. *European Journal of Organic Chemistry* **1869,** *150*, 242-252.
146. Stearns, B., Losee, K. A., Bernstein, J. Hydroxyurea. A new type of potential antitumor agent1. *Journal of medicinal chemistry* **1963,** *6*, 201-201.
147. Stock, C., Clarke, D., Philips, F., Barclay, R. Cancer chemotherapy screening data. *Cancer research* **1960,** *20*, 1.
148. Sneeden, J. L., Loeb, L. A. Mutations in the R2 subunit of ribonucleotide reductase that confer resistance to hydroxyurea. *Journal of Biological Chemistry* **2004,** *279*, 40723-40728.
149. Beckloff, G., Lerner, H., Frost, D., Russo-Alesi, F., Gitomer, S. Hydroxyurea (NSC-32065) in biologic fluids: dose-concentration relationship. *Cancer chemotherapy reports* **1965,** *48*, 57.
150. Gwilt, P. R., Tracewell, W. G. Pharmacokinetics and pharmacodynamics of hydroxyurea. *Clinical pharmacokinetics* **1998,** *34*, 347-358.
151. Ren, S., Wang, R., Komatsu, K., Bonaz-Krause, P., Zyrianov, Y., McKenna, C. E., Csipke, C., Tokes, Z. A., Lien, E. J. Synthesis, biological evaluation, and quantitative structure activity relationship analysis of new Schiff bases of hydroxysemicarbazide as potential antitumor agents. *Journal of medicinal chemistry* **2002,** *45*, 410-419.
152. Yen, Y., Grill, S. P., Dutschman, G. E., Chang, C. N., Zhou, B.-S., Cheng, Y. C. Characterization of a hydroxyurea-resistant human KB cell line with supersensitivity to 6-thioguanine. *Cancer research* **1994,** *54*, 3686-3691.
153. Aye, Y., Long, M. J., Stubbe, J. Mechanistic studies of semicarbazone triapine targeting Human ribonucleotide reductase in vitro and in mammalian cells tyrosyl radical quenching not involving reactive oxygen species. *Journal of Biological Chemistry* **2012,** *287*, 35768-35778.
154. Giles, F. J., Fracasso, P. M., Kantarjian, H. M., Cortes, J. E., Brown, R. A., Verstovsek, S., Alvarado, Y., Thomas, D. A., Faderl, S., Garcia-Manero, G. Phase I and

pharmacodynamic study of Triapine®, a novel ribonucleotide reductase inhibitor, in patients with advanced leukemia. *Leukemia research* **2003,** *27*, 1077-1083.
155. Karp, J. E., Giles, F. J., Gojo, I., Morris, L., Greer, J., Johnson, B., Thein, M., Sznol, M., Low, J. A phase I study of the novel ribonucleotide reductase inhibitor 3-aminopyridine-2-carboxaldehyde thiosemicarbazone (3-AP, Triapine®) in combination with the nucleoside analog fludarabine for patients with refractory acute leukemias and aggressive myeloproliferative disorders. *Leukemia research* **2008,** *32*, 71-77.
156. Alvero, A. B., Chen, W., Sartorelli, A. C., Schwartz, P., Rutherford, T., Mor, G. Triapine (3-aninopyridine-2-carboxaldehyde thiosemicarbazone) induces apoptosis in ovarian cancer cells. *Journal of the Society for Gynecologic Investigation* **2006,** *13*, 145-152.
157. Finch, R. A., Liu, M. C., Cory, A. H., Cory, J. G., Sartorelli, A. C. Triapine (3-aminopyridine-2-carboxaldehyde thiosemicarbazone, 3-AP): an inhibitor of ribonucleotide reductase with antineoplastic activity. *Advances in enzyme regulation* **1999,** *39*, 3-12.
158. Finch, R. A., Liu, M. C., Grill, S. P., Rose, W. C., Loomis, R., Vasquez, K. M., Cheng, Y. C., Sartorelli, A. C. Triapine (3-aminopyridine-2-carboxaldehyde-thiosemicarbazone): a potent inhibitor of ribonucleotide reductase activity with broad spectrum antitumor activity. *Biochemical pharmacology* **2000,** *59*, 983-991.
159. Kuo, M. L., Hwang, H. S., Sosnay, P. R., Kunugi, K. A., Kinsella, T. J. Overexpression of the R2 subunit of ribonucleotide reductase in human nasopharyngeal cancer cells reduces radiosensitivity. *The Cancer Journal* **2003,** *9*, 277-285.
160. Li, J., Zheng, L. M., King, I., Doyle, T. W., Chen, S. H. Syntheses and antitumor activities of potent inhibitors of ribonucleotide reductase 3-amino-4-nethylpyridine-2-carboxaldehyde-thiosemicarba-zone (3-Amp), 3-amino-pyridine-2-carboxaldehyde-thiosemicarbazone (3-Ap) and its water-soluble prodrugs. *Current medicinal chemistry* **2001,** *8*, 121-133.
161. Graser-Loescher, G., Schoenhuber, A., Ciglenec, C., Eberl, S., Krupitza, G., Mader, R. M., Jadav, S. S., Jayaprakash, V., Fritzer-Szekeres, M., Szekeres, T. Thiosemicarbazone derivatives, thiazolyl hydrazones, effectively inhibit leukemic tumor cell growth: Down-regulation of ribonucleotide reductase activity and synergism with arabinofuranosylcytosine. *Food and Chemical Toxicology* **2017,** *108*, 53-62.
162. Cotruvo Jr, J. A., Stubbe, J. Class I ribonucleotide reductases: metallocofactor assembly and repair in vitro and in vivo. *Annual review of biochemistry* **2011,** *80*, 733-767.
163. Popović-Bijelić, A., Kowol, C. R., Lind, M. E., Luo, J., Himo, F., Enyedy, É. A., Arion, V. B., Gräslund, A. Ribonucleotide reductase inhibition by metal complexes of Triapine (3-aminopyridine-2-carboxaldehyde thiosemicarbazone): A combined experimental and theoretical study. *Journal of inorganic biochemistry* **2011,** *105*, 1422-1431.
164. Mah, V., Alavi, M., Márquez-Garbán, D. C., Maresh, E. L., Kim, S. R., Horvath, S., Bagryanova, L., Huerta-Yepez, S., Chia, D., Pietras, R. Ribonucleotide reductase subunit M2 predicts survival in subgroups of patients with non-small cell lung carcinoma: effects of gender and smoking status. *PLoS One* **2015,** *10*, e0127600.
165. Aye, Y., Li, M., Long, M., Weiss, R. Ribonucleotide reductase and cancer: biological mechanisms and targeted therapies. *Oncogene* **2015,** *34*, 2011.

166. Siddique, M. U. M., Jadav, S. S., Graser, G., Saiko, P., Szekeres, T., Sinha, B. N., Jayaprakash, V. Design, Synthesis and biological evaluation of diazeno-thiazole derivatives as ribonucleotide reductase inhibitors. *Journal of Pharmeceutical Chemistry* **2017,** *4*, 20-24.
167. Mitsuya, H., Weinhold, K. J., Furman, P. A., St Clair, M. H., Lehrman, S. N., Gallo, R. C., Bolognesi, D., Barry, D. W., Broder, S. 3'-azido-3'-deoxythymidine (BW A509U): an antiviral agent that inhibits the infectivity and cytopathic effect of human T-lymphotropic virus type III/lymphadenopathy-associated virus in vitro. *Proceedings of the National Academy of Sciences* **1985,** *82*, 7096-7100.
168. Van der Donk, W. A., Stubbe, J., Gerfen, G. J., Bellew, B. F., Griffin, R. G. EPR investigations of the inactivation of E. coli ribonucleotide reductase with 2'-azido-2'-deoxyuridine 5'-diphosphate: Evidence for the involvement of the thiyl radical of C225-R1. *Journal of the American Chemical Society* **1995,** *117*, 8908-8916.
169. Livada, J., Martinie, R. J., Dassama, L. M., Krebs, C., Bollinger Jr, J. M., Silakov, A. Direct measurement of the radical translocation distance in the class I ribonucleotide reductase from Chlamydia trachomatis. *The Journal of Physical Chemistry B* **2015,** *119*, 13777-13784.
170. Wilson, E. B., Decius, J. C., Cross, P. C. Molecular vibrations: the theory of infrared and Raman vibrational spectra. *Courier Corporation* **1955.**
171. Hirschfeld, T. Fellgett's advantage in UV-Vis multiplex spectroscopy. *Applied Spectroscopy* **1976,** *30*, 68-69.
172. Luc, P., Gerstenkorn, S.,Fourier transform spectroscopy in the visible and ultraviolet range. *Applied optics* **1978,** *17*, 1327-1331.
173. Levin, I. W., Lewis, E. N. Fourier transform Raman spectroscopy of biological materials. *Analytical chemistry* **1990,** *62*, 1101-1111.
174. Murnaghan, F. The compressibility of media under extreme pressures. *Proceedings of the National Academy of Sciences* **1944,** *30*, 244-247.
175. Adamson, A., A textbook of physical chemistry. *Elsevier* **2012.**
176. Frueh, D. P., Goodrich, A., Mishra, S., Nichols, S. NMR methods for structural studies of large monomeric and multimeric proteins. *Current opinion in structural biology* **2013,** *23*, 734-739.
177. Sanders, J. K., Hunter, B. K. Modern NMR spectroscopy: a guide for chemists. *Analytical Chemistry* **1988,** 30, 320.
178. Ji, T., Urry, D. Correlation of light scattering and absorption flattening effects with distortions in the circular dichroism patterns of mitochondrial membrane fragments. *Biochemical and biophysical research communications* **1969,** *34*, 404-411.
179. Krimm, S., Bandekar, J. Vibrational spectroscopy and conformation of peptides, polypeptides, and proteins. *Advances in protein chemistry* **1986,** 38, 181-364.
180. Jackson, M., Mantsch, H. H. The use and misuse of FTIR spectroscopy in the determination of protein structure. *Critical reviews in biochemistry and molecular biology* **1995,** *30*, 95-120.
181. Byler, D. M., Purcell, J. M. FTIR examination of thermal denaturation and gel-formation in whey proteins. *International Society for Optics and Photonics* **1989,** 415-418.

182. Jackson, M., Mantsch, H. H. Protein secondary structure from FT-IR spectroscopy: correlation with dihedral angles from three-dimensional Ramachandran plots. *Canadian Journal of Chemistry* **1991,** *69*, 1639-1642.
183. Moore, W., Krimm, S. Transition dipole coupling in amide I modes of βpolypeptides. *Proceedings of the National Academy of Sciences* **1975,** *72*, 4933-4935.
184. Miyazawa, T. Perturbation treatment of the characteristic vibrations of polypeptide chains in various configurations. *The Journal of Chemical Physics* **1960,** *32*, 1647-1652.
185. Ambrose, E., Elliott, A. The structure of synthetic polypeptides. II. Investigation with polarized infra-red spectroscopy. *Proceedings of the Royal Society of London* **1951,** *205*, 47-60.
186. Elliott, A., Ambrose, E. Evidence of chain folding in polypeptides and proteins. *Discussions of the Faraday Society* **1950,** *9*, 246-251.
187. Pimentel, G. C., Sederholm, C. H. Correlation of infrared stretching frequencies and hydrogen bond distances in crystals. *The Journal of Chemical Physics* **1956,** *24*, 639-641.
188. Braiman, M. S., Rothschild, K. J. Fourier transform infrared techniques for probing membrane protein structure. *Annual review of biophysics and biophysical chemistry* **1988,** *17*, 541-570.
189. Mäntele, W. Reaction-induced infrared difference spectroscopy for the study of protein function and reaction mechanisms. *Trends in biochemical sciences* **1993,** *18*, 197-202.
190. Offenbacher, A. R., Vassiliev, I. R., Seyedsayamdost, M. R., Stubbe, J., Barry, B. A. Redox-linked structural changes in ribonucleotide reductase. *Journal of the American Chemical Society* **2009,** *131*, 7496-7497.
191. Offenbacher, A. R., Watson, R. A., Pagba, C. V., Barry, B. A. Redox-dependent structural coupling between the α2 and β2 subunits in E. coli ribonucleotide reductase. *The Journal of Physical Chemistry B* **2014,** *118*, 2993-3004.
192. Offenbacher, A. R., Minnihan, E. C., Stubbe, J., Barry, B. A. Redox-linked changes to the hydrogen-bonding network of ribonucleotide reductase β2. *Journal of the American Chemical Society* **2013,** *135*, 6380-6383.
193. Offenbacher, A. R., Burns, L. A., Sherrill, C. D., Barry, B. A. Redox-linked conformational control of proton-coupled electron transfer: Y122 in the ribonucleotide reductase β2 subunit. *The Journal of Physical Chemistry B* **2013,** *117*, 8457-8468.
194. Schowen, K., Limbach, H. H., Denisov, G., Schowen, R. Hydrogen bonds and proton transfer in general-catalytic transition-state stabilization in enzyme catalysis. *Biochimica et Biophysica Acta (BBA)-Bioenergetics* **2000,** *1458*, 43-62.

CHAPTER 2. REDOX-DEPENDENT STRUCTURAL COUPLING BETWEEN THE α2 AND B2 SUBUNITS IN *E. COLI* RIBONUCLEOTIDE REDUCTASE

2.1 Abstract

Ribonucleotide reductase (RNR) catalyzes the production of deoxyribonucleotides in all cells. In *E. coli* class Ia RNR, a transient α2β2 complex forms when a ribonucleotide substrate, such as CDP, binds to the α2 subunit. A tyrosyl radical (Y122O•)-diferric cofactor in β2 initiates substrate reduction in α2 via a long distance, proton-coupled electron transfer (PCET) process. Here, we use reaction-induced FT-IR spectroscopy to describe the α2β2 structural landscapes, which are associated with dATP and hydroxyurea (HU) inhibition. Spectra were acquired after mixing *E. coli* α2 and β2 with a substrate, CDP, and the allosteric effector, ATP. Isotopic chimeras, ^{13}Cα2β2 and α2^{13}Cβ2, were used to define subunit-specific structural changes. Mixing of α2 and β2 under turnover conditions yielded amide I (C=O) and II (CN/NH) bands, derived from each subunit. The addition of the inhibitor, dATP, resulted in a decreased contribution from amide I bands, attributable to beta strands and disordered structures. Significantly, HU-mediated reduction of Y122O• was associated with structural changes in α2, as well as β2. To define the spectral contributions of Y122O•/Y122OH in the quaternary complex, $^{2}H_4$ labeling of β2 tyrosines and HU-editing were performed. The bands of Y122O•, Y122OH, and D84,

a unidentate ligand to the diferric cluster, previously identified in isolated β2, were observed in the α2β2 complex. These spectra also provide evidence for a conformational rearrangement at an additional β2 tyrosine(s), Y_x, in the α2β2/CDP/ATP complex. This study illustrates the utility of reaction-induced FT-IR spectroscopy in the study of complex enzymes.

2.2 Introduction

A critical barrier in the development of new anti-cancer and anti-viral pharmaceuticals is an understanding of drug interactions with complex enzyme targets in solution. Ribonucleotide reductase (RNR) is a complex, multi-subunit enzyme that provides deoxynucleotides, the essential building blocks for DNA biosynthesis and repair in all organisms.[1] Therefore, RNR plays a pivotal role in nucleic acid metabolism and cell division and is a target for anti-cancer and anti-viral therapies (reviewed in [2-3]). Clinically relevant, chemotherapeutic agents, suppress the activity of RNR.[4] This inhibition impedes DNA replication and triggers tumor-cell death. In this paper, we use a new technique to provide detailed information about the interactions of one of these therapeutic agents with RNR.

In all RNRs, the reduction of ribonucleotides to deoxyribonucleotides proceeds through a free radical mechanism (reviewed in [2, 5]). The reaction is initiated by H atom abstraction at the ribose 3′-carbon using an active site, transient cysteine radical.[6-7] There are three classes of RNRs that are classified according to the cofactors used to generate the active site cysteine.[2, 8-9] Class Ia RNRs, found in mammals and bacteria, are composed of α2 and β2 subunits, and use a tyrosyl radical (Y122O•)-diferric cofactor to generate the

thiyl radical (see Figure 2.1). The prototype of the class Ia enzyme is derived from Escherichia coli. The binding and reduction of substrate occurs in the α2 subunit (Figure 2.1A). In addition, class Ia α2 contains two effector sites, one termed the specificity site and the other termed the overall activity site. ATP stimulates nucleotide reduction, while dATP is a reversible inhibitor that binds at the activity site.[10] In E. coli, dATP promotes formation of inactive, ring-like, α4β4 oligomers in which the β2 subunit is rotated away from its normal docking position.[11-13] The effectors, ATP and dATP, also bind to the specificity site and promote CDP reduction.[14] Binding of effectors, such as dATP, dTTP, and dGTP, stimulate interactions between α2 and β2.[11-13]

A tyrosyl radical,[15] Y122O•, located in the β2 subunit,[16-17] oxidizes the active site cysteine, C439, to initiate substrate reduction in the α2 subunit.[6, 18] This tyrosyl radical is generated by oxygen-requiring redox reactions at a diiron cluster and is required for activity.[19-21] Binding of substrate, such as CDP, and an effector, such as ATP, to α2 promotes the transient formation of the functional $(\alpha 2)_n\beta 2$ (n = 1 or 3) quaternary complex.[11-12, 22] A docking model, small angle X-ray scattering, and electron microscopy [11-12, 22-23] support the conclusion that radical propagation between Y122 and C439 occurs over 35 Å (see Figure 2.1A-C). This distance has also been substantiated by pulsed electron-electron double resonance spectroscopy.[24-25]

The transient thiyl radical, in the 170kDa α2 subunit, is generated from Y122O• by a reversible, multi-step proton coupled electron transfer (PCET) process, involving a conserved pathway (β2: Y122O• ⇋ [W48] ⇋ Y356 ⇋ α2: Y731 ⇋ Y730 ⇋ C439).[26] The role of these residues was suggested by site-directed mutagenesis[27-29] and the radical

transfer mechanism has been elucidated using site-specific incorporation of unnatural amino acids.[30-35] In the E. coli quaternary complex, the redox chemistry of Y122O• is rapid, but is gated by a conformational step.[36]

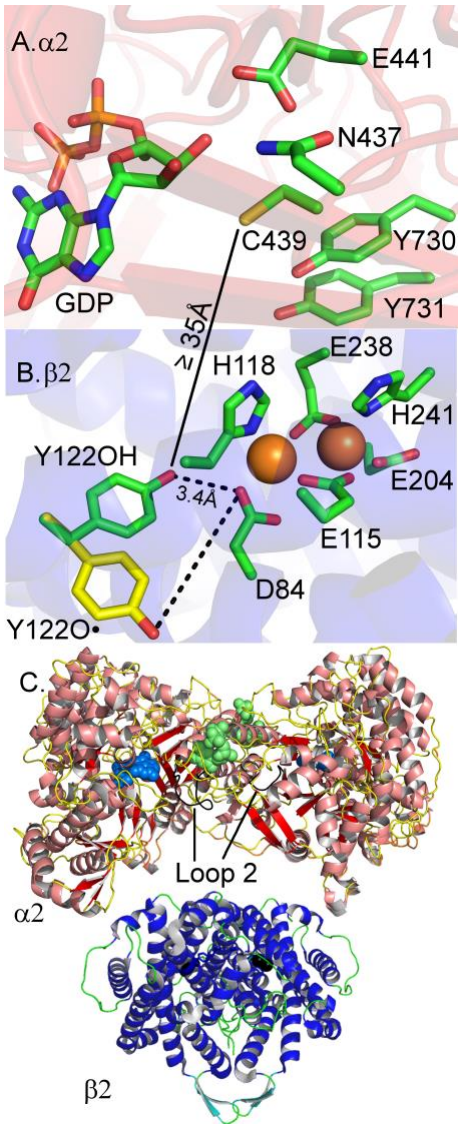

Figure 2.1 (A) Active site residues in the α2 subunit at 3.2 Å (PDB 4R1R) and containing the substrate, GDP.[37] (B) Y122OH-differric cluster in β2 at 1.9 Å (PDB 1MXR).[38] The solid line is the distance, as determined from the α2β2 docking model[23] and PELDOR[25] measurements, between β2 Y122 and α2 C439, which initiates

substrate reduction. The proposed conformational change at Y122O• in the isolated β2 subunit is superimposed in (B) in yellow, and is modeled in a YT dipeptide, as an A (backbone/ring dihedral angles: 173°/99°) to B (-69°/80°) conformational change.[38-39] Iron atoms are shown as orange spheres. (C) highlights the secondary structure of α2 (PDB 4R1R) and β2 (PDB 1MXR) subunits. The secondary structure elements are color-coded (α2: helix, salmon, beta, red, disordered, yellow and β2: helix, blue, beta, cyan, disordered, green). The substrates (GDP) and effectors (TTP) in α2 are represented as marine and lime spheres, respectively, the iron atoms in β2 are represented as black spheres. Loop 2 is highlighted in black and annotated. Note that (C) is presented to depict secondary structure and is not a docking model (see refs[23, 26]).

A complete description of this conformational gate is still not available. Currently, there is no high-resolution crystal structure of the class Ia α2β2 holoenzyme nor is there a structure of the isolated differic-Y122O• β2 subunit. Recent work has implicated an iron-bound water as the initial proton donor.[40-41] Therefore, the conformational gate could be linked to the proton transfer to Y122O•.[42] In the 1.4 Å structure of the diferric-Y122OH state (Met-β2), Y122OH is within hydrogen bonding distance (3.4 Å) of D84, a ligand of the diiron cluster (Figure 1B).[38] However, the radical state (Y122O•) is not hydrogen bonded.[43-44] Electron paramagnetic resonance (EPR)[38] and vibrational spectroscopic studies of isolated β2[39, 45] suggest that the phenoxyl ring translates away from D84 (Figure 1B, yellow), when Y122O• is oxidized. In isolated β2, this displacement has been shown to alter hydrogen bonding at D84.[46]

Reaction-induced FT-IR spectroscopy is a high-resolution technique, which can detect changes in protein structure in real time and with residue-specific resolution.[47-49] For RNR, this technique has been used to study reactions in the isolated β2 subunit,[39, 46, 50] but has not yet been used to study the α2β2 complex. Here, we use reaction-induced FT-IR vibrational spectroscopy to describe the conformational landscape of RNR under catalytic and inhibited conditions.

2.3 Materials and Methods

2.3.1 Materials.

HEPES, 4-(2-hydroxyethyl)-1-piperazineethanesulfonic acid, sodium hydroxide, and hydrochloric acid were purchased from Sigma (St. Louis, MO). Sodium deuteroxide (NaOD, 99.5%), deuterium oxide (D_2O, 98%), U-^{13}C-glucose (99%), and L-$^{2}H_4$-tyrosine ($^{2}H_{ring}$-tyrosine, 98%) were obtained from Cambridge Isotope Laboratories (Andover, MA). Hydroxyurea (HU) was purchased from Calbiochem (San Diego, CA).

2.3.2 Expression and purification of the E. coli α2 and β2 subunits of RNR.

Natural abundance, N-terminal His_6-tagged α (α2) was overexpressed using BL21(DE3) Star cells and purified by a Ni-NTA column, as described previously.[34] Natural abundance, wild-type β (β2) was overexpressed using BL21(DE3) cells and purified, as described previously.[51] Protein purity was assessed by SDS-PAGE (see Figure S1). Global ^{13}C labeling of all β2 carbons (^{13}C-β2) was conducted as described in ref[39, 52], global ^{13}C labeling of all α2 carbons (^{13}C-α2) was prepared by the same protocol. With this protocol, the extent of ^{13}C labeling has been quantified at > 90% using mass spec analysis.[52] Specific

$^{2}H_4$-tyrosine labeling of all β2 tyrosines ($^{2}H_4$Y-β2, 16 tyrosines per β monomer) was performed as described previously.[50] With this protocol, the extent of $^{2}H_4$ labeling at all β2 tyrosines has been quantified at 90% using mass spec analysis.[31] Average yields of α2 and ^{13}Cα2 were 60 and 56 mg per g of cell paste, respectively. Average yields of β2, ^{13}Cβ2, and $^{2}H_4$Yβ2 were 22, 15, and 5 mg per g of cell paste, respectively. The α and β homodimer concentrations were determined using UV-visible spectroscopy and the extinction coefficients, ε_{280} = 189 $mM^{-1}cm^{-1}$ for α2[53] and ε_{280} = 131 $mM^{-1}cm^{-1}$ for β2.[19] The tyrosyl radical (Y122O•) content in β2 (per homodimer) was determined spectrophotometrically by the drop-line method[54] and the average values for β2, ^{13}Cβ2, and $^{2}H_4$Yβ2 were 1.1, 1.0, and 0.9, respectively. The purities of the natural abundance and isotopically labeled samples was also assessed by Coomassie-stained SDS-PAGE[50] and were found to be similar (Figure S1). RNR activities were determined using the spectrophotometric assay, which monitors NADPH consumption in the coupled assay containing thioredoxin (TR) and thioredoxin reductase (TRR).[36] The assays were carried out at room temperature and contained 0.1 μM α2, 0.5 μM β2, 30 μM TR, 0.5 μM TRR, 0.2 mM NADPH, 3 mM ATP, 1.0 mM CDP, 15 mM $MgSO_4$, and 1 mM EDTA in 50 mM HEPES, pH 7.6. The buffer was mixed with $MgSO_4$, EDTA, DTT, ATP and CDP, then α2, TR, TRR and NADPH were added. The reaction was then initiated by the addition of β2 and by monitoring the absorbance at 340 nm. Typical α2 activity rates were 2000-2300 nmol $(min \times mg)^{-1}$, consistent with previous reports.[34, 36] Prior to UV-Vis kinetic or Fourier transform infrared (FT-IR) experiments, α2 and β2 samples were separately exchanged[50] using Ultracel-30 membrane into 5mM HEPES, pD 7.6 (pD values are reported without correction, see refs[55-

[56]). The buffer for the α2 samples also contained 5mM dithiothreitol (DTT) to maintain reduced α2.

2.3.3 Reaction-Induced FT-IR Spectroscopy.

Reaction-induced FT-IR spectra were collected at 20°C on a Nicolet Magna 550 II spectrometer, equipped with a MCT-A detector (Nicolet, Madison, WI). The protein samples were prepared at 300 μL volumes containing (final concentrations): 100 μM α2 (when present), 100 μM β2, 3 mM CDP, 1 mM ATP (or 1 mM dATP), 5 mM DTT, 15 mM $MgSO_4$, and 1 mM EDTA in 5 mM HEPES (pD 7.6). The reactions were prepared as described for the UV-Vis kinetic measurements below. HU, when applicable, was added immediately and last to a final concentration of 50 mM. The reaction was injected into a temperature-controlled CaF_2 flow cell, using a syringe pump (see refs[46, 50] for details). The path length used for these experiments was 50 microns. 120 s of data (4 cm^{-1} resolution, 595 interferograms, and 2.53 cm s^{-1} mirror velocity) were acquired, followed by a 360 s incubation, and then a second 120 s data acquisition was conducted. All data were processed using a Happ-Genzel apodization function, two levels of zero filling, and a Mertz phase correction. Each single beam set was ratioed to an open beam background, which consisted of the CaF_2 windows of the flow cell without buffer or sample and converted to absorption spectra. Individual absorption spectra (see Figure 2) were then subtracted to generate a difference spectrum (Scheme 2.1, part I). Absorption spectra of the reagents, CDP, HU, and ATP were recorded using the same conditions. FT-IR difference spectra (for example, see Figure 2.3A) were generated as before-minus-after the 360 s incubation. This time regime was chosen to maximize Y122O• reduction in the presence of HU, while

minimizing spectral artifacts from baseline drifts. For the HU reactions, these difference spectra reflect "Y122O•"-minus-"Y122OH" (Scheme 2.2, part I) and 50% reduction of Y122O•.[50] The data were reproducible, as shown in Figure S2. Isotope-edited spectra (Scheme 2.1, parts II and IV) were generated as NA-minus-isotope, prior to subtraction, the difference spectra were normalized for the Y122O• content (per β2 homodimer, for example, see ref [39]).

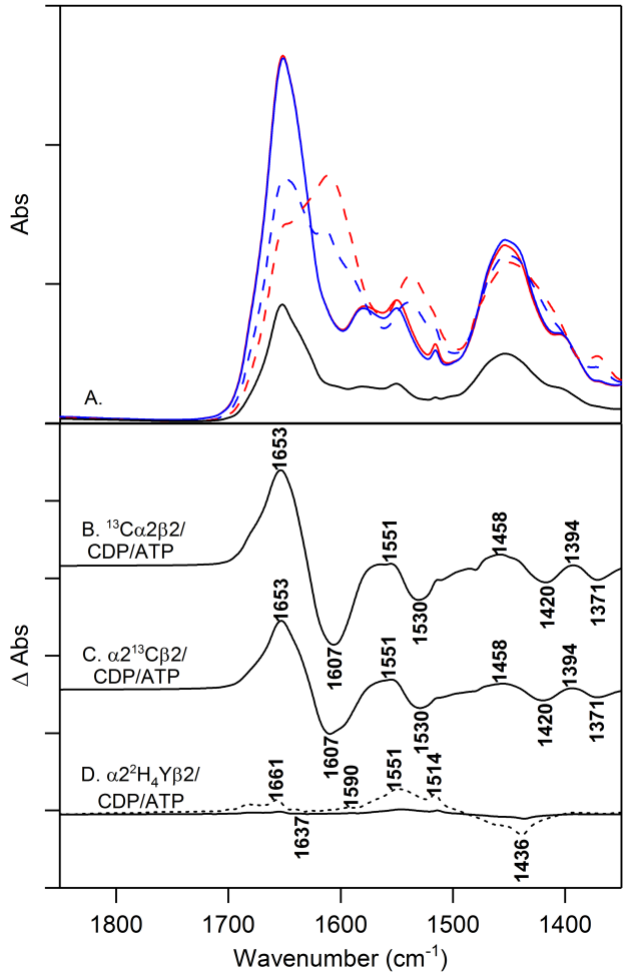

Figure 2.2 FT-IR absorption spectra. Samples were (A) α2β2 (solid red), 13Cα2-β2 (dashed red), α2-13Cβ2 (dashed blue), α2-2H4Yβ2 (solid blue), and β2 (black). The samples were prepared at 100 μM α2 (when present) and 100 μM β2 in 5 mM HEPES (pD 7.6) buffer, supplemented with 3 mM CDP, 1 mM ATP, 5 mM DTT, 15 mM $MgSO_4$, and 1 mM EDTA. Isotope-edited spectra (B-D) represent (B) α2β2-minus-

$^{13}C\alpha2$-β2, (C) α2β2-minus-α2-$^{13}C\beta2$, and (D) α2β2-minus-α2-$^{2}H_4Y\beta2$. To generate the dashed line in (D) the solid line was multiplied by a factor of 5 and is presented for comparison. The spectra are offset along the y-axis for comparison. Tick marks: 2×10^{-1} absorbance units. Averages: (A) 10 (solid red), 9 (solid blue), 10 (dashed red), 4 (dashed blue), and 8 (black) separate samples. The temperature was 20°C.

2.3.4 UV-Vis Kinetic Analysis of Y122O•.

The kinetic reactions (Figure S3) were performed at 20°C with a Varian Cary 50 (Varian, Walnut Creek, CA) spectrophotometer. The reactions contained (300 µL final volume) 35 µM α2, 35 µM β2, 3 mM CDP, 1 mM ATP, 5 mM DTT, 15 mM $MgSO_4$, and 1 mM EDTA in 5 mM HEPES (pD 7.6) buffer. The samples were prepared from concentrated stocks and added to buffer in the following order: DTT, $MgSO_4$/EDTA, ATP, CDP, and α2. β2 was subsequently added to initiate substrate reduction. Hydroxyurea was added immediately and last (50 mM final concentration) to reduce Y122O• in the experiments (see Figure S3A, B and D). In the absence of HU, no change in Y122O• was observed during the steady-state reactions over the 30 min time scans (Figure S3C). For each of the reactions, second-order HU rate constants were extracted from monoexponential fits to the % Y122O•, plotted at each time point (see insets in Figures S3A, B, and D). The Y122O• content was determined by the drop-line method, $[\mathrm{Y122O}\bullet] = \frac{A_{411nm} - \left[\frac{3\times(A_{416nm})+2\times(A_{406nm})}{5}\right]}{1784\ M^{-1}cm^{-1}}$.[54] The data in Figure S3 represent 3-4 averages for each decay fit. No corrections or normalizations were applied to the UV spectra before this data analysis. The values derived from this analysis were reproducible, as judged from the standard deviation (see error bars in Figure S3). For reactions containing dATP (Figure S3D), 1 mM dATP was added instead of 1 mM ATP.

Scheme 2.1 Methods used to generate reaction-induced FT-IR spectra.[a]

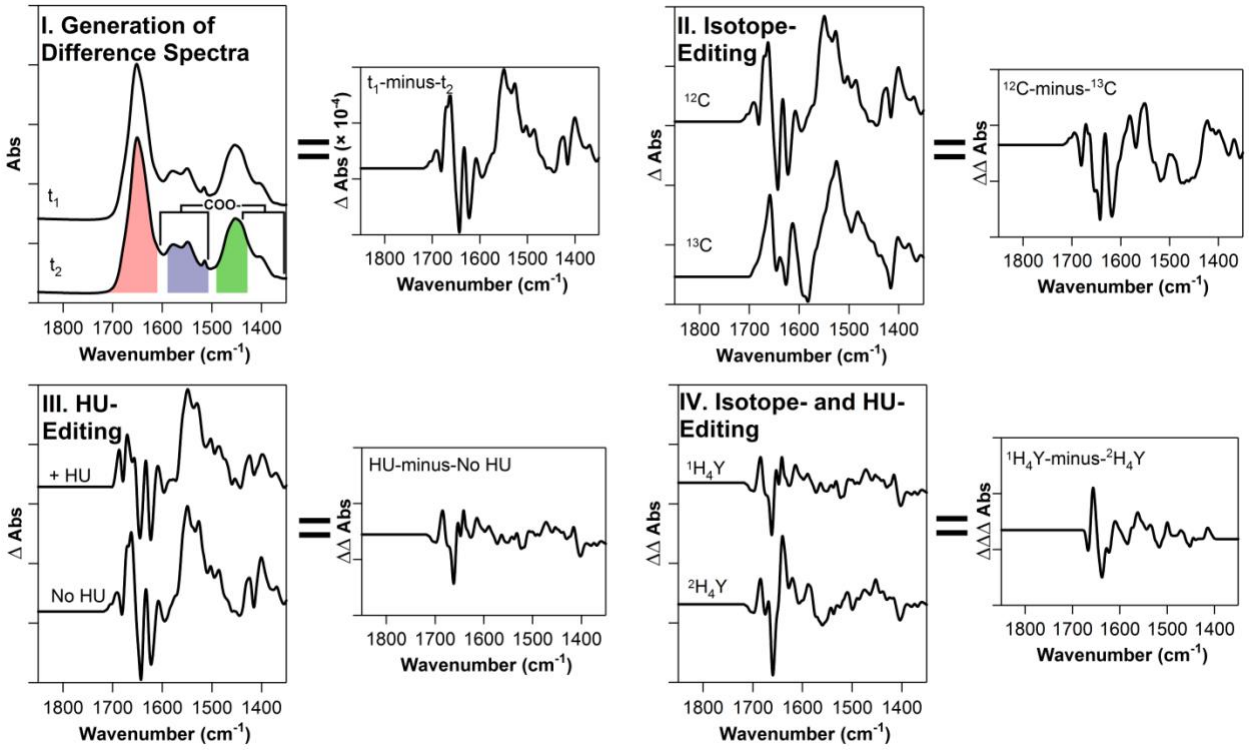

[a]In (I), the typical regions of carboxylate (COO^-) and amide (pink, amide I (C=O), blue, amide II (CN/NH, inaccessible to H/D exchange), and green, amide II′ (CN, accessible to H/D exchange)) vibrational modes are labeled. Time points, t_1 and t_2, represent data collected immediately (t_1) following rapid mixing and six minutes (t_2) after t_1.

2.4 Results

2.4.1 Isotope shifts derived from the FT-IR absorption spectrum of α2β2.

Figure 2.2A (solid red) displays the 1850-1350 cm^{-1} region of the FT-IR absorption spectra, recorded from the quaternary complex (QC), α2β2/CDP/ATP, under turnover conditions. This region is dominated by amide I, II, and III and carboxylate vibrations (see color coding in Scheme 2.1, part I). The frequency of the amide I (C=O) vibration (1690-

1620 cm^{-1}) is sensitive to changes in secondary structure (α-helix: 1660-1650, parallel and antiparallel β-sheet: 1690/1620, loop/unstructured: 1640 cm^{-1}) and in hydrogen bonding.[57-62] All protein samples were exchanged into D_2O buffer to downshift the water HOH bending (1640 cm^{-1}) band from the protein amide I region. Exchange of protein amide groups with deuterium is expected to shift the CN contribution of the amide II mode to ~1450 cm^{-1} and the NH contribution to ~1000 cm^{-1}. D_2O exhibits an intense vibrational band at 1200 cm^{-1}, thus preventing analysis below ~ 1300 cm^{-1}. To identify bands arising from α2 and β2 in the experiments, described below, the subunits were individually global-labeled with ^{13}C. The biosynthetic isotope enrichment approach has been shown to give >90% labeling.[52] The FT-IR absorption spectra of isotopic chimeras, in which one subunit is labeled and one subunit is globally labeled, are shown in Figure 2.2 B and C. A 46 cm^{-1} downshift of an amide I band component was observed in the isotopic chimera in which α2 was ^{13}C labeled and in which β2 was natural abundance ($^{13}C\alpha2\beta2$, Figure 2.2 B). A 46 cm^{-1} downshift was also observed in the isotopic chimera in which β2 was ^{13}C labeled and α2 was natural abundance ($\alpha2^{13}C\beta2$, Figure 2.2 C).

2.4.2 Preparations employed.

Scheme 2.2 introduces the preparations employed in reaction-induced FT-IR experiments. In Scheme 2.2, part 1, isolated β2 is treated with HU, which quenches the Y122 radical. In Scheme 2.2, part II, α2, β2, CDP, and ATP are mixed, in the presence of reductant, to generate the QC. In Scheme 2.2, part III, α2, β2, CDP, and dATP are mixed, this sample is inactive. Binding of dATP to the overall activity site prevents turnover and has been reported to promote oligomerization, generating an inactive α4β4 complex in E.

coli.[11-12] dATP also binds at the specificity site. In the presence of dATP, CDP may bind to reduced α2.[13-14, 37] In Scheme 2.2, part IV, HU is added to the QC, which is inactivated by this treatment. HU quenches the tyrosyl radical in a PCET process.[39, 63] In the quaternary complex, the HU reaction occurs with an accelerated rate, compared to isolated β2.[64] However, in D_2O, the reaction of HU with the quaternary complex is not accelerated, but occurs with the same rate as in isolated β2 (Figure S3 A and B).

Scheme 2.2 Preparations containing α2 and β2 subunits of *E. coli* RNR.

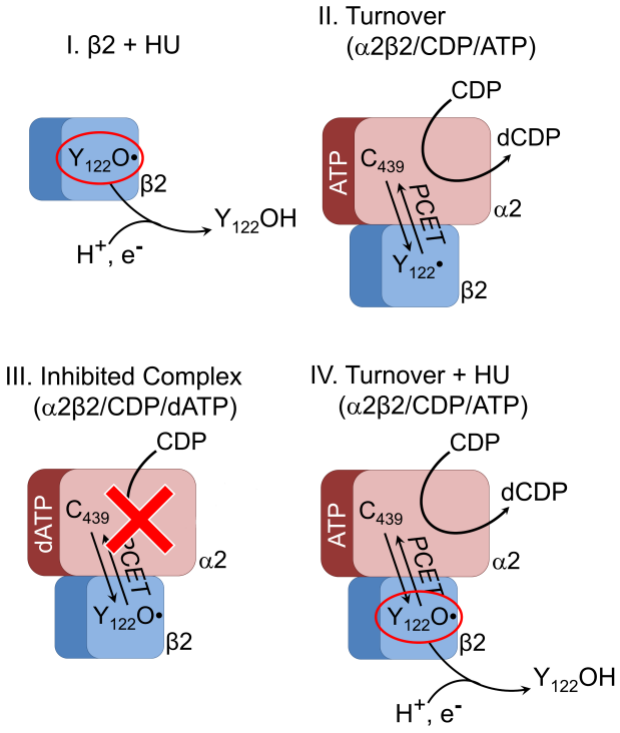

2.4.3 Methods used to construct reaction-induced FT-IR spectra.

Scheme 1 illustrates the method used to generate reaction-induced spectra. Starting with absorption spectra (such as the example in Figure 2.2), difference spectra were

constructed (Scheme 2.1, part 1). Spectra were acquired immediately following mixing, corresponding to a 2 min (t_1) time point. After 6 minutes, a second 2 min spectrum was acquired, corresponding to time point t_2. The t_1-minus-t_2 reflects the generation of the QC in samples that contain α2, β2, CDP, and ATP. At the t_2 time point, the reaction is complete, and the transient QC will not persist. On this timescale, all the available CDP substrate is predicted to be consumed. Thus, this spectrum reflects structural changes induced by formation of the QC and turnover. In HU-containing samples, the reaction-induced spectrum reflects structural changes induced by quenching of the β2 tyrosyl radical in the QC. This time frame was chosen to maximize signal while avoiding baseline drift. Reaction-induced FT-IR spectra were HU-edited by subtraction, HU treated-minus-no HU (Scheme 2.1, part III). Reaction-induced FT-IR spectra were isotope-edited by subtraction, natural abundance-minus-isotopically labeled (Scheme 2.1, part II). Isotopically labeled samples included globally ^{13}C labeled α2, globally ^{13}C labeled β2, and $^{2}H_4Y$-labeled β2.

2.4.4 Reaction-induced FT-IR spectra associated with mixing α2β2/CDP/ATP to form the QC.

Figure 2.3 A presents the reaction-induced FT-IR spectra of the QC (Scheme 2.1, part I). Complex spectral signatures were observed in the spectrum obtained from mixing DTT, α2, β2, ATP, and CDP (Figure 2.3 A). Note that mixing data recorded from a β2 control (Figure 2.3 F), containing no α2, but the same buffer and components as A, gave a flat baseline. In Figure 2.3 A, prominent bands in amide I (CO 1650 cm^{-1}) and amide II (CN/NH, 1550 cm^{-1}) regions reflect alterations in secondary structure and hydrogen bonding.[61] The appearance of these bands is attributable to formation of protein-protein

contacts and turnover-associated conformational alterations in the $\alpha 2\beta 2$ complex. The observation of amide II bands at 1550 cm^{-1} is potentially significant, because solvent-exposed regions of proteins into D_2O are observed at 1450 cm^{-1} (amide II′). The asymmetric stretching vibration of carboxylate side chains may also contribute in this region.[65] Bands in the 1425-1400 cm^{-1} region are assignable to the corresponding, symmetric carboxylate side chain vibrational bands.[65]

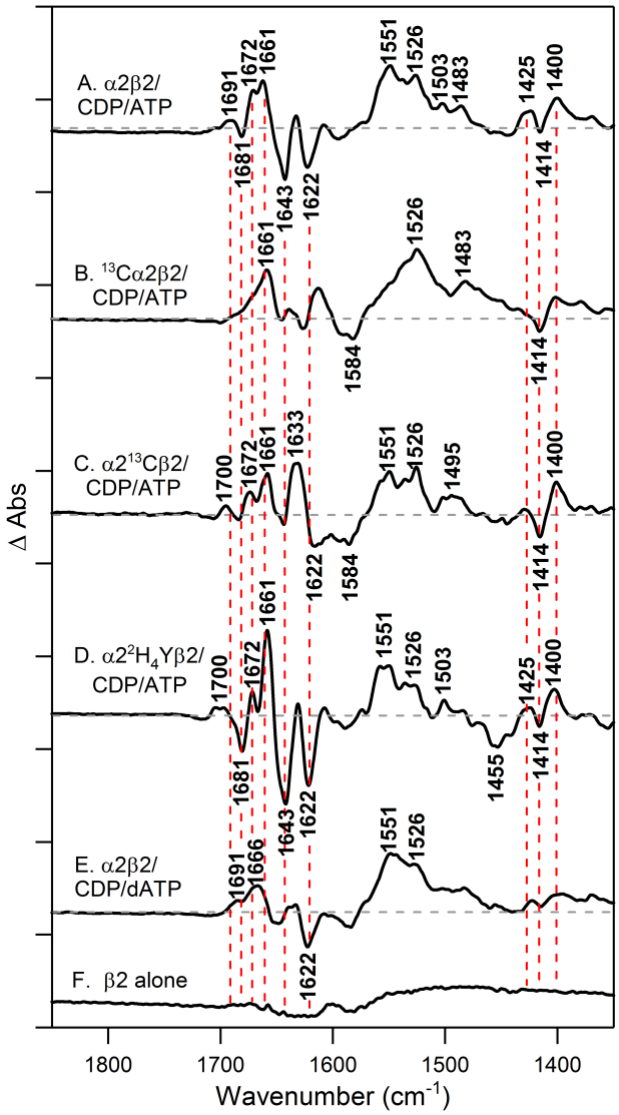

Figure 2.3 Reaction-induced FT-IR spectra of the α2β2 quaternary complex under turnover and dATP-inhibited conditions (Scheme 1, part 1). Samples were (A) α2β2/CDP/ATP, (B) 13Cα2-β2/CDP/ATP, (C) α2-13Cβ2/CDP/ATP, (D) α2-2H4Yβ2/CDP/ATP, and (E) the dATP-inhibited complex, α2β2/CDP/dATP. The spectrum in (F) was acquired from isolated β2 under the conditions used in (A). The samples were prepared at 100μM α2 (when present), 100μM β2 in 5mM HEPES (pD 7.6) buffer, supplemented with 3mM CDP, 1mM ATP (or dATP), 5mM DTT, 15mM $MgSO_4$, and 1mM EDTA. The spectra were offset along the y-axis for comparison. Tick marks: 1×10^{-3} absorbance units. Averages: (A) 10, (B) 10, (C) 4, (D) 9, (E) 10, and (F) 3 separate samples. The temperature was 20ºC.

2.4.5 Reaction-induced FT-IR spectra of globally ^{13}C labelled isotopic chimeras.

Reaction-induced FT-IR difference spectra were collected for the isotopic chimeras, $^{13}C\alpha 2\beta 2$ (Figure 3 B) and $\alpha 2^{13}C\beta 2$ (Figure 2.3 C), assembled into the QC. In Figure 2.3 B and C, spectral downshifts of amide I (~1650 cm^{-1}) and II (~1550 cm^{-1}) bands are apparent (Table 1). Isotope-sensitive amide I bands are consistent with a change in α2 and β2 structure following mixing. Moreover, as assessed from the isotope-edited spectra (see Figure S4 and Scheme 2.1, part II), the conformational changes arising in the two subunits are distinct. From the isotope shifts, bands at 1691, 1681, 1672 and 1622 cm^{-1} are assignable to α2 (Table 2.1). Bands at 1661 and 1643 have a contribution both from α2 and β2. Note that ^{13}C labeling of β2 causes small frequency shifts in the α2 bands in the 1691-1672 cm^{-1} region (Figures 2.3 C and S4B), as expected due to alterations in transition dipole coupling.[59] However, the pattern of intensities and frequencies is similar. Based on characteristic spectral regions, the 1643 cm^{-1} bands are assigned to disordered structure and the 1681-1622 cm^{-1} bands are assigned primarily to beta strands.[57, 60, 62, 66] Note that there may be overlap among these characteristic ranges.[60] The 1691 cm^{-1} band may arise either from a beta strand or from an amino acid side chain, such as asparagine or glutamine.[62, 67] Amide II and asymmetric carboxylate bands, derived from α2, are also observed in the 1550 cm^{-1} region of Figure 2.3 A. Symmetric carboxylate bands at 1425, 1414, and 1400 cm^{-1} are assigned to α2 (Table 2.1). The β2 subunit has an overlapping carboxylate contribution at 1425 and 1414 cm^{-1} (Figure 2.3C and Figure S4B).

Table 2.1 Assignment of amide I and carboxylate bands based on isotopic labeling and reaction-induced FT-IR spectroscopy, acquired in D2O buffers.

υ (cm^{-1})	Isotope-shifted υ	Subunit	Assignment	dATP sensitive?

Amide I bands identified by α2β2 mixing under turnover conditions (Figures 3 and S4)				
(+) 1691	1653 (^{13}C) (predicted[b] 1645)	α2	beta sheet or side chain	No
(–) 1681	N.D.[a] (predicted[b] 1635)	α2	beta sheet	Yes
(+) 1672	1622 (^{13}C) (predicted[b] 1626)	α2	beta sheet	Yes
(+) 1661	N.D. (predicted[b] 1615)	α2 and β2	beta sheet or alpha helix	No
(–) 1643	1607 (predicted[b] 1597)	α2 and β2	disordered	Yes
(–) 1622	1584 (^{13}C) (predicted[b] 1576)	α2	beta sheet	No

Carboxylate side chain bands identified by α2β2 mixing under turnover conditions (Figures 3 and S4)				
(+) 1425	N.D.	α2 and β2	asp/glu	Yes
(–) 1414	N.D.	α2 and β2	asp/glu	Yes
(+) 1400	N.D.	α2	asp/glu	Yes
Amide I bands, identified by HU reduction, either in α2β2 or in isolated β2 (Figures 4 and 5)				
(+) 1685/7	N.O.[c] α2 1644 (^{13}C β2)[d]	α2 and β2	beta sheet α2 D84 β2	No
(–) 1675	N.O. α2 1635 (^{13}C β2)[d]	α2 and β2	beta sheet α2 D84 β2	No
(–) 1661	N.O. α2 1621 (^{13}C)[d]	β2	D84/Y122 amide C=O	No
(+) 1653	1613 (^{13}C)[d]	β2	D84/Y122 amide C=O	No

[a]N.D. Not determined,

[b]Predicted based on average 46 cm^{-1} ^{13}C isotope shift (Figure 2.2),

[c]N.O. Not observed due to overlap with ^{13}C β,

[d]Isotope-shifted bands identified by specific Y and D β2 labeling in refs.[39, 46, 50]

2.4.6 Reaction-induced FT-IR spectra associated with dATP inhibition.

Figure 3 E presents a control (Scheme 2.2, part III), in which dATP was substituted for ATP. In the reaction-induced FT-IR spectrum, mixing α2 and β2 in the presence of dATP, CDP, and DTT altered the spectrum, compared to the ATP-containing sample (compare Figure 2.3 E to 2.3 A). The ATP-dependent bands were the 1681 and 1671 cm^{-1} bands of α2 and the 1643 cm^{-1} amide bands of α2 and β2 (Table 2.1). The intensities of the symmetric carboxylate bands of α2 and β2 were also ATP sensitive. The other α2 and β2 bands (Table 2.1) were observed both in the presence of dATP and in the presence of ATP. These spectral bands reflect secondary structural changes induced either by dATP or CDP binding.

2.4.7 Reaction-induced FT-IR spectra of the $^2H_4$-tyrosine labeled β2 chimera.

A third isotopic chimera was employed, in which β2 tyrosines were $^2H_4$ labeled and α2 was natural abundance (Figure 2.3 D). This labeling procedure has been described previously,[50] and results in 90% isotope enrichment of all tyrosine side chains (16 tyrosine residues per β monomer, including Y122O•). Interestingly, while there was no significant decrease in Y122O• content during turnover, as assessed by UV-Vis kinetics (Figure S3C), $^2H_4$ labeling of β2 significantly altered the reaction-induced FT-IR spectrum (Figure 2.3 D). In the isotope-edited spectrum (Figure S4C), bands 1521, 1501, 1455 and 1414 cm^{-1} are assignable to the natural abundance (1521 and 1501 cm^{-1}) and $^2H_4$Y labeled (1455, 1414 cm^{-1}) Y19a bands of a tyrosine in two different environments (Table 2.2). An ~80 cm^{-1} Y19a isotope shift is predicted by DFT calculations and model compound studies for $^2H_4$Y labeling.[39, 68] Isotope-sensitive amide I (CO) bands were also detected in Figure S4C. These isotope-sensitive bands provide evidence for a conformationally active tyrosine,

termed Y_x, in the β2 subunit, which is distinct from Y122 (see also discussion of the HU-edited spectrum, below).

Table 2.2 Assignment of Y122O•, Y122OH, and Yx spectral bands based on isotopic labeling and reaction-induced FT-IR spectroscopy, acquired in D2O buffers.

υ (cm^{-1})	Isotope-shifted υ	Subunit	Assignment
Y122OH/Y122O• bands, identified by HU reduction in α2β2 and in isolated β2 (Figure 6)			
(–) 1514	1436 (^2H_4Y)[a]	β2	(Y19a) ring Y122OH
(+) 1498	1480 (^2H_4Y)[a]	β2	(Y7a) CO Y122•
Y_x bands, identified by α2β2 mixing under turnover conditions or by reduction of the QC with HU (Figure 6)			
(–) 1521	1414 (^2H_4Y)	β2	(Y19a) Y_x
(+) 1501	1455/1436 (^2H_4Y)	β2	(Y19a) Y_x

[a]Isotope-shifted bands also identified in refs.[39, 46, 50]

Quantitation of Y_x in the $^2H_4$-tyrosine edited spectrum. The peaks of the 1680-1630 cm^{-1} region in the isotope-edited spectrum (Figure 2.3 D), which are attributed to Y_x, were integrated and compared to that of the ^2H_4Y-edited absorption spectrum, which reflects the isotope shifts of all 16 β2 tyrosines (Figure 2.2 D). This analysis estimates that ~2 tyrosines in the β2 homodimer contribute to Figure 2.3 D. Therefore, we attribute these bands to spectral shifts arising from two Y_x residues per β2 dimer.

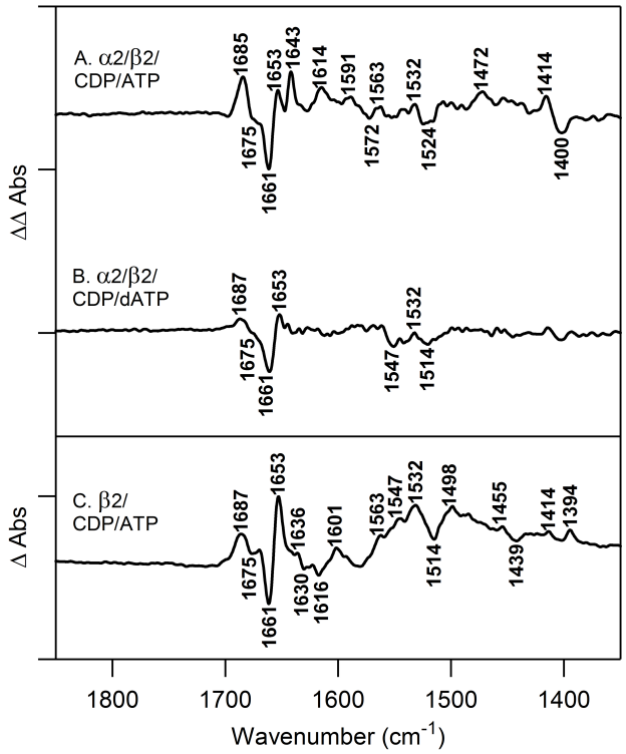

Figure 2.4 HU-edited, reaction-induced FT-IR spectra (HU-minus-no HU, Scheme 1, part III). Samples were (A) α2β2/CDP/ATP, (B) the dATP-inhibited complex, α2β2/CDP/dATP, and (C) isolated β2 under the conditions used in (A). Tick marks: 1 × 10-3 absorbance units. Averages: (A) 19, (B) 21, and (C) 8 separate samples. The temperature was 20ºC.

2.4.8 *HU-editing of the reaction-induced FT-IR spectra.*

To define Y122O• redox-linked changes in the α2β2 complex, HU editing was employed (Scheme 2.1, part III). As shown in Figure 2.4 A, HU addition to the QC altered the mixing spectrum and led to a well-defined HU-edited spectrum, which is associated with quenching of the tyrosyl radical in the QC (see Scheme 2.2, part IV).

The HU-edited spectrum, acquired from a sample containing dATP, was found to be distinct (Figure 2.4 B), compared to the one acquired in the presence of ATP (Figure 2.4 A). An overall decrease in intensity was observed, consistent with the decreased rate of HU-mediated Y122O• reduction in the presence of dATP (Figure S3 A and D). Also, Figure 2.4 A and B were distinguishable from the HU-edited spectrum acquired from isolated β2 (Figure 2.4 C and Scheme 2.2, part I) under the same conditions as A. In Figure 2.4A, positive bands at 1643 and 1614 cm-1 may be attributable to the consumption of the substrate, CDP, which occurs in the ATP-containing sample, but does not occur in the dATP-containing control. Comparison to the spectrum of CDP in solution (Figure S5) shows that solution CDP does have overlapping contributions in this region. However, the frequencies are shifted and narrow, when compared to the solution spectrum, as expected if CDP is bound at the substrate binding site. These results are consistent with the expectation that CDP oxidation is redox-linked with Y122O•.[26] However, an amide I contribution in this region cannot be completely excluded.

2.4.9 HU-editing and isotopic labelling, amide bands.

The assignment of bands in the HU-edited spectrum was investigated by isotopic labeling (Figure S6). Global ^{13}C labeling of α2 (Figure 2.5 B) downshifted (expected Δ=46 cm^{-1}) a component of the 1685/1675 cm^{-1} bands (Figure 2.5 A, repeated from Figure 2.4 A) in the HU-edited spectrum. Global ^{13}C labeling of β2 also shifted vibrational bands, including the 1687, 1675, 1661, and 1653 cm^{-1} bands previously assigned to redox-linked changes at Y122 (amide) and D84 (asymmetric stretch, amide) in β2 (Figure 2.5 C). This result demonstrates that the effect of HU on Y122 and D84 structure is similar in the QC

and the isolated β2.[39, 46, 50] However, in the QC, HU reduction leads to secondary structural changes in α2. These HU-mediated structural changes are not dATP sensitive (Table 2.1).

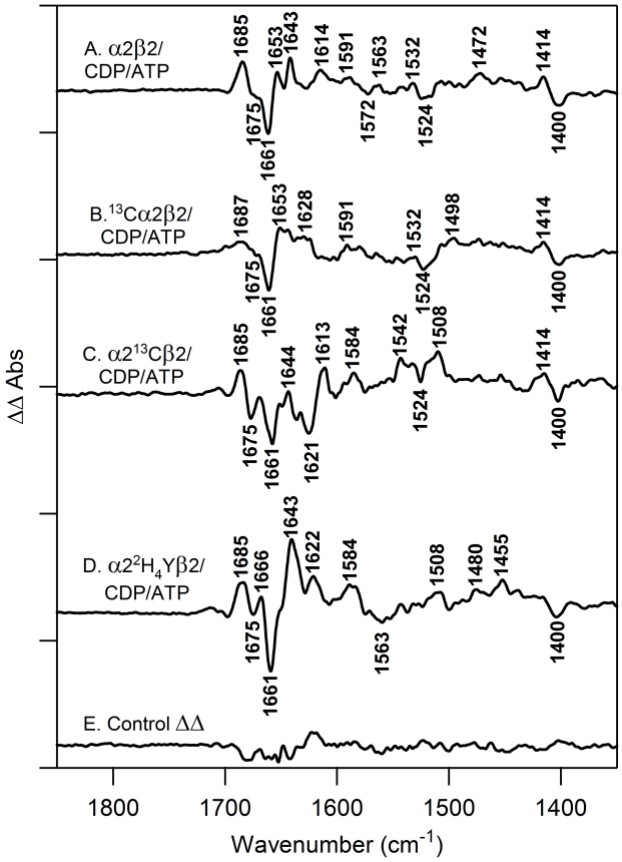

Figure 2.5 HU-edited, reaction-induced FT-IR spectra (HU-minus-no HU, Scheme 1, part III). Samples were (A) α2β2/CDP/ATP, (B) 13Cα2-β2/CDP/ATP, (C) α2-13Cβ2/CDP/ATP, and (D) α2-2H4Tyrβ2/CDP/ATP. (E) is a control double difference spectrum, generated by subtraction of ½ of the data in Figure 3 A from the other ½ and division by √2. Tick marks: 1 × 10^{-3} absorbance units. Averages: (A) 19, (B) 21, (C) 11, (D) 19, and (E) 10 separate samples. The temperature was 20°C.

2.4.10 HU-editing and isotopic labelling, tyrosine and tyrosyl radical bands.

To identify the β2 bands due to tyrosine in the HU-edited spectrum, HU-editing experiments were conducted on the $^{2}H_{4}$Yβ2 isotopic chimera (Figure 2.5 D). In this

spectrum, spectral changes are evident, which are accentuated by construction of an isotope-edited spectrum (Figure 2.6 A and Scheme 2.1, part IV). To appear in this spectrum, bands must be sensitive to incorporation of the isotopic label and reduction with HU. In $\alpha 2^{2}H_{4}Y\beta 2$/CDP/ATP (Figure 2.6 A), bands at (–) 1514 and (+) 1498 cm^{-1} were observed, similar to those observed in isolated β2 under the same conditions (Figure 2.6 B and Table 2.2). The isotope-shifted bands were observed at (+) 1436 and (–) 1480 cm^{-1} in isolated β2 (Figure 2.6 B). Previously, these bands have been assigned to the CO stretch (Y7a) of Y122O• and the ring stretch (Y19a) of Y122OH in the β2 subunit, based on DFT calculations and isotopic labeling.[39, 50] This result shows that the local environments of Y122O• and Y122OH are similar in isolated β2 and in the QC.

However, when Figure 2.6 A (QC) and Figure 2.6 B (isolated β2) were compared, the isotope-edited/HU edited spectra were distinct in the amide I region. We hypothesized that Figure 2.6 A reflects oxidation/reduction of Y122 and also a contribution from the β2 tyrosine, Y_x. To test this hypothesis, the Y122 contributions, measured in isolated β2 (Figure 2.6 B), were subtracted from the spectrum of the QC (Figure 2.6 A). This procedure generates Figure 2.6 C. The FT-IR spectra in Figure 2.6 A and B were normalized for Y122O• content, and the rate of Y122O• reduction was measured to be similar in the QC and in isolated β2 (Figure S3, D_2O buffers). Therefore, the Y122O• and Y122OH contributions are expected to subtract out in Figure 2.6 C. However, Figure 2.6 C still exhibits $^{2}H_{4}Y$ isotope-sensitive bands at (–) 1521, (+) 1501, (–) 1455/1436, and (+) 1414 cm^{-1}, assignable to natural abundance and $^{2}H_{4}$ labeled Y_x (Table 2.2). The 1501 cm^{-1} Y19a band is distinguishable from Y122• Y7a (CO) at 1498 cm^{-1}, because the ring stretching vibration, Y19a, is expected to exhibit a larger isotope-shift (Table 2.2).[39, 50]

Note that a similar set of bands, at 1521, 1501, 1455, and 1414 cm^{-1}, were also assigned to Y_x, based on mixing experiments (Figure S4C). In the mixing experiments, there was no detectable decay of Y122• over the time course of these experiments (Figure S3). Taken together, these data provide evidence that a second $\beta 2$ tyrosine, Y_x, is conformationally active in the QC.

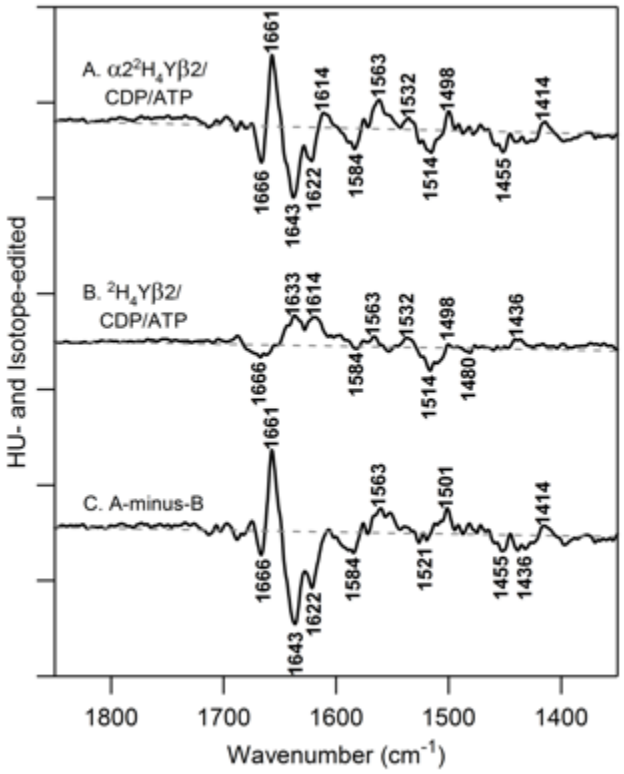

Figure 2.6 (A) Isotope-edited and HU-edited spectra of the isotopic chimera, α2-$^2H_4$Tyrβ2/CDP/ATP (Scheme 1, part IV). For comparison, the isotope-edited and HU-edited spectrum of isolated $^2H_4$Tyrβ2, under the conditions used in (A), is shown in (B). Data were derived from Figure 5 and S6, respectively, the conditions are described in those legends. The spectrum in (C) is the subtraction of the spectrum (A)-minus-(B). Tick marks: 5×10^{-4} absorbance units.

2.5 Discussion

2.5.1 Summary.

In biological systems, PCET processes can be gated by conformational changes.[69] Ribonucleotide reductase is an excellent model, in which conformational gating regulates the catalytic PCET events.[26, 36, 42] Also, RNR is subject to complex allosteric regulation, which is still not completely understood. There are relatively few ways to define the structure of inhibited and catalytic RNR complexes in solution.[11-12] Here, reaction-induced FT-IR spectroscopy was applied to define conformational motions in RNR that are linked to catalysis and to inhibition with HU and dATP.

2.5.2 Secondary structural changes accompany formation of the QC.

Our data indicate that mixing of α2 and β2 in the presence of ATP, CDP, and DTT alters hydrogen bonding and secondary structure both in α2 and β2. X-ray structures of α2 show three structural domains (Figure 2.1 C). The N-terminal, alpha helical dATP binding domain is a four-helix bundle that is capped with a small beta sheet. The other two domains are a central, 10-strand alpha/beta barrel, which contains the essential thiyl radical essential in a beta loop, and a smaller 5-strand alpha/beta barrel. The two active site cysteines that reduce substrate are found on adjacent beta strands to the beta loop. The specificity site is found at a four-helical bundle interface between the two α monomers. Allosteric control is mediated by changes in conformation in the flexible loops at the specificity site.[14]

2.5.3 Amide I bands at 1681, 1672, and 1643 cm^{-1} are dATP/ATP sensitive.

Our reaction-induced FT-IR spectra show that formation of the QC is associated with changes in the frequency and intensity of α2 and β2 amide I bands. From the frequencies, the observed amide I bands at 1681 and 1671 cm^{-1} (Table 2.1) were assignable to hydrogen bonding changes involving antiparallel and parallel beta strands.[57-62] A band at 1643 cm^{-1} was assigned to disordered secondary structural regions. The intensities of the 1681, 1671, and 1643 cm^{-1} bands were dependent on the presence of ATP, these bands were not observed when dATP is bound to the activity site. These ATP/dATP-sensitive bands are therefore assignable to a transition from a disordered to a beta strand domain, which accompanies formation and turnover in the QC. dATP binding is known to prevent formation of the active complex, to promote the formation of inactive oligomers, and to bind at the specificity site.[11-13] X-ray crystallography has shown that the structure of a loop (loop 2, see Figure 2.1 C) in the specificity domain is sensitive to occupancy at this binding site.[37, 70-71] The ATP/dATP-dependent 1681, 1671, and the α2 component of the 1643 cm^{-1} band can be accounted for by such a conformational change in loop 2. The intensity of the β2 amide band at 1643 cm^{-1} was also dATP/ATP sensitive. The β2 subunit is primarily alpha helical, but the carboxyl terminal domain, which binds to α2, is disordered and not resolved in X-ray structures.[16, 38] The loss of intensity in the 1643 cm^{-1} β2 band may reflect decrease in disorder in the QC, due to the formation of contacts between α2 and β2 in the QC. These data provide evidence for activity-induced, conformational rearrangements in the α2 and the β2 subunits.

2.5.4 Amide bands at 1691, 1661, and 1622 cm^{-1} are not dATP/ATP sensitive.

The 1691, 1661, and 1622 cm^{-1} bands may represent internal α2 and β2 hydrogen bonding changes associated with ATP/dATP binding or with CDP binding under reducing conditions.[13-14, 37]

2.5.5 Formation of the QC alters the frequency of dATP/ATP sensitive α2 and β2 carboxylate bands.

Our data identified isotope-sensitive bands at 1425, 1414, and 1400 cm^{-1} in α2, which are altered in frequency and intensity in the QC. These bands arise from the symmetric stretch of carboxylate side chains. Overlapping carboxylate bands at 1425 and 1414 cm^{-1} arise from β2 (Table 2.1). The intensities of these carboxylate bands were altered by dATP, suggesting that the environment of these carboxylates is modulated by formation of the QC and turnover. Therefore, these carboxylates may be located at the α2β2 interface. The β2 linker peptide, which interacts with α2 to form the α2β2 quaternary complex, includes one glutamate and four aspartate residues. α2 also contains carboxylate residues (including Asp: 227, 520, 608, 630, Glu: 224, 231, 281, 519, 524) that may be located at the α2β2 interface.[23]

2.5.6 The Y122 and D84 structural landscapes are similar in α2β2 and isolated β2.

Reaction-induced FT-IR spectra also monitored the HU reaction in the QC. HU reduces Y122O• in a PCET reaction, leading to vibrational bands from radical and singlet in the reaction-induced spectrum. The isotopic chimera, in which the β2 subunit was $^{2}H_{4}Y$ labeled, was employed to assign bands to β2 tyrosines. As in isolated β2, (Figure 2.6 B and ref [50]) the 1498 and 1514 cm^{-1} bands, which are characteristic of Y122O• (Y7a) and

Y122OH (Y19a), were observed with $^{2}H_{4}Y$ labeling (Table 2). The similarity of the frequencies suggests that hydrogen bonding environments of Y122O• and Y122OH are similar in isolated β2 and in the α2β2 complex. Bands at 1687 and 1675 cm^{-1} bands were observed in the β2 subunit after formation of the QC (Table 1). These bands were previously assigned to the asymmetric carboxylate stretching mode of β2 D84 by ^{13}C aspartate labeling in the isolated β2 subunit.[46] D84 is a unidentate ligand to the iron cluster and undergoes a coupled hydrogen bonding change when Y122O• is reduced. The frequency of the asymmetric stretching vibration is a marker for this hydrogen bonding change, which occurs in isolated β2[46] and also, as shown here, in the QC. In the QC, the D84 bands overlap with α2 bands, but the contributions can be evaluated separately in the $^{13}C\alpha2\beta2$ and $\alpha2^{13}C\beta2$ chimeras. Global ^{13}C labeling of β2 also reveals amide I bands (Table 2.1) previously assigned to D84, Y122O•, and Y122OH in isolated β2.[39, 46] When compared to density functional theory calculations, these data support a redox-linked conformational change from the A (singlet) to the B (radical) conformer of Y122 (see Figure 2.1B). Observation of these bands in the QC indicates that redox-driven structural changes at Y122 and D84 are relevant to catalysis.

2.5.7 In the QC, HU reduction alters secondary structure in α2.

In addition to changes in β2, HU reduction led to structural changes in α2, as assessed by the appearance of α2 1685/1675 cm^{-1} bands in the HU-edited spectrum of the QC (Table 2.1). These results demonstrate that the α2 subunit is conformationally malleable and responsive to the HU-mediated reduction of Y122O•.

2.5.8 Evidence for a conformationally active β2 tyrosine, Y_x.

Our data provide evidence that a second β2 tyrosine, termed Y_x, undergoes a structural change when the QC forms or when HU is used to reduce the QC. HU-editing and ^2H_4Y labeling of the β2 subunit led to the detection of these additional tyrosine bands at (–) 1521 and (+) 1501 cm^{-1} (Figure 2.6 C). These spectral features have a frequency and an isotope shift (Table 2.2) consistent with assignment to a tyrosinate ring stretching vibration, Y19a, in two different environments. Tyrosine ring vibrations are known to be altered in frequency by changes in side chain protonation and hydrogen bonding. For example, a model compound, tyrosine in solution, was reported to have a Y19a band at 1518 cm^{-1}, while tyrosinate had a Y19a band at 1499 cm^{-1}.[72] Thus, the (+) 1501 cm^{-1} band in Figure 2.6 C, may represent a tyrosinate species, Y_x^-, and the negative (–) 1521 cm^{-1} band arise from tyrosine, Y_x. The isotope-shifted bands are assigned with opposite sign at (–) 1455/1436 and (+) 1414 cm^{-1} (Figure 2.6 C, Table 2.2). Note that the another ring vibrational mode, Y8a, expected at ~1600 cm^{-1}, may be observable, but is expected to be much less intense compared to Y19a.[68, 72] Interestingly, ^2H_4Y labeling also altered the spectrum obtained after mixing α2 and β2 in the presence of ATP, CDP, and excess reductant (Figure 2.3 D) with no HU. Similar bands were observed at 1521, 1501, and 1414 cm^{-1} (Figure S4 C). This result provides support for the conclusion that a conformational change at Y_x is associated with formation of the QC. This conformational change may be a Y_x protonation reaction. One possible explanation is that the spectra reflect a protonation change at β2 Y356, which is known to be required for intersubunit PCET.[26] However, site-selective NO_2Y modification has shown that the pK_a of Y356 is not perturbed in the QC or in isolated β2.[30, 73] Alternatively, more modest shifts in Y19a frequency have been associated with changes in hydrophobicity in the RAS protein.[74] The

sign of the Y_x bands is of interest. In the experiment described in Scheme 2.2, part II, i.e., mixing to form the QC, the 1521 cm^{-1} band is positive and the 1501 cm^{-1} band is negative (Figure S4C). This sign change is consistent with an increase in hydrophobicity or a protonation of Y_x, when the QC at t_1 (Scheme 2.1, part I) is compared to the sample after the consumption of substrate (t_2). In this experiment, one isotope-shifted band at 1455 cm^{-1} is observed. In the isotope-edited and HU-edited spectrum (Scheme 2.2, part IV, HU-minus-no HU), the signs of the 1521 and 1501 cm^{-1} bands were reversed, as expected if the conformational change occurs in the QC. Interesting, two putative isotope-shifted bands were observed at 1455 and 1436 cm^{-1} (Figure 6 C, Scheme 2.1, part IV). The origin and assignment of Y_x bands will be investigated in future studies.

2.5.9 HU-editing and ^2H_4Y tyrosine labeling reveals complexity in the amide I region of the QC.

^2H_4Y isotope- and HU-editing in the QC led to a change in the amide I region, when the spectra were compared to data acquired from $^2H_4Y\beta2$ alone. Side chain labeling can alter amide frequencies if the vibrational motions are similar in frequency and coupled.[46] For example, ^2H_4Y sensitive amide I bands were observed in photosystem II (PSII), which contains two redox-active tyrosines. Reaction-induced FT-IR spectra, collected for the redox active tyrosine, YZ, revealed amide I contributions that were shifted by tyrosine ring labeling.[75] The ^2H_4Y-sensitive bands were attributed to redox-linked backbone dynamics,[75] which may also occur for Y_x .This suggestion that Y_x is conformationally flexible in the QC may be consistent with an assignment to Y356 in β2. Y356 is located in a C-terminal domain of β2 that is not resolved in the crystal structure.[16, 38] This C-terminal domain interacts with the α2 subunit.[76] Recently, it was shown that Y356 has a relative redox

potential, which is (~100 mV) lower than the active site cysteine in α2.[35] Thus, a forward electron transfer, mediated by Y356, is thermodynamically uphill and likely to be conformationally gated.[30]

2.5.10 Inhibitors of RNR, HU and dATP.

In this paper, experiments employed the RNR inhibitors, HU and dATP. HU is a clinically-relevant anti-cancer and anti-viral treatment.[77] In *E. coli*, HU reduces Y122O•, but retains the differic cluster. Kinetic experiments show no saturation of HU on the reaction, suggesting HU has no specific interaction with β2.[63] However, a mutation at a β2 surface residue near Y122 generates HU resistance, supporting direct electron transfer.[78] Consistent with this, the HU reaction in isolated β2 is associated with a large solvent isotope effect.[39] In the quaternary complex, HU-mediated Y122O• reduction is 10-fold faster compared to the rate in isolated β2.[64] It was hypothesized that HU participates in multiple reduction pathways, one of which is the physiologically-relevant PCET pathway.[79] Our results agree with this suggestion, because the HU reduction pathway in the QC involves a secondary structure change in α2, as well as secondary structural changes in β2. In *E. coli* class Ia RNR, dATP is a reversible inhibitor that modulates the overall activity of the enzyme by interaction with the N-terminal activity site. X-ray structures of a α2-AMPPNP complex showed no significant changes associated with binding of this compound to the activity site.[37] However, dATP also binds to the specificity site, which contains a conformationally flexible loop region.[80] The structure of this loop is specific to the bound effector.[70] In our reaction-induced FT-IR spectra, ATP promoted secondary structural changes in α2, which were inhibited by dATP. The frequencies and

signs were consistent with a change from beta sheet (initial state, QC) to disordered structure (final, substrate consumed state). dATP inhibits this conformational change, mostly likely caused by binding interactions at the specificity sites. X-ray structural data have provided evidence for a loop 2 structural change when the effectors, dTTP, dATP, and dGTP, are bound to the specificity site. In class II α2, loop 2 is disordered until deoxynucleotide binding induces ordering and alters main chain interactions.[14, 70, 80] This pattern of allosteric control also occurs in the class Ia enzymes.[13, 80] The reaction-induced FT-IR technique provides a novel way to monitor these conformational rearrangements in the QC.

2.6 Conclusions

Proteins exhibit conformational motions on multiple timescales, this dynamic landscape facilitates catalysis and provide opportunities to design specific inhibitors.[81-84] NMR describes these motions, but this technique is typically limited to small, diamagnetic proteins. FT-IR spectroscopy can be applied to large, complex proteins and provides high signal-to-noise, which allows spectral assignment at single amino acid resolution. This method is facilitated by the use of isotope-edited spectra in which spectral assignments are based on specific isotopic labeling. Reaction-induced FT-IR spectroscopy provides an incisive, new method to describe the RNR structural landscape.

2.7 Acknowledgements

The authors thank Prof. J. Stubbe and Dr. E. Minnihan for the α2 plasmid, some of the reagents used in the activity measurements, and helpful discussions. We also thank Prof. J. Soper for use of the temperature-controlled Cary UV spectrophotometer.

ASSOCIATED CONTENT

Supporting Information. Additional experimental data including SDS-PAGE (Figure S1), reaction-induced FT-IR spectra (Figure S2 and Figure S6), UV kinetic measurements (Figure S3), isotope-edited FT-IR spectra (Figure S4), and FT-IR absorption spectra (Figure S5). This material is available free of charge via the Internet at http://pubs.acs.org.

2.8 References

1. Stubbe, J., Nocera, D. G., Yee, C. S., and Chang, M. C. Y. Radical Initiation in the Class I Ribonucleotide Reductase: Long-Range Proton-Coupled Electron Transfer? *Chemical Reviews* **2003**, *103*, 2167–2201.
2. Jordan, A., and Reichard, P. Ribonucleotide Reductases. *Annual Reviews of Biochemistry* **1998**, *67*, 71–98.
3. Shao, J., Liu, X., Zhu, L., and Yen, Y. Targeting Ribonucleotide Reductase for Cancer Therapy. *Expert. Opin. Ther. Targets* **2013**, *17*, 1423–1437.
4. Shao, J., Zhou, B., Chu, B., and Yen, Y. Ribonucleotide Reductase Inhibitors and Future Drug Design. *Current Cancer Drug Targets* **2006**, *6*, 409–431.
5. Stubbe, J., and Van der Donk, W. A. Ribonucleotide Reductases: Radical Enzymes with Suicidal Tendencies. *Chemical Biology* **1995**, *2*, 793–801.
6. Stubbe, J. Ribonucleotide Reductases: Amazing and Confusing. *J. Biol. Chem.* **1990**, *265*, 5329–5332.
7. Stubbe, J., and van der Donk, W. A. Protein Radicals in Enzyme Catalysis. *Chem. Rev.* **1998**, *98*, 705–762.
8. Contruvo, J. A., Jr., and Stubbe, J. Class I Ribonucleotide Reductases: Metallocofactor Assembly and Repair *In Vitro* and *In Vivo*. *Annu. Rev. Biochem.* **2011**, *80*, 733–767.
9. Tomter, A. B., Zoppellaro, G., Andersen, N. H., Haersleth, H.-P., Hammerstad, M., Røhr, Å. K., Sandvik, G. K., Strand, K. R., Nilsson, G. E., Bell, C. B., III, Barra, A.-L., Blasco, E., Le Pape, L., Solomon, E. I., and Andersson, K. K. Ribonucleotide Reducase Class I with Different Radical Generating Clusters. *Coord. Chem. Rev.* **2013**, *257*, 3–26.
10. Larsson, A., and Reichard, P. Enzyme Synthesis of Deoxyribonucleotides IX. Allosteric Effects in the Reduction of Pyrimidine Ribonucleotides by the Ribonucleoside Diphosphate Reductase System of *Escherichia coli*. *J. Biol. Chem.* **1966**, *241*, 2533–2539.
11. Rofougaran, R., Crona, M., Vodnala, M., Sjöberg, B.-M., and Hofer, A. Oligomerization Status Directs Overall Activity Regulation of the *Escherichia coli* Class Ia Ribonucleotide Reductase. *J. Biol. Chem.* **2008**, *283*, 35310-35318.
12. Ando, N., Bringnole, E. J., Zimanyi, C. M., Funk, M. A., Yokoyama, K., Asturias, F. J., Stubbe, J., and Drennan, C. L. Structural Interconversions Modulate Activity of *Escherichia coli* Ribonucleotide Reductase *Proc. Natl. Acad. Sci. U.S.A.* **2011**, *108*, 21046–21051.

13. Zimanyi, C. M., Ando, N., Brignole, E. J., Asturias, F. J., Stubbe, J., and Drennan, C. L. Tangled Up in Knots: Structures of Inactivated Forms of *E. coli* Class Ia Ribonucleotide Reductase. *Structure* **2012**, *20*, 1374–1383.
14. Reichard, P. Ribonucleotide Reductases: Substrate Specificity by Allostery. *Biochem. Biophys. Res. Commun.* **2010**, *396*, 19–23.
15. Sjöberg, B.-M., Reichard, P., Gräslund, A., and Ehrenberg, A. The Tyrosine Free Radical in Ribonucleotide Reductase from *Escherichia coli*. *J. Biol. Chem.* **1978**, *253*, 6863–6865.
16. Nordlund, P., Sjöberg, B.-M., and Eklund, H. Three Dimensional Structure of the Free Radical Protein of Ribonucleotide Reductase. *Nature* **1990**, *345*, 593–598.
17. Nordlund, P., and Eklund, H. Structure and Function of the *Escherichia coli* Ribonucleotide Reductase. *J. Mol. Biol.* **1993**, *232*, 123–164.
18. Stubbe, J., and Riggs-Gelasco, P. Harnessing Free Radicals: Formation and Function of the Tyrosyl Radical in Ribonucleotide Reductase. *Trends Biochem. Sci.* **1998**, *23*, 438–443.
19. Atkin, C. L., Thelander, L., and Reichard, P. Iron and Free Radical in Ribonucleotide Reductase. Exchange of Iron and Mössbauer Spectroscopy of the Protein B2 Subunit of the *Escherichia coli* Enzyme. *J. Biol. Chem.* **1973**, *248*, 7464–7472.
20. Larsson, Å., and Sjöberg, B.-M. Identification of the Stable Free Radical Tyrosine Residue in Ribonucleotide Reductase. *Embo J.* **1986**, *5*, 2037–2040.
21. Bollinger, J. M., Jr., Edmondson, D. E., Huynh, B. H., Filley, J., Norton, J. R., and Stubbe, J. Mechanism of Assembly of the Tyrosyl Radical-Dinuclear Iron Cluster Cofactor of Ribonucleotide Reductase. *Science* **1991**, *253*, 292–298.
22. Minnihan, E. C., Ando, N., Brignole, E. J., Olshansky, L., Chittuluru, J., Asturias, F. J., Drennan, C. L., Nocera, D. G., and Stubbe, J. Generation of a Stable, Aminotyrosyl Radical-Induced a2b2 Complex of *Escherichia coli* Class Ia Ribonucleotide Reductase. *Proc. Natl. Acad. Sci. U.S.A.* **2013**, *110*, 3835–3840.
23. Uhlin, U., and Eklund, H. Structure of Ribonucleotide Reductase Protein R1. *Nature* **1994**, *370*, 533–539.
24. Bennati, M., Robblee, J. H., Mugnaini, V., Stubbe, J., Freed, J. H., and Borbat, P. EPR Distance Measurements Support a Model for Long-Range Radical Initiation in *E. coli* Ribonucleotide Reductase. *J. Am. Chem. Soc.* **2005**, *127*, 15014–15015.
25. Seyedsayamdost, M. R., Chan, C. T. Y., Mugnaini, V., Stubbe, J., and Bennati, M. PELDOR Spectroscopy with DOPA-β2 and NH_2Y-α2s: Distance Measurements between Residues Involved in the Radical Propagation Pathway of *E. coli* Ribonucleotide Reductase. *J. Am. Chem. Soc.* **2007**, *129*, 15748–15749.
26. Minnihan, E. C., Nocera, D. G., and Stubbe, J. Reversible, Long-Range Radical Transfer in *E. coli* Class Ia Ribonucleotide Reductase. *Acc. Chem. Res.* **2013**, *46*, 2524–2535.
27. Rova, U., Goodtzova, K., Ingemarson, R., Behravan, G., Gräslund, A., and Thelander, L. Evidence by Site-Directed Mutagenesis Supports Long-Range Electron Transfer in Mouse Ribonucleotide Reductase. *Biochemistry* **1995**, *34*, 4267–4275.
28. Ekberg, M., Sahlin, M., Eriksson, M., and Sjöberg, B.-M. Two Conserved Tyrosine Residues in Protein R1 Participate in an Intermolecular Electron Transfer in Ribonucleotide Reductase. *J. Biol. Chem.* **1996**, *271*, 20655–20659.

29. Rova, U., Adrait, A., Pötsch, S., Gräslund, A., and Thelander, L. Evidence by Mutagenesis that Tyr370 of the Mouse Ribonucleotide Reductase R2 Protein is the Connecting Link in the Intersubunit Radical Transfer Pathway. *J. Biol. Chem.* **1999**, *274*, 23746–23751.
30. Yee, C. S., Chang, M. C. Y., Ge, J., Nocera, D. G., and Stubbe, J. 2,3-Difluorotyrosine at Position 356 of Ribonucleotide Reductase R2: A Probe of Long-Range Proton-Coupled Electron Transfer. *J. Am. Chem. Soc.* **2003**, *125*, 10506–10507.
31. Seyedsayamdost, M. R., Reece, S. Y., Nocera, D. G., and Stubbe, J. Mono-, Di-, Tri-, and Tetra-Substituted Fluorotyrosines: New Probes for Enzymes that Use Tyrosyl Radicals in Catalysis. *J. Am. Chem. Soc.* **2006**, *128*, 1569–1579.
32. Seyedsayamdost, M. R., Yee, C. S., Reece, S. R., Nocera, D. G., and Stubbe, J. pH Profiles of FnY356-R2s (n =2,3,4) in *Escherichia coli* Ribonucleotide Reductase: Evidence that Y356 is a Redox-Active Amino Acid Along the Radical Propagation Pathway. *J. Am. Chem. Soc.* **2006**, *128*, 1562–1568.
33. Seyedsayamdost, M. R., Xie, J., Chan, C. T. Y., Schultz, P. G., and Stubbe, J. Site-Specific Insertion of 3-Aminotyrosine into Subunit a2 of *E. coli* Ribonucleotide Reductase: Direct Evidence for Involvement of Y730 and Y731 in Radical Propagation. *J. Am. Chem. Soc.* **2007**, *129*, 15060–15071.
34. Minnihan, E. C., Seyedsayamdost, M. R., Uhlin, U., and Stubbe, J. Kinetics of Radical Intermediate Formation and Deoxynucleotide Production in 3-Aminotyrosine-Substituted *Escherichia coli* Ribonucleotide Reductases. *J. Am. Chem. Soc.* **2011**, *133*, 9430–9440.
35. Yokoyama, K., Smith, A. A., Corzilius, B., Griffin, R. G., and Stubbe, J. Equilibration of Tyrosyl Radicals (Y356•, Y731•, Y730•) in the Radical Propagation Pathway of the *Escherichia coli* Class Ia Ribonucleotide Reductase. *J. Am. Chem. Soc.* **2011**, *133*, 18420–18432.
36. Ge, J., Yu, G., Ator, M. A., and Stubbe, J. Pre-Steady-State and Steady-State Kinetic Analysis of *E. coli* Class I Ribonucleotide Reductase. *Biochemistry* **2003**, *42*, 10071–10083.
37. Han, W.-G., and Noodleman, L. DFT Calculations for Intermediate and Active States of the Diiron Center with a Tryptophan or Tyrosine Radical in *Escherichia coli* Ribonucleotide Reductase. *Inorg. Chem.* **2011**, *50*, 2302–2320.
38. Wörsdörfer, B., Conner, D. A., Yokoyama, K., Livada, J., Seyedsayamdost, M. R., Jiang, W., Silakov, A., Stubbe, J., Bollinger, J. M., Jr., and Krebs, C. Function of the Diiron Cluster of *Escherichia coli* Class Ia Ribonucleotide Reductase in Proton-Coupled Electron Transfer. *J. Am. Chem. Soc.* **2013**, *135*, 8585–8593.
39. Yokoyama, K., Uhlin, U., and Stubbe, J. A Hot Oxidant, 3-NO_2Y122 Radical, Unmasks Conformational Gating in Ribonucleotide Reductase. *J. Am. Chem. Soc.* **2010**, *132*, 15368–15379.
40. Högbom, M., Galander, M., Andersson, M., Kolberg, M., Hofbauer, W., Lassmann, G., Nordlund, P., and Lendzian, F. Displacement of the Tyrosyl Radical Cofactor in Ribonucleotide Reductase Obtained by Single-Crystal High-Field EPR and 1.4-Å X-Ray Data *Proc. Natl. Acad. Sci. U.S.A.* **2003**, *100*, 3209–3214.
41. Backes, G., Sahlin, M., Sjöberg, B.-M., Loehr, T. M., and Sanders-Loehr, J. Resonance Raman Spectroscopy of Ribonucleotide Reductase. Evidence for a

Deprotonated Tyrosyl Radical and Photochemistry of the Binuclear Iron Center. *Biochemistry* **1989**, *28*, 1923–1929.
42. Bender, C. J., Sahlin, M., Babcock, G. T., Barry, B. A., Chandrashekar, T. K., Salowe, S. P., Stubbe, J., Lindstroem, B., and Petersson, L. An ENDOR Study of the Tyrosyl Free Radical in Ribonucleotide Reductase from *Escherichia coli*. *J. Am. Chem. Soc.* **1989**, *111*, 8076–8083.
43. Barry, B. A., Chen, J., Keough, J., Jenson, D. L., Offenbacher, A. R., and Pagba, C. Proton-Coupled Electron Transfer and Redox-Active Tyrosines: Structure and Function of the Tyrosyl Radicals in Ribonucleotide Reductase and Photosystem II. *J. Phys. Chem. Lett.* **2012**, *3*, 543–554.
44. Offenbacher, A. R., Burns, L. A., Sherrill, C. D., and Barry, B. A. Redox-Linked Conformational Control of Proton-Coupled Electron Transfer: Y122 in the Ribonucleotide Reductase β2 Subunit. *J. Phys. Chem. B* **2013**, *117*, 8457–8468.
45. Offenbacher, A. R., Minnihan, E. C., Stubbe, J., and Barry, B. A. Redox-Linked Changes to the Hydrogen-Bonding Network of Ribonucleotide Reductase β2. *J. Am. Chem. Soc.* **2013**, *135*, 6380–6383.
46. Vogel, R., and Siebert, F. Vibrational Spectroscopy as a Tool for Probing Protein Function. *Curr. Opin. Chem. Biol.* **2000**, *4*, 518–523.
47. Kötting, C., and Gerwert, K. Proteins in Action Monitored by Time-Resolved FT-IR Spectroscopy. *ChemPhysChem* **2005**, *6*, 881–888.
48. Siebert, F., and Hildebrandt, P. *Vibrational Spectroscopy in Life Science*, Wiley-VCH: Weinheim, 2008.
49. Offenbacher, A. R., Vassiliev, I. R., Seyedsayamdost, M. R., Stubbe, J., and Barry, B. A. Redox-Linked Structural Changes in Ribonucleotide Reductase. *J. Am. Chem. Soc.* **2009**, *131*, 7496–7497.
50. Salowe, S. P., and Stubbe, J. Cloning, Overproduction, and Purification of the B2 Subunit of Ribonucleoside-Diphosphate Reductase. *J. Bacteriol.* **1986**, *165*, 363–366.
51. Hutchison, R. S., Betts, S. D., Yocum, C. F., and Barry, B. A. Conformational Changes in the Extrinsic manganese Stabilizing Protein Can Occur upon Binding to the Photosystem II Reaction Center: An Isotope Editing and FT-IR Study. *Biochemistry* **1998**, *37*, 5643–5653.
52. Thelander, L. Physicochemical Characterization of Ribonucleoside Diphosphate Reductase from *Escherichia coli*. *J. Biol. Chem.* **1973**, *248*, 4591–4601.
53. Bollinger, J. M., Jr., Hangtong, W., Ravi, N., Huynh, B. H., Edmondson, D., and Stubbe, J. Use of Rapid Kinetics Methods to Study the Assembly of the Diferric-Tyrosyl Radical Cofactor of *E. coli* Ribonucleotide Reductase. *Methods Enzymol.* **1995**, *258*, 278–303.
54. Schowen, K. B., and Schowen, R. L. Solvent Isotope Effects on Enzyme Systems. *Methods Enzymol.* **1982**, *87*, 551–606.
55. Jenson, D. L., and Barry, B. A. Proton-Coupled Electron Transfer in Photosystem II: Proton Inventory of a Redox Active Tyrosine. *J. Am. Chem. Soc.* **2009**, *131*, 10567–10573.
56. Miyazawa, T., and Blout, E. R. The Infrared Spectra of Polypeptides in Various Conformations : Amide I and II Bands. *J. Am. Chem. Soc.* **1961**, *83*, 712–719.
57. Blyer, D. M., and Susi, H. Examination of the Secondary Structure of Proteins by Deconvoluted FTIR Spectra. *Biopolymers* **1986**, *25*, 469–487.

58. Krimm, S., and Bandekar, J. Vibrational Spectroscopy and Conformation of Peptides, Polypeptides, and Proteins. *Adv. Protein Chem.* **1986**, *38*, 181–364.
59. Surewicz, W. K., Mantsch, H. H., and Chapman, D. Determination of Protein Secondary Structure by Fourier Transform Infrared Spectroscopy: A Critical Assessment. *Biochemistry* **1993**, *32*, 389–394.
60. Barth, A. Infrared Spectroscopy of Proteins. *Biochim. Biophys. Acta* **2007**, *1767*, 1073–1101.
61. Korkmaz-Özkan, F., Köster, S., Kühlbrandt, W., Mäntele, W., and Yildiz, Ö. Correlation between the OmpG Secondary Structure and Its pH-Dependent Alterations Monitored by FTIR. *J. Mol. Biol.* **2010**, *410*, 56–67.
62. Eriksson, M., Uhlin, U., S., R., Ekberg, M., Rengström, K., Sjöberg, B.-M., and Eklund, H. Binding of Allosteric Effectors to Ribonucleotide Reductase Protein R1: Reduction of Active-Site Cysteines Promotes Substrate Binding. *Structure* **1997**, *5*, 1077–1092.
63. Lassmann, G., Thelander, L., and Gräslund, A. EPR Stopped-Flow Studies of the Reaction of the Tyrosyl Radical of Protein R2 from Ribonucleotide Reductase with Hydroxyurea. *Biochem. Biophys. Res. Commun.* **1992**, *188*, 879–887.
64. Karlsson, M., Sahlin, M., and Sjöberg, B.-M. *Escherichia coli* Ribonucleotide Reductase. Radical Susceptibility to Hydroxyurea is Dependent on the Regulatory State of the Enzyme. *J. Biol. Chem.* **1992**, *267*, 12622–12626.
65. Hutchison, R. S., Steenhuis, J. J., Yocum, C. F., Razeghifard, M. R., and Barry, B. A. Deprotonation of the 33-kDa, Extrinsic, Manganese-stabilizing Subunit Accompanies Photooxidation of Manganese in Photosystem II. *J. Biol. Chem.* **1999**, *274*, 31987–31995.
66. Brauner, J. W., Dugan, C., and Mendelsohn, R. ^{13}C Isotope Labeling of Hydrophobic Peptides. Origin of the Anomalous Intensity Distribution in the Infrared Amide I Spectral Region of Beta-Sheet Structures. *J. Am. Chem. Soc.* **2000**, *122*, 677–683.
67. Iwata, T., Zhange, Y., Hitomi, K., Getzoff, E. D., and Kandori, H. Key Dynamics of Conserved Asparagine in a Cryptochrome/Photolyase Family Protein by Fourier Transform Infrared Spectroscopy. *Biochemistry* **2010**, *49*, 8882–8891.
68. Range, K., Ayala, I., York, D., and Barry, B. A. Normal Modes of Redox-Active Tyrosine: Conformation Dependence and Comparison to Experiment. *J. Phys. Chem. B* **2006**, *110*, 10970–10981.
69. Davidson, V. L. Protein Control of True, Gated, and Coupled Electron Transfer Reactions. *Acc. Chem. Res.* **2008**, *41*, 730–738.
70. Larsson, K.-M., Jordan, A., Eliasson, R., Reichard, P., Logan, D. T., and Nordlund, P. Structural Mechanism of Allosteric Substrate Specificity Regulation in a Ribonucleotide Reductase. *Nat. Struct. Mol. Biol.* **2004**, *11*, 1142–1149.
71. Xu, H., Faber, C., Uchiki, T., Fariman, J. W., Racca, J., and Dealwis, C. Structures of Eukaryotic Ribonucleotide Reductase I Provide Insights into dNTP Regulation. *Proc. Natl. Acad. Sci. U.S.A.* **2006**, *103*, 4022–4027.
72. Hellwig, P., Pfitzner, U., Behr, J., Rost, B., Pesavento, R. P., v. Donk, W., Gennis, R. B., Michel, H., Ludwig, B., and Mäntele, W. Vibrational Modes of Tyrosines in Cytochrome c Oxidase from *Paracoccus denitrificans*: FTIR and Electrochemical Studies on Tyr-D_4-labeled and on Tyr280His and Tyr35Phe Mutant Enzymes. *Biochemistry* **2002**, *41*, 9116–9125.

73. Yokoyama, K., Uhlin, U., and Stubbe, J. Site-Specific Incorporation of 3-Nitrotyrosine as a Probe of pKa Perturbation of Redox-Active Tyrosines in Ribonucleotide Reductase. *J. Am. Chem. Soc.* **2010**, *132*, 8385–8397
74. Warscheid, B., Brucker, S., Kallenbach, A., Meyer, H. E., Gerwert, K., and Kötting, C. Systematic Approach to Group-Specific Isotopic Labeling of Proteins for Vibrational Spectroscopy. *Vib. Spectrosc.* **2008**, *48*, 28–36.
75. Pujols-Ayala, I., Sacksteder, C. A., and Barry, B. A. Redox-Active Tyrosine Residues: Role for the Peptide Bond in Electron Transfer. *J. Am. Chem. Soc.* **2003**, *125*, 7536–7538.
76. Zhang, Y., An, X., Stubbe, J., and Huang, M. Investigation of *In Vivo* Roles of the C-terminal Tails of the Small Subunit (ββ′) of *Saccharomyces cerevisiae* Ribonucleotide Reductase. Contribution to Cofactor Formation and Intersubunit Assocation within the Active Holoenzyme. *J. Biol. Chem.* **2013**, *288*, 13951–13959.
77. Saban, N., and Bujak, M. Hydroxyurea and Hydroxamic Acid Derivatives as Antitumor Drugs. *Cancer Chemother. Pharmacol.* **2009**, *64*, 213–221.

78. Sneeden, J. L., and Loeb, L. A. Mutations in the R2 Subunit of Ribonucleotide Reductase that Confer Resistance to Hydroxyurea. *J. Biol. Chem.* **2004**, *279*, 40723–40728.
79. Jiang, W., Xie, J., Varano, P. T., Krebs, C., and Bollinger, J. M., Jr. Two Distinct Mechanisms of Inactivation of the Class Ic Ribonucleotide Reductase from *Chlamydia trachomatis* by Hydroxyurea: Implications for the Protein Gating of Intersubunit Electron Transfer. *Biochemistry* **2010**, *49*, 5340–5349.
80. Nordlund, P., and Reichard, P. Ribonucleotide Reductases. *Annu. Rev. Biochem.* **2006**, *75*, 681–706.
81. Boehr, D. D., McElheny, D., Dyson, H. J., and Wright, P. E. The Dynamic Energy Landscape of Dihydrofolate Reductase Catalysis. *Science* **2006**, *313*, 1638–1642.
82. Henzler-Wildman, K. A., Thai, V., Lei, M., Wolf-Watz, M., Fenn, T., Pozharski, E., Wilson, M. A., Petsko, G. A., Karplus, M., Hübner, C. G., and Kern, D. Intrinsic Motions Along an Enzymatic Reaction Trajectory. *Nature* **2007**, *450*, 838–844.
83. Masterson, L. R., Shi, L., Metcalfe, E., Gao, J., Taylor, S. S., and Veglia, G. Dynamically Committed, Uncommitted, and Quenched States Encoded in Protein Kinase A Revealed by NMR Spectroscopy. *Proc. Natl. Acad. Sci. U.S.A.* **2011**, *108*, 6969–6974.
84. Shittier, S. K., Hengge, A. C., and Loria, J. P. Conformational Motions Regulate Phosphoryl Transfer in Related Protein Tyrosine Phosphatases. *Science* **2013**, *341*, 899–903.

Overall work contributed to this project includes the overexpression of both the α2 and β2 subunits involved in all experiments. This work involves the expression of the natural abundance as well as the isotope labeled samples. I was also responsible for the purification of each subunit involving column chromatography procedures discussed in the text. I was further involved in the discussion of experimental FT-IR spectroscopy results obtained with these purified samples.

CHAPTER 3. INVESTIGATION OF STRUCTURAL BINDING INTERACTIONS IN *E. COLI* RIBONUCLEOTIDE REDUCTASE

3.1 Abstract

Ribonucleotide reductase (RNR) is a multiple subunit enzyme solely responsible for the production the deoxyribonucleotides from the corresponding ribonucleotides required for both DNA replication and repair. RNR supplies cellular deoxynucleotide triphosphate (dNTP) pools by using a stable radical cofactor to convert nucleotides to deoxynucelotides.[1-3] Class Ia RNR consists of homodimeric α2β2 active complex.[4] The β2 subunit contains a stable Y122O• differic cofactor.[5-7] Long-range proton-coupled electron transfer generates a transient C439• located 35Å away in the active site of the functional α2β2 complex.[3, 8-10] The conformational effects related to substrate (CDP/UDP) and effector (ATP/TTP) binding to the active and specificity sites, respectively, are studied by reaction-induced FT-IR difference spectroscopy. Hydroxyurea (HU) and Fe(II)-Triapine (Fe(II)-3AP) are two radical scavengers that inhibit α2β2 by quenching the tyrosyl radical. Investigation of the reduction mechanism by HU and Fe(II)-3AP describe the conformational changes associated with the inhibited enzyme complex. Previously, we identified an aspartate 84 contribution is observed with HU inhibition.[11-12] This assignment was further investigated using a potent inhibitor, Fe(II)-3AP. Conformational rearrangements that take place during catalysis mask the radical chemistry from direct observation. Radical trap 2′-azido-2′-deoxyuridine 5′-diphosphate (AzUDP) isolates the radical in the active site near C439 and prevents reformation of the resting state Y122O•. Conformational changes associated with the radical "hole" being propagated to the active

site can be seen for the first time. Amide I (C=O) and II (CN/NH) bands were observed as well as the previously identified Asp84 during inhibition. The addition of the effector ATP resulted in the appearance of bands 1872 and 1040 cm^{-1}, likely due to increased interactions between the substrate binding in the specificity site and the induced conformational response by nearby protein backbone. This ordered structure is not observed upon incubation with the effector TTP. Under HU inhibition a band at 1687 cm^{-1} was previously assigned to D84 hydrogen bond formation with Y122OH. However, upon inhibition by Fe(II)-3AP this band is no longer present, but displays negative features seen at 1633 and 1624 cm^{-1}. Spectral similarities are observed between AzUDP-inhibited and HU-inhibited complexes. Contributions at 1687, 1657, and 1649 cm^{-1} which have been previously assigned as D84 amide I vibrational modes in isolated β2 have never been seen in AzUDP-inhibited α2β2. RIFT-IR difference spectroscopy exposes how the inhibitors HU and Fe(II)-3AP interact with the active α2β2 complex in different methods to accomplish the indistinguishable radical quenching in isolated β2. The distinctive inhibitor, AzUDP, induces structurally significant rearrangements due to radical generation in the active site resulting in the formation of a hydrogen bond between Y122OH and D84 and deconvolutes conformational masking.

3.2 Introduction

In all organisms, ribonucleotide reductase (RNR) drives the production of deoxynucleotides by using a diiron metallo-cofactor and molecular oxygen to generate a stable radical species. RNR is the enzyme responsible for preserving the proper ratios of dNTP reservoirs for DNA synthesis and repair.[13-15] If these cellular concentrations were to become imbalanced, the fidelity of DNA decreases leading to point mutations and

ultimately genomic instability.[16] Due to its necessity for cell replication, the over production of RNR in cancerous tissue has characterized it as a key target for chemotherapeutics.[17] In its active form, RNR is composed of two homodimers, α2 and β2 (Figure 3.1). The α2 can be separated into two domains. The N-terminal-domain of the α2 subunit contains the activity site, a site of allosteric regulation.[18-19] The catalytic body encompasses a different site of allosteric regulation, the specificity site, and the catalytic active site. The allosteric sites tightly synchronize RNR activity.[20] Adenosine triphosphate (ATP) binding to the activity site induces conformational changes and increases RNR production. Comparatively, when dATP binds to the N-terminal-domain an overall decrease in activity is observed. The binding of distinct effectors to the specificity site triggers unique conformational responses from loops 1, 2, and 3 and results in the binding of CDP, UDP, GDP, and ADP substrates for reduction.[21-22] Catalysis in α2 is driven by the binding of substrate and effectors leading to the formation of the QC.[23-24]

Class Ia RNRs are comprised of human and *E. coli* RNRs and contain fundamental amino acids necessary for radical initiation. *In vitro*, *E. coli* RNR retains the β2's ability to store the radical at Y122 (*E. coli*) until turnover is initiated by allosteric regulation. A conserved radical transfer pathway between the active site and the radical generation site is required in both human and *E. coli* RNR. The conformational changes in the *E. coli* α and β subunits during catalysis and inhibition will be explored.

These studies are conducted using *E. coli* RNR as a model RNR. Identifying how the α subunit responds to substrate and effector binding will uncover a discernable and detectable conformational response from if ATP is bound in the specificity site versus if TTP is bound. The diferric cluster, molecular oxygen, and a conserved tyrosine residue,

Y122 in the β2 subunit (Figure 3.1 B) are necessary to generate the radical responsible for nucleotide reduction. However, nucleotide reduction takes place 35 Å away from where the radical is generated. Production of dNTPs is carried out in the active site of the larger α2 subunit.[3-4, 25-26] Various forms of cancer and other oxidative stress related diseases have all been linked to free radical production in the body.[27-29] Free radicals form naturally from biological processes and rigorous exercise,[5, 30-31] as well as being induced by commonly used house hold chemicals[32] and global pollution.[33] However, formation of high concentrations of free radicals can cause a cascade that can produce cellular damage, ultimately leading to genomic instability if antioxidants are not present in sufficient concentrations.[34] Evolution has selected organisms that exploit the power of free radicals to drive the assembly of deoxynucleotides to maintain nucleotide concentrations for DNA synthesis and repair.[35-36]

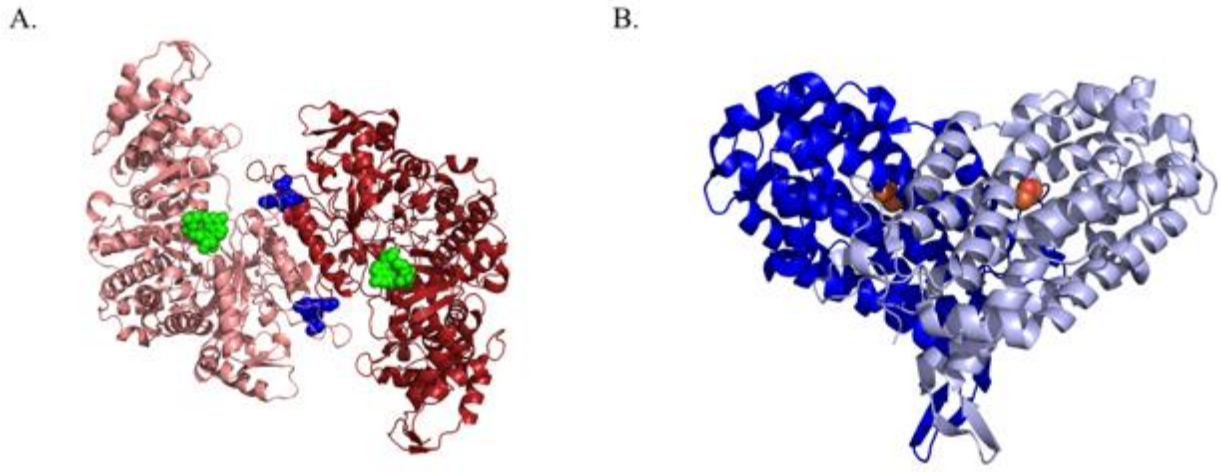

Figure 3.1 (A) Structure of α2 subunit at 3.2 Å (PDB 4R1R) containing substrate (green) GDP in the active sites and effector (blue) TTP bound to the specificity sites. This subunit is the site of nucleotide reduction. (B) Structure of β2 subunit at 2.2 Å (2XOF), the Fe-O-Fe clusters responsible for radical generation at Y122 are shown in orange (iron) and red (oxygen).

After the radical is generated by the diferric cluster, the radical hole must be transported 35 Å from the β subunit, across the α:β interface, into the α subunit, and finally resides on the conserved cysteine-439 (C439) residue in the catalytic site. The radical transfer pathway has been studied extensively using the incorporation of unnatural amino acids, as well as different types of experimental techniques.[8-9, 37-45] This has led to compelling evidence of a well-established radical hopping pathway. [9-10, 46] This pathway is proposed as follows: β-Y122O• → β-Y356 → α-Y731 → α-Y730 → α-C439 allows for reversible, long-range proton-coupled electron transfer (PCET). Rapid transfer is gated by conformation responses of the enzyme that are not fully understood, however, recent work suggests the protein dynamics are directly related to an iron bound water ligand to the diferric cofactor supplying the proton in the concerted PCET reaction to Y122O•.[47] Y356 provides the electron in the long-range PCET that fills the radical hole and propagates this radical into the active site. Interestingly, proton and electron donation differ from the α to the β subunit, where proton and electron transfer occurs orthogonally in the β2 subunit but occurs collinearly in the α2 subunit. Once the radical is in the active site, C439• induces reduction of the nucleotide substrate and release of the deoxyribonucleotide for DNA synthesis or repair. After release of the product, the pathway is used to reform the stable Y122O• by reversible PCET.[43, 48] Despite high-resolution crystal structures of the β2 enzyme, there remains no specificity regarding the position of β-Y356 due to the high variability of the C-terminal tail in isolated β2.[49]

The inhibition of RNR has been a major focus in cancer treatment to control and inhibit the overexpressed activity of RNR in cancerous cells. Chemical inhibition of the active quaternary complex (QC) using substrate and effectors has been of great interest to

understand the interactions that lead in RNR inactivity.[50-52] The mode of inhibition of RNR is significant for the design and applications of innovative anti-cancer therapeutics, like radical scavengers hydroxyurea (HU) and Triapine (3AP).[53-54] In contrast to HU and 3AP, 2′-azido-2′-deoxyuridine 5′-diphosphate (AzUDP) acts as a radical trap in the active site, generating a nitrogen radical that is moderately stable (Figure 3.2 A).[55-56] AzUDP and gemcitabine, a FDA approved cancer therapeutic in that they both inhibit with the α2 subunit.[57] Gemcitabine competes with dCTP for incorporation into DNA during synthesis and prevents the reformation of the essential radical for substrate reduction.[58] Gemcitabine is can be used with cisplatin to treat various forms of cancerous cells.[40, 59-60] Cisplatin creates cross links in DNA to prevent DNA synthesis and trigger apoptosis.[61] Although AzUDP is not being proposed as a potential option for cancer treatment in this study, we are proposing its uses to unmask the conformational changes associated with PCET.[11, 47, 62-63] COH29 is a promising inhibitor that binds to the ligand binding pocket of β2, preventing the formation of the α2β2 complex.[64] Other promising inhibitors that prevent protein-protein contact formation have been discovered using peptidomimetic compounds that have shown antiviral activity with HIV.[65] Another possible avenue for investigating RNR would be with iron chelators that cause radical loss by depletion of intracellular iron concentration,[66-67] and could be a direction pursued in future work. As seen in Figure 3.2 B, reaction-induced Fourier transform infrared (RIFT-IR) difference spectroscopy allows for the detection of subtle perturbations as small as a single amino acid conformational changes in RNR as a result of catalysis or inhibition due to radical quenching or trapping.[68-71] The FTIR spectra highlight the distinction of protein conformations in the presence of different substrates and effectors during active turnover noticing key features of the spectra

to occur independently of whether the enzyme is active or inhibited, and the conformational significance of QC inhibition.

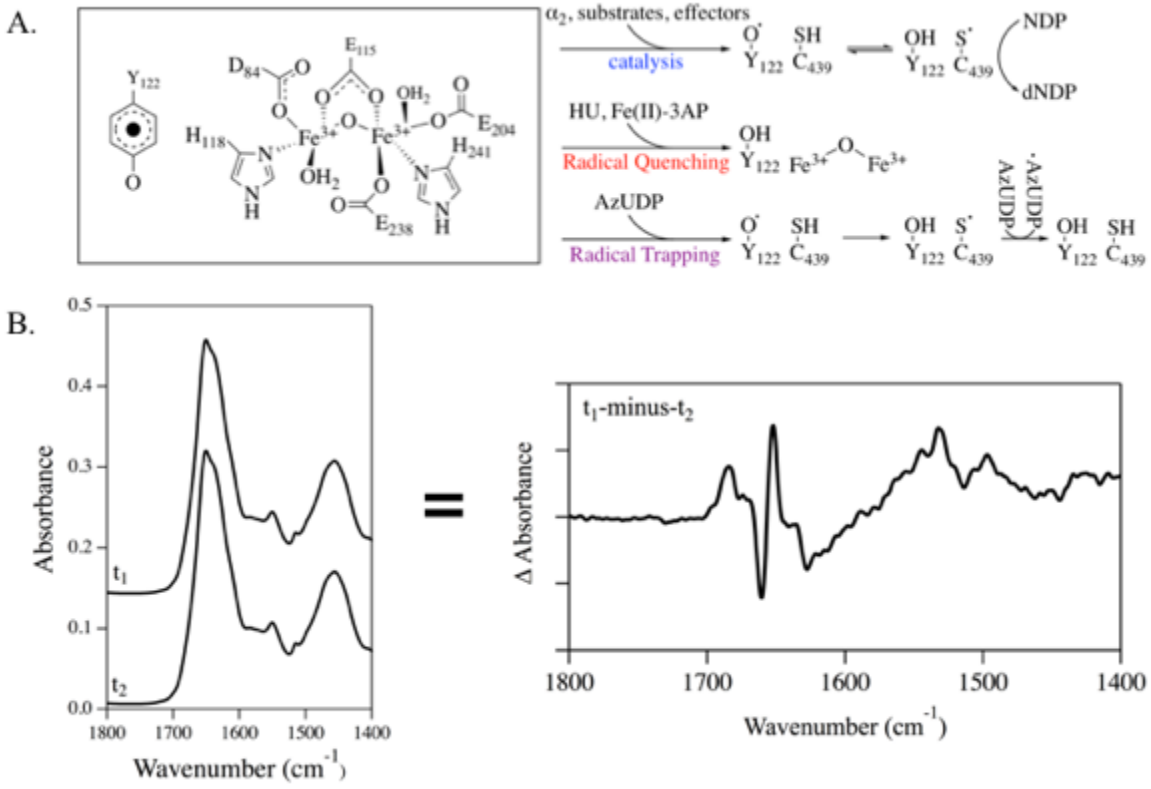

Figure 3.2 (A) A tyrosyl radical, Y122O•, is generated by an oxygen requiring diiron cluster and is required for catalysis. Separate modes of inhibition, radical quenching and trapping, are illustrated. HU and Fe(II)-3AP quench the tyrosyl radical prohibiting substrate reduction. AzUDP acts as a substrate analog and allows PCET to occur and generate a nitrogen centered radical (N•). (B) Method to generate reaction-induced FTIR difference spectra. These regions investigated have amide and carboxylate (COO^-) vibrational mode contributions.

3.3 Materials and Methods

3.3.1 Materials.

Hydrochloric acid (HCl), HEPES, 4-(2-hydroxyethyl)-1-piperazineethanesulfonic acid, and sodium hydroxide (NaOH) purchased from Sigma (St. Louis, MO) were used for

experimental and purification buffer solutions. UV-Vis kinetic experiments and FTIR spectroscopy samples were prepared in deuterium oxide (D_2O, 98%) and pH was adjusted using sodium deuteroxide (NaOD, 99.5%) to pD 7.6. Samples were obtained from Cambridge Isotope Laboratories (Andover, MA). Triapine (3AP) was a gift from Alan C. Sartorelli, Yale (New Haven, CT). 2′-azido-2′-deoxyuridine 5′-diphosphate (AzUDP) was a gift from Lisa Olshansky and JoAnne Stubbe, MIT (Cambridge, MA). Hydroxyurea (HU) was acquired from Calbiochem (San Diego, CA).

3.3.2 Overexpression and isolation of RNR E. coli α2 and β2 homodimers.

BL21 cells containing N-terminal His_6-tagged α2 were overexpressed and purified by Ni-NTA column chromatography. Wild-type β2 was overexpressed using BL21 cells and purified using size exclusion and ion-exchange chromatography. Identification of purified α2 or β2 was performed by gel electrophoresis. Average yield of β2 was 20 mg/g of cell paste. UV−Visible absorbance spectroscopy was used to calculate the concentrations of the α and β dimers with the extinction coefficients, ε_{280} = 189 mM^{-1} cm^{-1} and ε_{280} = 131 mM^{-1} cm^{-1}, for α2 and β2, respectively. The drop-down baseline method was used to quantify the concentration of tyrosyl radical (Y122O•) in β2 spectroscopically, and the average value was 1.19 Y122O•/β2.

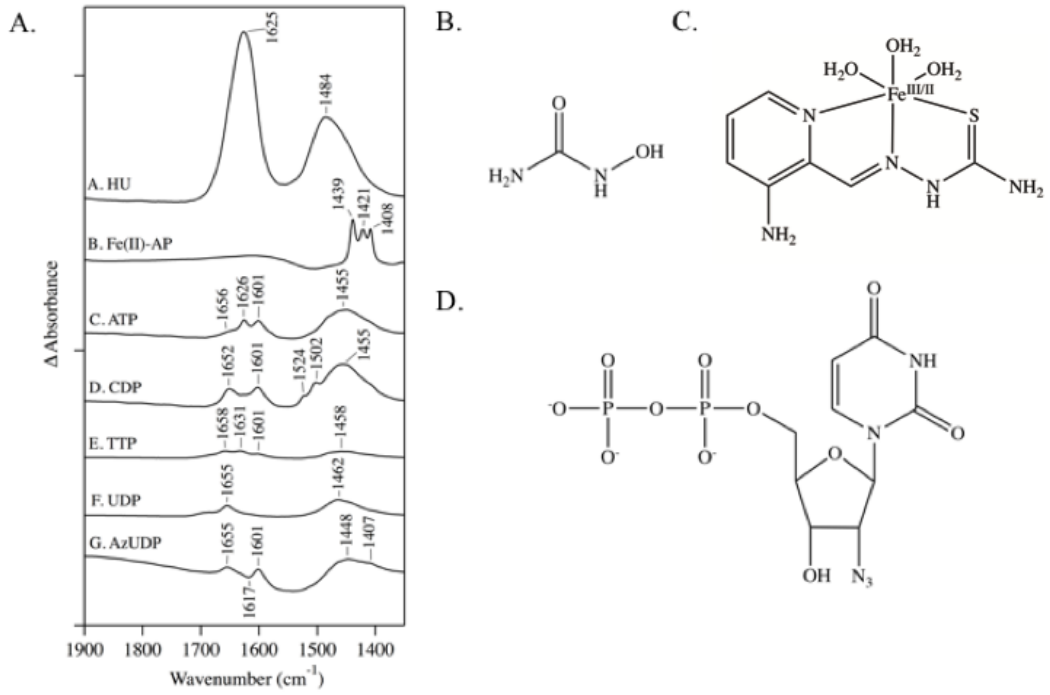

Figure 3.3 (A) FT-IR absorption spectra. Substrates, effectors, and inhibitors were tested to identify specific individual contributions in each spectrum. (B-D) Structures of inhibitors used throughout this study. Hydroxyurea, Fe(II)-3AP, and AzUDP, respectively.

3.3.3 Decay kinetics of Y122O• by UV−Vis spectroscopy

Kinetic analysis of tyrosyl radical reduction was monitored with a Varian Cary 50 (Varian, Walnut Creek, CA) spectrophotometer at 20°C by use a Peltier cell. The QC mixing experiments involved 35 μM α2, 35μM β2, 3 mM CDP (or 1 mM UDP/AzUDP), 1 mM ATP (or 0.8 mM TTP), 5 mM DTT, 15 mM $MgSO_4$, 1 mM EDTA, and 50 mM HU or 40 μM Fe(II)-3AP, where applicable, in 5 mM HEPES, pD 7.6 buffer (300 μL final volume). All samples were prepared in D_2O. Turnover and inhibition trials were prepared identically as follows: DTT, $MgSO_4$/EDTA, ATP (or TTP), CDP (or UDP/AzUDP), α2, and finally, β2 was added to initiate radical transfer. Fe(II)-3AP was prepared in D_2O in the presence

of oxygen with equal amounts of $FeCl_3$ and 3AP. DMSO was used to increase the solubility of 3AP and excess DTT was present in solution to continuously reduce the Fe(III)-3AP to Fe(II)-3AP. AzidoUDP was prepared in 5mM HEPES, D_2O. Inhibitor samples were stored at -80ºC until ready for use. Figure 3.2 A describes the conditions under which RNR is studied in this investigation. When inhibitors were present, they were added immediately following β2 addition to reduce Y122O•. The sequence of addition, including inhibitors, is consistent with FT-IR spectroscopy experiments discussed below. In the absence of inhibitors (Figure 3.4 A, 3.4 C, 3.5 A, and 3.5 D), no discernable change was observed for radical concentration during kinetic analysis. In Figure 3.4 (B, D, isolated β2), and 3.5 (B, C, E, α2β2), a monoexponential fit was used to calculate the rate constants of tyrosyl radical reduction by hydroxyurea by measuring the absorbance of 410 nm over time, a characteristic band of the tyrosyl radical. The concentration is displayed as percent remaining radical concentration as a function of time. Figure 3.6 uses Fe(II)-3AP and AzUDP, that inhibit the enzyme by radical quenching and radical trapping, respectively. It can be seen clearly that, in each case, both therapeutics result in loss of the tyrosyl radical over the course of kinetic analysis. Baseline drop-down method: $[Y122O\bullet] = (A_{411nm} - [(3(A_{416nm}) + 2(A_{406nm}))/5)/(1784\ M^{-1}\ cm^{-1})$ was used to evaluate the radical concentration. The standard deviations in Figures 3.4-6 display the reproducibility of all conditions observed.

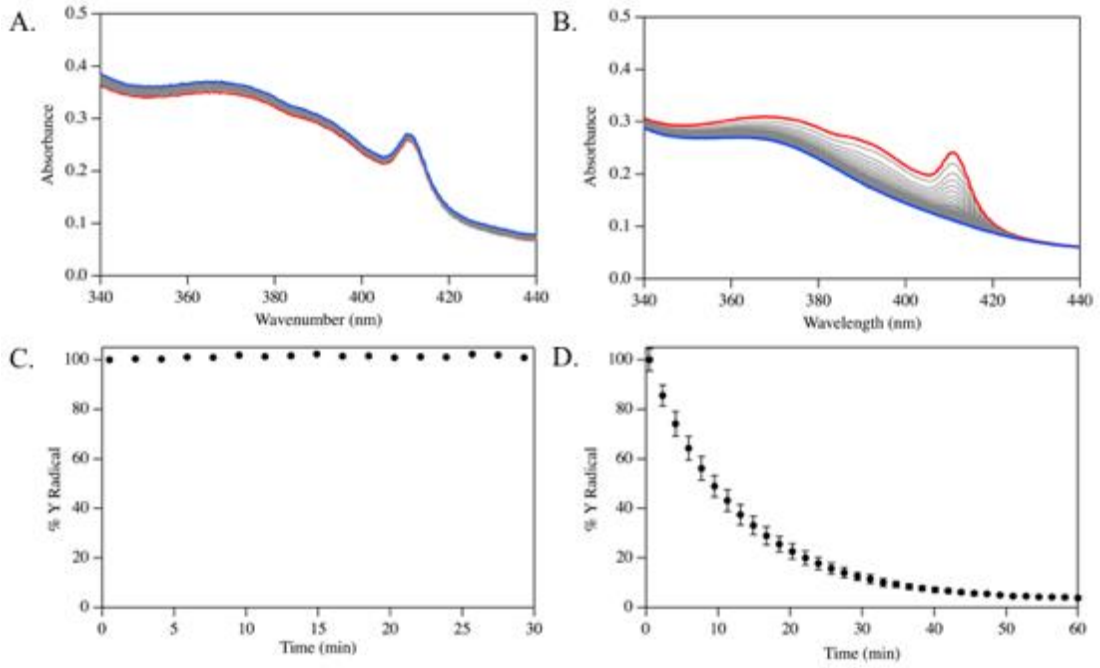

Figure 3.4 UV-Vis kinetic spectroscopic studies of (A) 40 µM isolated β2 and (B) 40 µM isolated β2 with 50 mM HU (C) Measure of percent radical present in A over the course of the 30-minute runs. (D) Measure of percent radical in B that is subsequently quenched by HU over the course of 60-minute runs. Averages: (A) 12 and (B) 11.

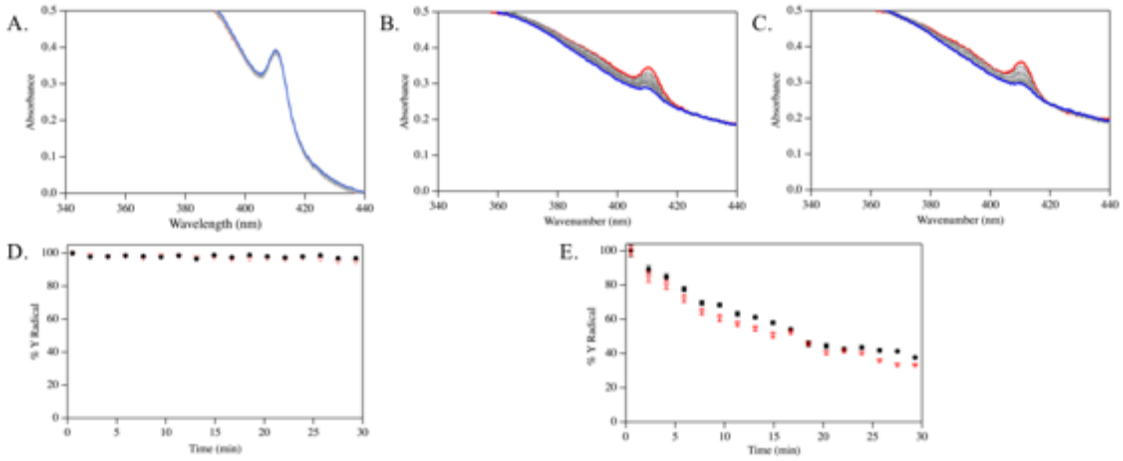

Figure 3.5 UV-VIS kinetic spectroscopic radical scavenger (HU) mixing studies (A) 35 µM α2, 35 µM β2, 1 mM ATP (0.8 mM TTP), 3 mM CDP (1 mM UDP) with no inhibitor. (B) 35 µM α2, 35 µM β2, 1 mM ATP, 3 mM CDP, and 50 mM HU. (C) 35 µM α2, 35 µM β2, 0.8 mM TTP, 1 mM UDP and 50 mM HU. (D) Measure of percent radical in A over the course of 30-minute runs. (E) Measure of percent radical in B

and C that is subsequently quenched by HU over the course of 30-minute runs. Averages: (A) 9, (B) 9, and (C) 9.

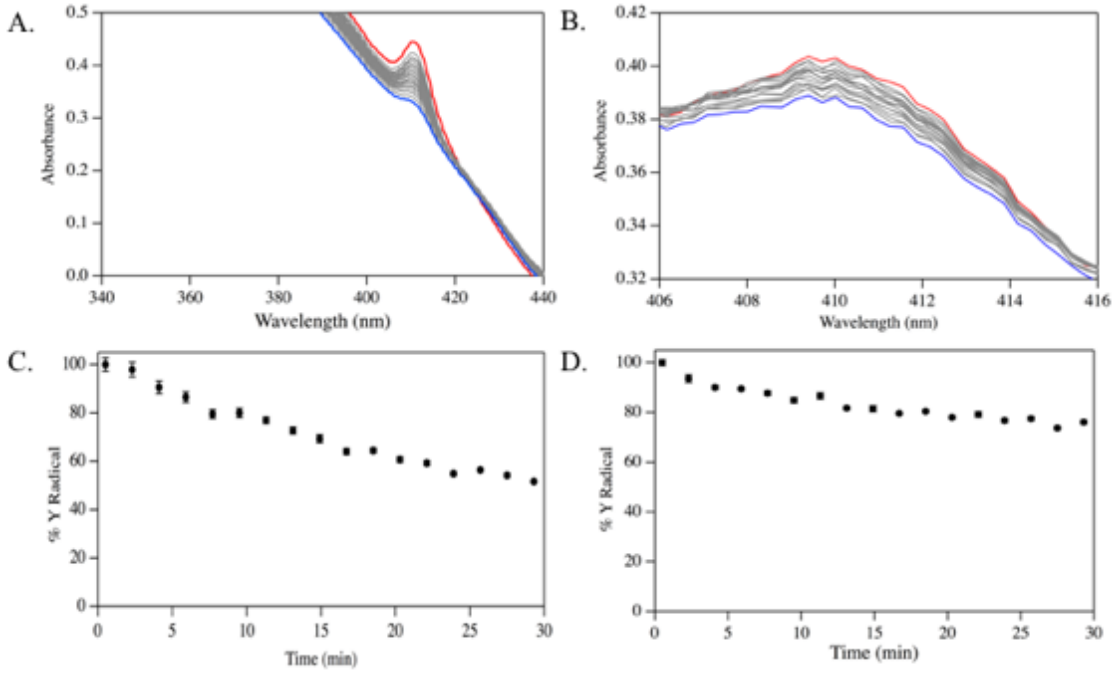

Figure 3.6 UV-Vis kinetic spectroscopic studies of radical scavenger (Fe(II)-3AP) and radical trapping substrate analog (AzUDP) (A) 35 µM α2, 35 µM β2, 1 mM ATP, 3 mM CDP and 40 µM Fe(II)-3AP. (B) 35 µM α2, 35 µM β2, 0.8 mM TTP, and 1 mM AzUDP. (C) Measure of percent radical quenched in A over the course of 30-minute runs. (D) Measure of percent radical in B that is trapped in the active site over the course of 30-minute runs. Averages: (A) 9 and (B) 9.

3.3.4 Reaction-Induced FT-IR Spectroscopy.

A temperature-controlled Nicolet Magna 550 II spectrometer was used to collect reaction-induced FT-IR spectra (Nicolet, Madison, WI). All of the FT-IR spectra shown in this work were collected at 20°C using a MCT-A detector. All reaction-induced FT-IR mixing samples were prepared in deuterium oxide (D_2O) with the final concentrations of 100 µM α2, 100 µM β2, 3 mM CDP (or 1 mM UDP/AzUDP), 1 mM ATP (or 0.8 mM TTP), 5 mM DTT, 15 mM $MgSO_4$, and 1 mM EDTA in 5 mM HEPES (pD 7.6) in the final 300 µL

sample. Figure 3.3 shows absorbance spectra of all substrates, effectors, and inhibitors that were collected to disregard any contributions not specifically from QC interactions. Immediately upon addition of either the β2 subunit for turnover or an inhibitor to quench the radical, a computer-controlled pump injected the prepared sample into the CaF_2 flow cell with a path length of 50 μm. Data was collected for difference spectroscopy for 2 min followed by 6 min of incubation, followed by another 2 min of data collection. This experimental parameter as well as inhibitor concentration was decided on based off the half-life of tyrosyl radical reduction monitored by UV-Vis absorbance kinetics to maximize signal intensity to baseline drift. Each 2 min scan was performed using a 4 cm^{-1} resolution, collection of 595 total interferograms, and a mirror velocity of 2.53 cm s^{-1}. Happ−Genzel apodization function, two levels of zero filling, and a Mertz phase correction were used for Fourier transform and generation of the energy spectra. A ratio to a previously collected open beam composed of the empty CaF_2 flow cell windows and the energy spectra generated the absorption spectra. The difference of each absorption spectra from each 10 min scan was taken to generate the difference spectra (t_1-minus-t_2). All subsequent absorption spectra were collected and processed identically to show individual contributions based on the substrate, effector or inhibitor.

3.4 Results

3.4.1 UV-Vis spectroscopic analysis of tyrosyl radical reduction

3.4.1.1 β2 with radical scavenging hydroxyurea

UV-Vis spectroscopy is used to optimize RIFT-IR spectroscopy to examine ribonucleotide reduction. Here we monitor *E. coli* α2β2 radical which has a characteristic

410 nm peak coupled with a shoulder band at 390 nm. In these spectra we also see contributions from the diferric metallo-cofactor at 325 and 375 nm. In Figure 3.4 B, we present UV-VIS derived kinetic studies of isolated β2 with HU and the characteristic spectra, single reduction by HU. The band contributed a sharp radical peak at 410 nm. This is compared to Figure 3.4 A where HU was not added. In C and D, the data have been converted to % tyrosyl radical with the baseline drop down approach. Kinetics shows that in Figure 3.4 B, 50% percent of the radical has been reduced by HU in the given parameter. Without HU there is no reduction of the radical. This is consistent with previous results.

3.4.1.2 *E. coli* α2β2 with various substrates, effectors, and inhibitors

In Figure 3.5, we add α2, along with substrates and effectors to examine the inhibition by HU in the active complex. Figure 3.5 A, serves are a control where α2, β2, substrates (CDP or UDP) and effectors (ATP or TTP) were mixed together without inhibitor. In Figure 3.5 B, mixing of α2, β2, ATP, CDP, and HU. In Figure 3.5 C, mixing of α2, β2, TTP, UDP, and HU were monitored by UV-VIS spectroscopy. Figure 3.5 D and E involve conversion of the data to % tyrosyl radical with the baseline drop down approach. In Figure 3.5 E, (•) represents ATP and CDP and (∇) represents TTP and UDP, both of which have no inhibitor, and there is no radical reduction observed. In Figure 3.5 F, HU has been introduced into the solution, and with ATP and CDP (•) and TTP and UDP (∇), 35 to 40% tyrosyl radical has been reduced over the course of the 10-minute experimental run, respectively.

In Figure 3.6, we introduce two separate inhibitors to the QC, a radical scavenger Triapine (3-AP) and a substrate analog azido-2′-deoxyuridine 5′-diphosphate

(AzUDP). In Figure 3.6 A, the α2, β2, ATP, CDP, and active form, Fe(II)-3AP (discussed in Figure 3.25), show the sharp radical peak at 410 nm being reduced of over the course of the 30-min reaction. In Figure 3.6 B, α2, β2, TTP, and AzUDP the tyrosyl radical has been amplified to observe the smaller loss in radical than has been previously discussed. In Figures 3.6 C and D, show data conversion to % tyrosyl radical. In Figure 3.6 C, 20% of the tyrosyl radical has been reduced over 10 minutes, as designated by the experimental design of the FT-IR spectroscopy. In Figure 3.6 D, there is ~20% tyrosyl radical reduction.

3.4.2 Reaction-induced FT-IR difference spectra derived from α2β2/ATP/CDP mixing.

Previously we examined clear distinctions between the contributions that results from isotopically labelled *E. coli* α and β subunits, where we looked at active turnover with a single substrate (CDP) and effector (ATP). [72] In addition, we exposed the active complex to the radical scavenging inhibitor hydroxyurea (HU). [12, 73] Here we look to build upon that work by examining additional substrates and effector, as well as investigating the consequences associated with inhibition of the active complex.

Ribonucleotide reductase has strict control over the active site in the α subunit by allosteric regulation in the specificity site. [13-14, 74] Using two different effectors, ATP and TTP, allows the observation of how the binding of these effectors influence the spectra during active turnover or inhibition conditions (Figure 3.7). This figure displays 1750-1450 cm^{-1} region of the FTIR spectra composed of amide and carboxylate vibrations. The amide I (C=O) frequency is sensitive to changes in hydrogen bonding and secondary structure (α-helix, β-sheet, and loop). All samples were either prepared or buffer exchanged into D_2O to shift the water bending mode whose contributions are so large that it would wash out the

protein amide I region. Deuterium exchange will also shift the CN and NH contributions to 1450 and 1000 cm^{-1}, respectively allowing for clearer spectral assignments.

3.4.3 Comparison of reaction-induced FT-IR spectra of the QC with altered substrate and effectors from 1750 to 1450 cm^{-1}.

In Figure 3.7, we present the average data corresponding to absorbance mixtures with ATP/CDP compared to TTP/UDP. Even under active turnover clear distinctions can be seen in Figure 3.7 B and D. When α2, β2, TTP, and UDP are mixed into solution and turnover occurs as seen in Figure 3.7 D, peaks can be seen at 1706 and 1685 cm^{-1} that were not previously observed with ATP and CDP. In Figure 3.7 B, α2, β2, ATP, and CDP, both of these peaks are absent from the spectra. However, bands seen at 1676 and 1659 cm^{-1} with ATP and CDP display similar patterns and frequencies when compared to 1668 and 1657 cm^{-1}. The amide I (C=O) vibrations (1690-1620 cm^{-1}) are sensitive to alterations in secondary structure. The large negative peaks at 1635 and 1618 cm^{-1} (Figure 3.7 D) are associated with the production of dUDP over the course of the experiment, as well as loop/unstructured regions (1640 cm^{-1}). In Figure 3.7 B, these bands are similar at 1631 and 1622 cm^{-1}, however, with ATP and CDP, the spectrum has an additional negative band at 1644 cm^{-1} unique to its turnover spectra. Additionally, both Figure 3.7 B and D contain a large positive peak at 1547 cm^{-1}. In contrast, Figure 3.7 B, has an additional band with near equal intensity at 1527 cm^{-1} that is absent from Figure 3.7 D. Studies provide evidence that these signals could be a result of the modifications associated with the binding of the TTP in the specificity site.[74-76] These changes suggest the ability to distinguish between active

turnover due to conformational responses to specific effectors in this highly regulated enzyme.

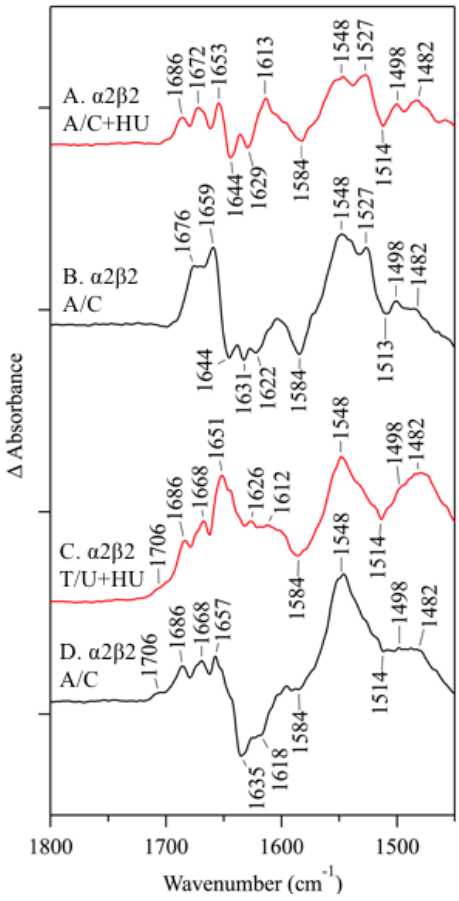

Figure 3.7 Averaged α2β2 RIFT-IR spectra with and without HU were vertically offset for comparison: (A) 100 µM α2, 100 µM β2, 1 mM ATP, 3 mM CDP and 50 mM HU (B) 100 µM α2, 100 µM β2, 1 mM ATP, 3 mM CDP (C) 100 µM α2, 100 µM β2, 0.8 mM TTP, 1 mM UDP and 50 mM HU (D) 100 µM α2, 100 µM β2, 0.8 mM TTP, 1 mM UDP. Tick marks for the spectra are 2 x 10^{-3} absorbance units. Averages: (A) 10 (B) 9 (C) 7 (D) 6.

3.4.4 Inhibition of the active α2β2 complex with radical scavenger, Hydroxyurea, from 1750 to 1450 cm^{-1}.

In Figure 3.7, exposure of the QC to HU yielded results not previously seen with ATP and CDP compared to TTP and UDP. Inhibition of the quaternary complex (QC) by

HU was monitored by UV-VIS spectroscopy in Figures 3.4 (isolated β2) and 3.5 (α2β2 complex) to insure similar time scales of inhibition. In Figure 3.7 C, we still observe the 1706, 1686, and 1668 cm^{-1} bands that previously observed in Figure 3.7 D. Observation of the 1706 cm^{-1} band in turnover and inhibition suggest the contribution could be due to binding of by substrate or effector to the α2 specificity or active sites. Where differences begin to appear between inhibition with TTP and UDP are at 1651 cm^{-1} which is 1657 cm^{-1} in turnover reactions. Moreover, in Figure 3.7 C, there is a large, broad band with positive signals at 1626 and 1612 cm^{-1}. In Figure 3.7 D, this region is negative with large peaks at 1635 and 1618 cm^{-1} believed to correspond to dUDP production. Both Figure 3.7 C and D have large intensity peaks at 1547 and 1482 cm^{-1}.

In Figure 3.7 A and C, the data were derived from ATP and CDP (A), and TTP and UDP (C) with both holoenzymes being exposed to the inhibitor HU. These two inhibited structures display clear changes in the mid-IR. In Figure 3.7 C, the band at 1706 cm^{-1} is present as stated previously, but is absent in Figure 3.7 A. Other bands in the amide I region between the inhibited complexes are remain similar. In Figure 3.7 C, these bands are 1686, 1668, and 1651 cm^{-1} compared in Figure 3.7 A as 1686, 1672, and 1654 cm^{-1}. There are small shifts in some of these bands. Most likely due to slight changes in the electrostatic environment of the protein. As previously stated in Figure 3.7 C, there is a large, broad band with positive signals at 1626 and 1612 cm^{-1}. In Figure 3.7 A, the spectrum has a similar negative region when compared to Figure 3.7 B and D with two negative bands at 1644 and 1629 cm^{-1}. Interestingly, the spectrum displays a solitary positive peak at 1614 cm^{-1} similar to Figure 3.7 C's 1612 cm^{-1}. Both Figure 3.7 A and C show identical signals

at 1547 cm^{-1}, but similar to the comparison of the active turnover complexes, the 1527 cm^{-1} peak is absent from the inhibited TTP/UDP mixing spectrum.

3.4.5 Reaction-induced FT-IR spectra associated with AzUDP inhibition from 1750 to 1450 cm^{-1}.

The process of radical transfer into the active site happens too rapidly for direct monitoring and is conformationally masked by the protein. [2, 77] To overcome this obstacle, we implemented the use of a radical trap 2'-Azido-2'-deoxyuridine 5'-Diphosphate (AzUDP). AzUDP traps the radical in the active site and, as a result, allows us to observe conformational changes associated with forward PCET in this conformationally "locked" state that would have been, previously, undetectable to us. [25-27] In Figure 3.8 A-C, we examined the effects of AzUDP with isolated β2 compared to HU. In Figure 3.8 A and B, we repeated previous results of isolated β2 with HU and with TTP, UDP, and HU, respectively. These spectra display previously assigned the iron ligand aspartate, D84, at 1685 and 1675 cm^{-1} with contributions to the 1661 and 1653 cm^{-1} bands, as well as the Y122• at 1498 cm^{-1} and Y122OH at 1514 cm^{-1}. However, in Figure 3.8 C, AzUDP shown in discernable interaction with isolated β2. This is expected as AzUDP should interact solely with the α subunits active site.

In Figure 3.8 F, AzUDP spectra displays similar bands at 1685, 1674, and 1548 cm^{-1} that are observed in all spectra regardless of substrate, effector, turnover or inhibition. It also exhibits a band seemingly unique to the presence of TTP and UDP at 1706 cm^{-1}. This band is present in the active complex with TTP and UDP (Figure 3.7 D), the inhibited complex with HU (Figure 3.8 E) or AzUDP (Figure 3.8 F). Interestingly, AzUDP also

displays a negative band at 1657 cm^{-1} and a positive feature at 1649 cm^{-1}. These bands are consistent with amide I vibrations indicating changes to the secondary structure and in hydrogen bonding. Under inhibition conditions in Figure 3.8 D and E, this region has remained positive around 1650 cm^{-1}, which makes the negative band curious and unique to the substrate analog inhibitor. Clearly distinct from active QC (Figure 3.7 B and 3.7 D), as well as inhibition by HU (Figure 3.8 D and 3.8 E), this feature shows clear evidence of hydrogen bonding changes, conformational changes associated with PCET, and generation of a trapped radical species in the active site generated by way of AzUDP. The AzUDP spectrum also has two negative bands at 1640 and 1625 cm^{-1}. These bands are interestingly more similar to Figure 3.8 D with ATP, CDP, and HU which correspond to 1644 and 1629 cm^{-1}, respectively whereas this region is positive in Figure 3.8 E. Figure 3.8 F, also displays the same loss of the peak at 1527 cm^{-1} that remains present under ATP and CDP conditions suggesting a contribution by ATP/CDP that is lost under TTP/UDP conditions. As a result of the radical having moved into the active site, clear conformational changes have occurred that are quite distinct from the active QC. AzUDP behaves as a substrate mimic in the active site of $\alpha 2$, [55-56, 68] but demonstrates conformational changes not detectable when the enzyme is left to function naturally.

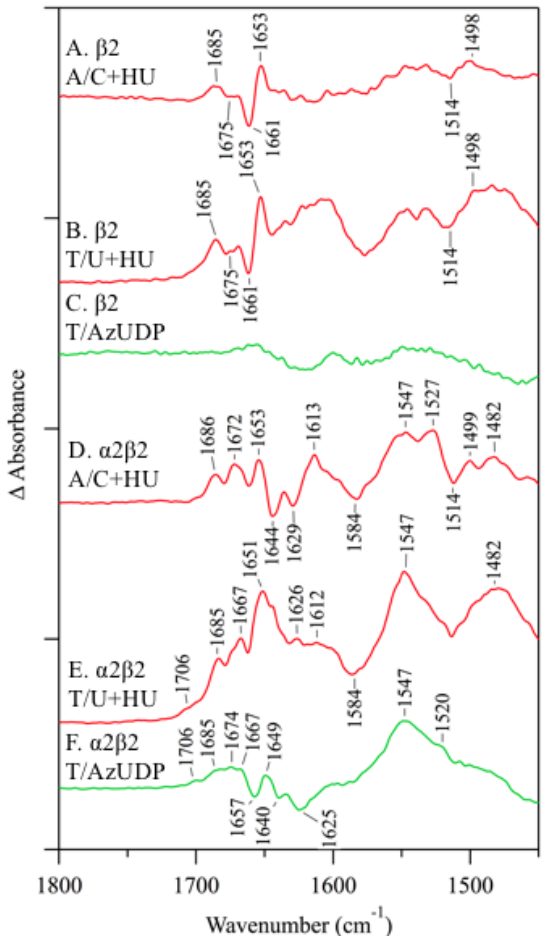

Figure 3.8 Averaged α2β2 RIFT-IR spectra with HU and AzUDP were vertically offset for comparison (A) 40 µM β2 and 50 mM HU (B) 40 µM β2, 0.8 mM TTP, 1 mM UDP, and 50 mM HU (C) 40 µM β2, 0.8 mM TTP, and 1 mM AzUDP (D) 100 µM α2, 100 µM β2, 1 mM ATP, 3 mM CDP and 50 mM HU (E) 100 µM α2, 100 µM β2, 0.8 mM TTP, 1 mM UDP and 50 mM HU (F) 100 µM α2, 100 µM β2, 0.8 mM TTP and 1 mM AzUDP. Spectra D and E are reproductions of spectra in Figure 3.7 A and C, respectively. Tick marks for the spectra are 2 x 10^{-3} absorbance units. Averages: (A) 10 (B) 8 (C) 8 (D) 10 (E) 7 (F) 9.

3.4.6 Inhibition of the active α2β2 complex with potent radical scavenger, Triapine from 1750 to 1450 cm^{-1}.

Lastly, we wanted to examine another radical scavenging inhibitor similar to HU, but one that is far more potent, Triapine.[53-54, 78-79] In Figure 3.9 A, control experiments were conducted, where iron was titrated into the 3AP sample and monitored by UV-VIS

spectroscopy to ensure that the 3AP was saturated at a 1:1 ratio. Titration of the iron from 0.5:1 (black) up to 2:1 (blue) iron:triapine displays no UV-Vis changes once equal concentrations of triapine and iron are reached suggesting they form a 1:1 complex. Radical decay was monitored as previously reported and displayed in Figure 3.9 C and in Figure 3.6 C based on % tyrosyl radical. In figure 3.9 B, additional controls were used to establish that Fe(II)-3AP was the active complex used to inhibit RNR. UV-VIS spectroscopy was used to monitor absorbance spectra generated by 3AP, Fe(III)-3AP, and Fe(II)-3AP. Both 3AP (blue) and Fe(III)-3AP (aqua) show similar spectroscopic contributions with a sharp distinct band at 355 nm, Fe(II)-3AP (pink) is distinct in that it displays a broadening of the 355 nm band seen with 3AP and Fe(III)-3AP and shifts its peak to 365 nm with a clear shoulder at 425 nm. Individual spectra were recorded for DMSO and DTT. DMSO was used to fully solubilize the 3-AP into solution. DTT was used to reduce the Fe(III)-3AP to Fe(II)-3AP based on absorbance spectra controls.

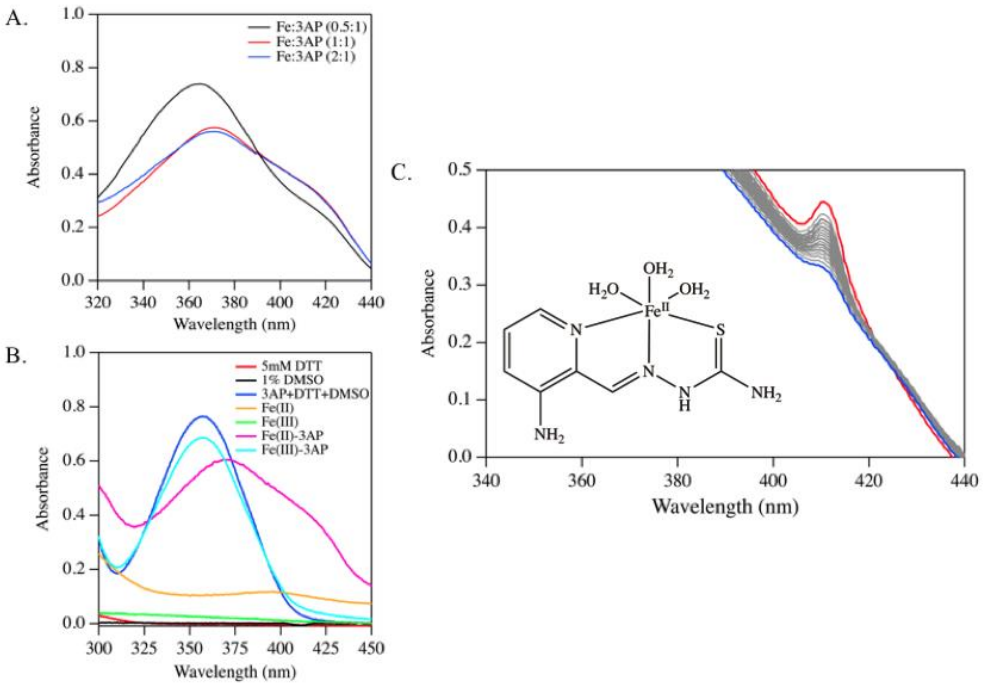

Figure 3.9 UV-VIS Spectroscopy 3AP controls and kinetic experiments. (A) Iron solution was titrated into 3AP containing sample to examine Iron:Triapine stoichiometry. (B) Absorbance spectra to determine individual spectral contributions. (C) 100 µM β2 and 40 µM Fe(II)-3AP in 5 mM Hepes, pD 7.6 over 30 minutes (Red: Indicates experimental start. Blue Indicates experimental end).

Both HU and Fe(II)-3AP are radical scavengers and are thought to behave similarly when exposed to RNR.[11-12, 52, 73, 80-83] In Figure 3.10 A and 3.10 B, isolated β2 FTIR spectroscopy display similar modes of inhibition by HU and Fe(II)-3AP, respectively. These spectra highlight D 85 bands at 1685 and 1675 cm^{-1}, as well as amide I conformational changes at 1661 and 1653 cm^{-1} to which D84 also contributes. They both also feature Y122• at 1498 cm^{-1} and Y122OH at 1514 cm^{-1}. Interesting to note, is that the concentrations used were 50 mM HU and 40 µM for Fe(II)-3AP. Nearly identical quenching of the tyrosyl radical done at over x1000-fold less in concentration. Could a binding site or multiple binding locations be the cause of such an increase in potency?

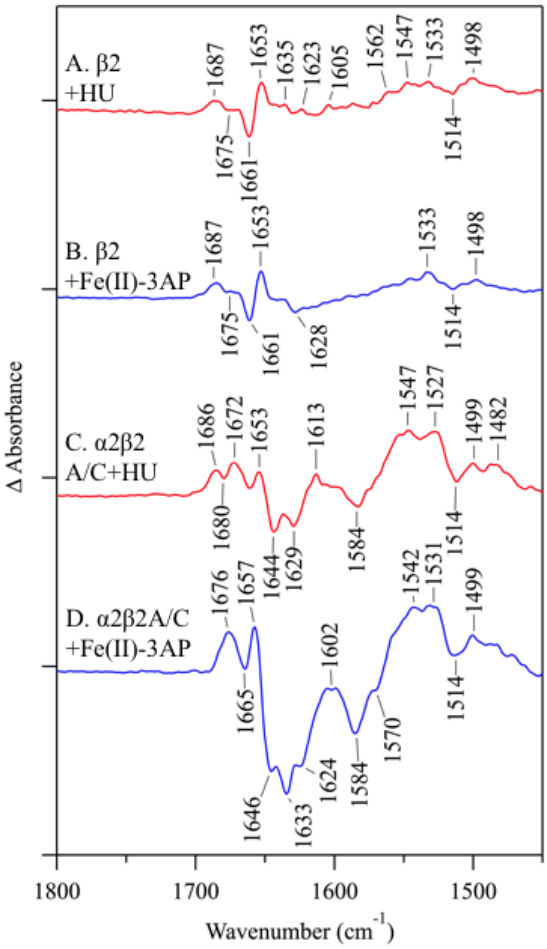

Figure 3.10 Averaged α2β2 RIFT-IR spectra for HU and Fe(II)-3AP were vertically offset for comparison (A) isolated 100 µM β2 and 50 mM HU (B) isolated 100 µM β2 and 40 µM Fe(II)-AP (C) 100 µM α2, 100 µM β2, 1 mM ATP, 3 mM CDP and 50 mM HU (D) 100 µM α2, 100 µM β2, 1 mM ATP, 3 mM CDP, and 40 µM Fe(II)-AP. Tick marks for the spectra are 2 x 10^{-3} absorbance units. Averages: (A) 11 (B) 9 (C) 10 (D) 8.

These inhibitors were investigated further with the QC, as well, to see if Fe(II)-3AP displayed a similar potency, and if the inactivation of the QC was a similar to HU as it was observed in the isolated β2. In Figure 3.10 C and D, modes of inhibition do not appear to be as comparable as previously imagined. In figure 3.10 D, a discrete duo of peaks is observed in the amid I region at 1676 and 1657 cm^{-1}. These two bands would correspond to 1672 and 1653 cm^{-1} as seen in Figure 3.10 C with HU. However, Fe(II)-3AP does not

have a positive band at 1886 cm^{-1}. In both Figure 3.10 C and D, they both have negative bands at 1644, 1629 cm^{-1}, and 1646 and 1633 cm^{-1}, respectively, while Fe(II)-3AP has an additional negative feature at 1624 cm^{-1}. The Triapine spectrum in Figure 3.10 D shares further similarities at 1602, 1584, 1542, 1531, 1514, and 1499 cm^{-1} to those seen in the HU Figure 3.10 C at 1614, 1584, 1547, 1527, 1514, and 1499 cm^{-1}. The slight changes in wavenumbers suggest small variations in the electrostatic environments based on the different inhibitors.

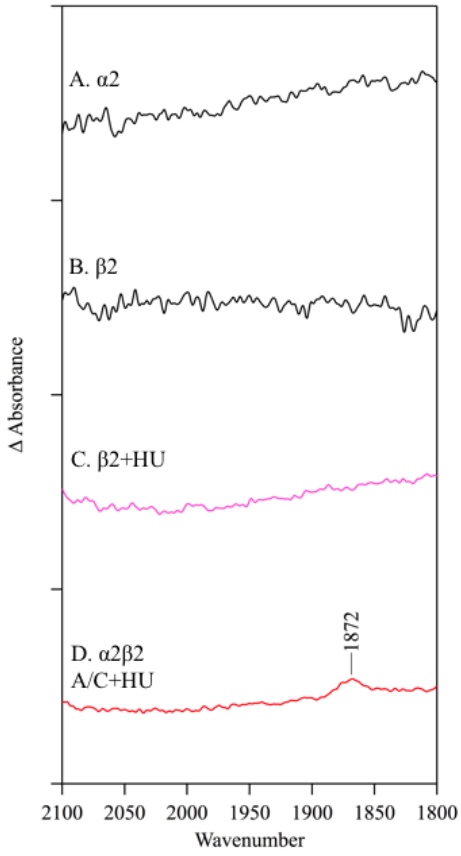

Figure 3.11 Averaged RIFT-IR spectra in the SD stretching region (A) α2, (B) β2, (C) β2 with HU, (D) α2β2, ATP, CDP with HU. (+) 1872 cm-1 band observed with α2β2, ATP, CDP with HU mixing experiment. The same band is not observed with isolated samples alone. Averages: (A) 7 (B) 6 (C) 11 (D) 10.

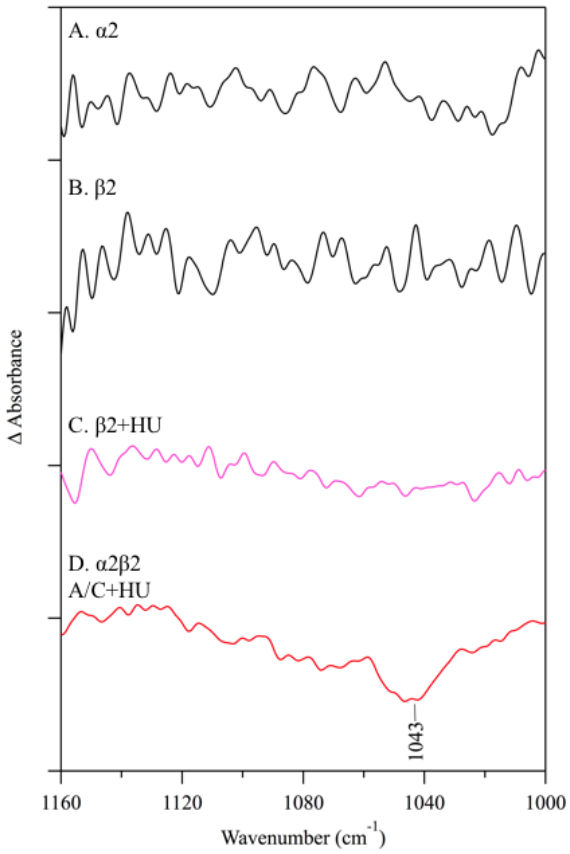

Figure 3.12 (A) α2, (B) β2, (C) β2 with HU, (D) α2β2, ATP, CDP with HU. (–) 1040 cm-1 band observed with α2β2, ATP, CDP with HU mixing experiment. This negative feature is not observed with isolated samples alone. Averages: (A) 7 (B) 6 (C) 11 (D) 10.

3.4.7 Investigation of the active α2β2 complex from 2200 to 1800 cm^{-1}, 1160 to 1000 cm^{-1}, and 3700 to 3100 cm^{-1} during turnover and inhibition.

Upon thorough examination of each region of the RIFT-IR spectra collected, two unique features presented themselves in the regions from 2200 to 1800 cm^{-1} and 1160 to 1000 cm^{-1}. In Figure 3.11, α2β2 mixing experiments with ATP/CDP and HU (Figure 3.11 D) exhibit a (+) 1872 cm^{-1} band not previously observed with control experiments α2 alone (Figure 3.11 A), β2 alone (Figure 3.11 B), or β2 with HU (Figure 3.11 C). After examination of other spectral ranges, it was also observed that controls showed no

contributions at the near IR in Figure 3.12 A-C. However, the mixing experiment in Figure 3.12 D yielded a unique contribution at (–) 1040 cm^{-1}. These new features were examined with other mixing experiments performed. Figure 3.13, presents data corresponding to $\alpha 2\beta 2$ mixing experiments performed in the presence and absence of HU. Figure 3.13 A contains $\alpha 2\beta 2$ with ATP, CDP and HU. Figure 3.13 B contains $\alpha 2\beta 2$ with ATP and CDP. Figure 3.13 C contains $\alpha 2\beta 2$ with ATP, CDP and Fe(II)-3AP. Figure 3.13 D contains $\alpha 2\beta 2$ with TTP, UDP and HU. Figure 3.13 E contains $\alpha 2\beta 2$ with TTP and UDP. Figure 3.13 F contains $\alpha 2\beta 2$ with TTP and AzUDP. As observed in Figure 3.13, there is a unique band at 1872 cm^{-1}. This signal is observed in mixing experiments which contain $\alpha 2\beta 2$ with ATP and CDP and is present regardless of turnover or inhibition. In Figure 3.13 D, E and F, which contains $\alpha 2\beta 2$ with TTP and UDP, there is no such signal to be observed in either case. Other inhibitors were analyzed for this same feature.

In the near IR region from 1160 to 1000 cm^{-1}, there is a similar distinction seen in the comparison of ATP/CDP vs TTP/UDP. In Figure 3.14 all spectra are displayed. Spectra A, B, and C correspond to ATP/CDP mixing spectra with HU, no inhibitor, and Fe(II)-3AP, respectively. Spectra D, E, and F correspond to TTP/UDP (where applicable) mixing spectra with HU, no inhibitor, and AzUDP, respectively. In Figure 3.14 A-C, there is a negative band at 1040 cm^{-1} that is, again, present regardless of turnover or inhibition conditions. In Figure 3.14 D-F, there is no characteristic feature with TTP/UDP experiments under any condition.

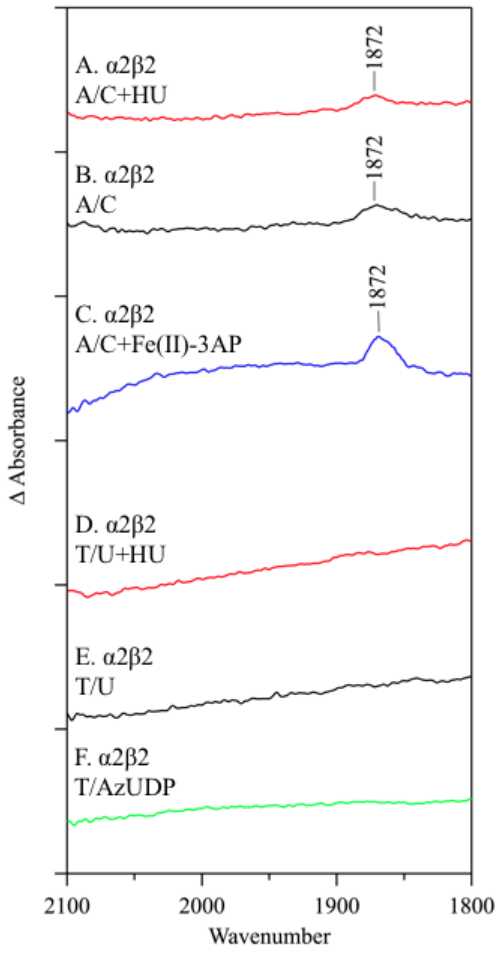

Figure 3.13 Averaged α2β2 RIFT-IR spectra in the SD stretching region (A) 100 µM α2, 100 µM β2, 1 mM ATP, 3 mM CDP and 50 mM HU (B) 100 µM α2, 100 µM β2, 1 mM ATP, 3 mM CDP (C) 100 µM α2, 100 µM β2, 1 mM ATP, 3 mM CDP and 40 µM Fe(II)-3AP (D) 100 µM α2, 100 µM β2, 0.8 mM TTP, 1 mM UDP, and 50 mM HU (E) 100 µM α2, 100 µM β2, 0.8 mM TTP, 1 mM UDP (F) 100 µM α2, 100 µM β2, 0.8 mM TTP, 1 mM AzUDP. Tick marks for the spectra are 1 x 10^{-3} absorbance units. Averages: (A) 10 (B) 9 (C) 8 (D) 7 (E) 6 (F) 9.

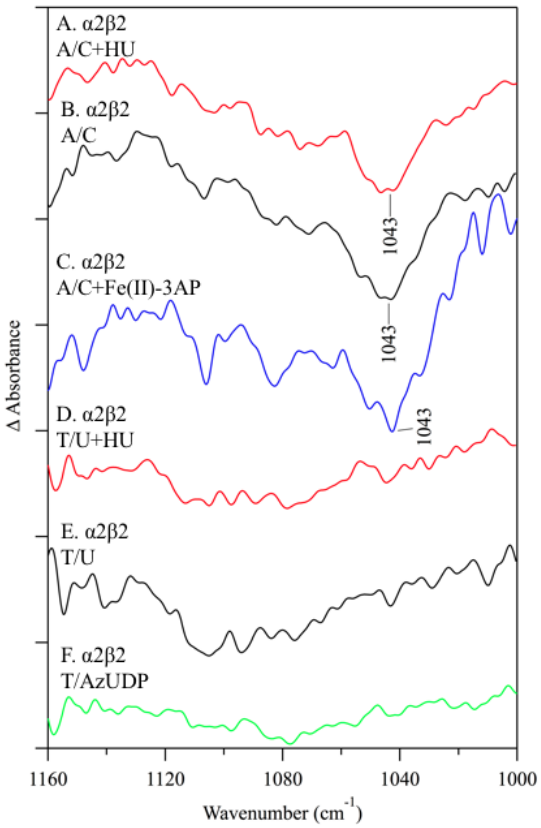

Figure 3.14 Averaged α2β2 RIFT-IR spectra in the 1300 cm-1 IR region. (A) 100 µM α2, 100 µM β2, 1 mM ATP, 3 mM CDP and 50 mM HU (B) 100 µM α2, 100 µM β2, 1 mM ATP, 3 mM CDP (C) 100 µM α2, 100 µM β2, 1 mM ATP, 3 mM CDP and 40 µM Fe(II)-3AP (D) 100 µM α2, 100 µM β2, 0.8 mM TTP, 1 mM UDP and 50 mM HU (E) 100 µM α2, 100 µM β2, 0.8 mM TTP, 1 mM UDP (F) 100 µM α2, 100 µM β2, 0.8 mM TTP and 1 mM AzUDP. Tick marks for the spectra are 1 x 10^{-3} absorbance units. Averages: (A) 10 (B) 9 (C) 8 (D) 7 (E) 6 (F) 9.

3.5 Discussion

3.5.1 Summary.

Illumination of how diverse substrate and effectors are able to regulate and maintain deoxynucleotides pools is fundamental in designing novel cancer therapeutics. Here we use reaction-induced FT-IR spectroscopy to highlight that the QC is conformationally

responsive and that these minute changes associated with binding to the enzyme are detectable and can be monitored as a function of time.

3.5.2 Binding of effectors influence disordered secondary structure in the α subunit

Previous studies focused on the assignment of contributions to the specific α or β subunits when ATP and CDP are bound. [72] Table 3.1 summarizes the findings of this work to examine the influence of varying reactants. When TTP and UDP are incorporated into the QC, Figure 3.7 exhibits clear distinctions that begin to arise. Under turnover or inhibitory conditions, a band at 1706 cm^{-1} is observed that is not present with ATP and CDP and is most likely a conformational response of α2. In Figure 3.7, spectral features from 1686-1651 cm^{-1} are observed independent of experimental condition and are assignable to α2 as previously reported.[72] These subtle changes in frequency are most likely due to small changes in the electrostatic environments as a result of larger conformational changes resulting from the varying of binding partners. TTP and UDP spectra no longer contain the (−) 1644 cm^{-1} band. This band was assigned to disordered regions of the α and β subunits when CDP and ATP operate as substrate and effector.[84-85] It is known that as different allosteric regulators bind to the α2 subunit, structural modifications impact ordered and disordered observed regions of the protein.[18, 20] As reported on in cryo-EM studies, loop 2 contains several imperative residues for specificity site stability and recognition. TTP and UDP experiments retain (−) 1629, (−) 1584, and (+) 1548 cm^{-1}, while losing the positive 1527 cm^{-1}, assignable to β sheets of the α subunit and amide II and asymmetric carboxylate bands. These extreme alterations seen in Figure 3.7 C and D between these two spectra are most likely a result of conformational changes that

are occurring in the α loop 2 region. Further spectral contributions could be due to loops 1 and 3 as a result of specificity site binding interactions. (Individual spectra of each of these conditions can be seen in Figures 3.15, 3.16, 3.18, and 19).

3.5.3 Spectral contributions at 1872, 1040, and 1706 cm^{-1}: sustainable regardless inhibition conditions.

Based on the influence by substrate and effector binding resulting in changes to disordered structure, it stands to reason that these ordered structures would present distinctive features in RIFT-IR spectra about the inner workings of RNR turnover and inhibition. The peak at 1872 cm^{-1} that was observed with ATP and CDP was not present under any experimental condition measured with TTP and UDP. A typical S-H functional group appear from 2600-2500 cm^{-1} in FTIR spectroscopy for the stretching vibration. Exchange of the hydrogen with deuterium to produce S-D, typically results in a down shift to lower frequencies by approximately 700 cm^{-1} (1900-1820 cm^{-1}) upon deuterium exchange in agreement with our 1872 cm^{-1} peak.[86] To observe significant contributions, mixing experiments are performed in D_2O so that functional groups are not washed out by water contribution. As laid out in chapter 1, the effector forms hydrogen bonds with Asp287 and Gly289 in loop 2. Binding of purine versus pyrimidine into the specificity site influences Gln288 to adopt either a "Gln-In" or "Gln-Out" position.[20] The conformational dynamics associated with loop 2 which has a conserved cysteine (C292) has the potential to act as a sensor to perturbations occurring in the active and specificity sites. This interaction is the most likely explanation for a signal in this area. Other possible explanations would be the conserved active site cysteines (C225 and C462) and cysteines found on the exterior of the active site and function as a transfer system (C754 and C759).

However, the presence of this unique band in Figure 3.13 is uninfluenced by any experimental parameter when ATP and CDP are present and is no longer detected when replaced by TTP and UDP under any variable. Therefore, this signal is attributed to the binding influence of the substrate or effector in the α2 subunit. Without additional controls, the assignment of the 1872 cm^{-1} signal cannot be definitely assigned to either subunit.

Table 3.1 Assignment of amide region bands based on reaction-induced FT-IR spectroscopy, acquired in HEPES D2O buffer, pD 7.6.

υ (cm^{-1})	α2β2 A/C	α2β2 A/C HU	α2β2 A/C Fe(II)-3AP	α2β2 T/U	α2β2 T/U HU	α2β2 T AzUDP	Subunit	Putative Assignment
1872	+	+	+	−	−	−	α2	Loop 2
1706	−	−	−	+	+	+	α2	Loop 1-3
1686	−	+	−	+	+	+	α2, β2	β-sheet/ side chain
1672	+	+	+	+	+	+	α2	β-sheet
1657	+	+	+	+	+	+	α2, β2	β-sheet / α-helix
1644	+	+	+	−	−	−	α2, β2	disordered

1635	+	+	+	+	−	−	α2, β2	Substrate consumption
1620	−	−	+	+	−	+	α2, β2	β-sheet
1613	+	+	+	−	−	−	α2	β-sheet
1584	+	+	+	+	+	+	α2, β2	β-sheet
1527	+	+	+	−	−	−	α2	β-sheet
1514	+	+	+	+	+	+	β2	Y122OH
1498	+	+	+	+	+	+	β2	Y122•
1040	+	+	+	−	−	−	α2	Loop 2

Upon examination of the near IR region in Figure 3.14, we also observed a negative band at 1040 cm^{-1} that is again observed when ATP or CDP are bound and not TTP and UDP. These signals lend further evidence to effector binding being the driving force for this new spectral contributions.[18, 87] The specificity site in the α subunit consists of positively charged residues that intermingle with the negatively charged phosphates of the nucleotide. Because these experiments are performed in D_2O, a deuterated cysteine signal, such as Cys292, in the low IR region is consistent with the signal at 1040 cm^{-1} due to the region being an indicator for S-H bending (1060 cm^{-1}).[88] The steric constraint of a purine bound in the active site demonstrates interactions not seen when the smaller pyrimidine,

TTP, is bound in the specificity site. Loop 2 associates with the effector leading to conformational rearrangement. Loop 2 is in contact with other nearby loops 1 and 3 that stabilize the phosphates of the bound effector. The position of one loop influences the position of each of the other loops leading to conformational cascade throughout the α subunit ultimately facilitating communication with the substrate binding site.[18] Inclusion of purine ATP leads to a conformational response that is not observable when TTP is bound to the specificity site.[89-90]

In Figure 3.7 C and D, 1706 cm^{-1} is present under turnover in the α2β2/TTP/UDP and is uninfluenced by the incorporation of inhibitors. In Figure 3.7 A and B, this band is not detected in α2β2/ATP/CDP experiments. This band, as well as 1872 cm^{-1} and 1040 cm^{-1}, is attributable to never before seen conformational changes and hydrogen bonding by the α2β2 complex outside of x-ray crystallography. The loops surrounding the specificity site are highly variable and stabilized by the interaction with the bound effector. The QC exhibits small differences in response to inhibition by HU conceivably due to distinct conformational arrangements adopted in response to effectors. Mixing experiments with TTP, UDP, and HU exhibit the same amide I 1706 cm^{-1} signal (Figure 3.7 C), but also reveal positive peaks at 1626 and 1612 cm^{-1} and the loss of negative signals at 1644, 1629 cm^{-1} and a positive amide II signal at 1527 cm^{-1} that were previously seen with ATP and CDP mixing experiments during turnover and inhibition (Figure 3.7 A and B). When TTP is bound, loops 1-3 adopt a more ordered structure that have defined positions, unlike its partially disordered structure when ATP is bound.[18, 89-90] This structure gives rise to discrete peaks observed at 1872, 1706, and 1040 cm^{-1} regardless of experimental conditions.

3.5.4 Conformational Position of QC Displayed by Catalytic Site Radical Trap

To this point, our investigation has been solely focused on examining the RNR under either turnover conditions or consequences resulting from quenching the tyrosyl radical with HU or Fe(II)-3AP. Observation of hydrogen bonding and conformational changes responsible for making radical transfer into the active site possible, is made even more difficult by the rapid speed at which the radical transfer process occurs and ultimately the enzyme masking the process altogether.[2, 77] To overcome these obstacles, the use of a radical trap, AzidoUDP was implemented. This inhibitor traps the radical in the active site of the α subunit where it forms a nitrogen radical species.[55-56, 68] This permits the detection of conformational changes that arise solely and specifically due to the forward PCET. In Figure 3.8 B, isolated β2 with TTP, UDP, and HU mixing experiments were performed as controls to monitor how substrate and effector influenced the spectra in an enzyme that is being actively reduced. This control was compared to β2 and HU alone, and the two spectra are nearly identical excluding a general broadening at 1610 cm^{-1} that was observed with TTP and UDP. In Figure 3.8 C, isolated β2 experiments with AzUDP shows no interaction like HU (Figure 3.8 A and B) nor should there be because there is no α subunit for AzUDP to interact with the radical. In Figure 3.6 B and D, UV-VIS spectroscopy exhibits loss of Y• when exposing the substrate analog to the active QC. In the QC, inhibition is presented that is unique from other inhibitory conditions. In Figure 3.8 F, the 1706 cm^{-1} signal is present again with AzUDP, in alignment with our assignment of TTP/UDP binding and existing with or without inhibitor. We also observe changes in the amide I region at (–)1657 and (+) 1649 cm^{-1} consistent with the conserved radical pathway being conformationally active and secondary structure transformations during radical transfer into the active site.

Amide I (C=O) vibrational band characteristically appear in this region. This suggests that propagation of the hole to the active site, leaving Y122• reduced, is coupled with structural changes in the β2 subunit. Individual spectra show that for a third condition, the 1872 cm^{-1} (Figure 3.13 F) and 1040 cm^{-1} (Figure 3.14 F) signals are not present when TTP is bound to the specificity site. Our previous work highlighted the Y122 residue undergoes a structural change during PCET, Y•→Y-OH,[11] and there is potentially a second conformational active tyrosine, most likely Y356, during PCET.[72] These experiments support these claims and probe the conformational dynamics associated with radical transfer into the active site causing the enzyme as a whole to be observed in a conformationally "locked," structurally meaningful approach.

3.5.5 Potent Radical Scavenger Alters the Secondary Structure of the QC.

Finally, we explored another radical scavenging inhibitor comparable to HU. Triapine is a very effective RNR inhibitor. In Figure 3.6 A and C, UV-VIS spectroscopy demonstrates quenching of the tyrosyl radical in the QC by Fe(II)-3AP. In Figure 3.10, isolated β2 experiments show very similar modes of radical quenching by HU (Figure 3.10 A) and Fe(II)-3AP (Figure 3.10 B) using 50mM HU and 40μM Fe(II)-3AP, but still displaying similar rates of inhibition. HU has no defined binding site or a particularly high affinity for RNR,[91-92] which causes it to have devastating side effects.[80] Figure 3.10 C and D compares the QC with the two radical scavenging inhibitors but yield vastly diverse spectra. There is a complete loss of the positive 1687 cm^{-1} band, an α subunit amide I contribution by β sheet or side chain,[72] that was observed under HU inhibition with both ATP/CDP and TTP/UDP. This reinforces that the α subunit is in communication with the

β subunit and has a conformational response during inhibition. We also detected large negative characteristics at 1646, 1633, and 1624 cm^{-1}. These mixing experiments involve ATP and CDP as substrate and effectors and we immediately see reformation of the disordered 1646 cm^{-1} band. The 1633 and 1624 cm^{-1} negative features could be a result of specific, and potentially multiple, binding locations for Fe(II)-3AP. These binding site(s) provide a cause as to why Triapine has such a high potency compared to other inhibitors and maintains a distinct spectrum from the other radical scavenger, HU. Inspection of the SD and low-IR regions provide the same unique signal for a third condition with ATP and CDP. The bands at 1872 and 1040 cm^{-1} are present and again seem to be uninfluenced by inhibition and rely solely on the presence of ATP. In Figure 3.13 F, the spectrum illustrates the presence of the 1872 cm^{-1} band for the inhibitor Fe(II)-3AP, while Figure 3.14 F displays the negative band at 1040 cm^{-1}. These bands, that are detected in the company of ATP and CDP, are detectable under turnover conditions and 2 separate types of inhibitors. In addition, these signals are not detected in the presence of TTP and UDP under turnover, inhibition by radical scavenging, or inhibition by radical trapping. The most likely explanation of these signals is the binding of ATP versus TTP to the specificity site which crystals structures have shown loop 2 of the α subunit to vary when the effector is.[20] However, the assignment of these features is not entirely clear. Uniformly, isotopically labeling both subunits will conclusively assign these features to the conformationally active Cys292 residue in the α2 subunit.

3.6 Conclusion

The conformational landscape of proteins provides an intricate quandary to decipher. FT-IR spectroscopy paired with radical activity allow us to untangle the dynamic conformational changes occurring during catalysis and inhibition. This technique allows for the observation of single amino acid changes taking place in this substantial enzyme. These experimental data begin to understand a host of natural processes in RNR that remain clouded. Understanding the conformational responsiveness of RNR to numerous substrates and effectors to maintain and regulate deoxynucleotides pools for DNA synthesis will mean understanding the regulatory controls for the enzyme itself. In the work presented, we have observed the enzymes conformational response to different allosteric effectors by the (–) 1644 cm^{-1} disordered region observed with ATP/CDP being absent with TTP/UDP. If this region is no longer disordered in TTP/UDP mixing experiments, then contributions should arise in another aspect of the spectra and could explain the appearance of the (+) 1706 cm^{-1} peak that is observed with TTP/UDP. Advancing our knowledge of anti-cancer therapy interactions to include how they specifically interact with the protein is of vital importance. Determination of a single path or potentially multiple paths to inhibition will influence how drugs are designed, which are tested, and ultimately used as viable treatment options. HU and Fe(II)-3AP interact with isolated β2 in nearly identical routes to quench the tyrosyl radical but diverge in the assembled QC while still maintaining similar rates of reduction. Future work will aim to elucidate these two pathways further. The radical pathway has remained a fascinating enigma. Attempting to break down the radical progression into manageable phases (i.e. radical traps) to unbundle the biological procedures will provide a better understanding of such a vital process of life. We have presented exactly that with AzUDP. This radical trap illustrates clear coupling of

conformational dynamics to Y122• reduction. This work displays clear and dynamic structural perturbations associated with redox-linked structural changes in RNR.

3.7 Acknowledgements

The authors thank Prof. J. Stubbe and Dr. E. Minnihan for the α2 plasmid, some of the reagents used in the activity measurements, AzUDP, and helpful discussions. We also thank Prof. J. Soper for use of the temperature-controlled Cary UV spectrophotometer.

3.8 Supporting Information

As observed in Figure 3.2 B, FT-IR difference spectra were generated by 2 min of data collection, known as t_1. The reaction was allowed to incubate for 6 min and then an additional 2 min of data was collected, t_2. Data was subtracted (t_1-minus-t_2) to generate the difference spectra (Δ Abs) highlighting specific interactions due to either turnover or inhibition. This reaction scheme allows the direct monitoring of RIFT-IR spectroscopy to observe minimal baseline drift while maximizing Y122O• reduction. For the HU, Fe(II)-3AP, and AzUDP (structures shown in figure 3.3 B-D) reactions, these difference spectra reflect radical state-minus-singlet state and 20-50% reduction of Y122O•. In Figure 3.15, we present RIFT-IR spectra recorded from α2β2 mixtures in the presence of ATP and CDP. In Figure 3.16, we present RIFT-IR spectra recorded from α2β2 mixtures in the presence of ATP, CDP, and HU. In Figure 3.17, we present RIFT-IR spectra recorded from α2β2 mixtures in the presence of ATP, CDP, and Fe(II)-3AP. In Figure 3.18, we present RIFT-IR spectra recorded from α2β2 mixtures in the presence of TTP and UDP. In Figure 3.19, we present RIFT-IR spectra recorded from α2β2 mixtures in the presence of TTP, UDP, and HU. In Figure 3.20, we present RIFT-IR spectra recorded from α2β2 mixtures in the

presence of TTP and AzUDP. In Figure 3.21, we present FT-IR spectra recorded from isolated β2. The average spectrum is presented in black above the individual spectra shown in red. In Figure 3.22, we present RIFT-IR spectra recorded from isolated β2 in the presence of HU. The average spectrum is again presented in black above the individual spectra shown in red. The data in Figures 3.15-3.22 are individual spectra to display reproducibility. The letters denote different days of data acquisition as pointed out in the figure legend.

The data in Figures 3.23-3.29 are individual spectra to display reproducibility. The letters denote different days of data acquisition as pointed out in the figure legend. In Figure 3.25, this spectrum contains α2β2, ATP, and CDP with Fe(II)-3AP and the individual spectra (red) as well as the average (black) exhibit the same band at 1872 cm^{-1} that was previously observed with other spectra containing ATP and CDP. In Figure 3.28, α2β2, TTP with AzUDP, in agreement with other TTP/UDP spectra display no trace of this band. In Figure 3.29, isolated β2 controls were analyzed for the presence of the putative S-D 1872 cm^{-1} band.

The water region (3700 to 3100 cm^{-1}) was surveyed to find discrepancies either between substrate and effector influence or turnover and inhibitory conditions. The region can be highly variable. Further investigation will be required in this region to gain meaningful data of either substrate and effector binding variances or the mechanism of the long range PCET pathway.

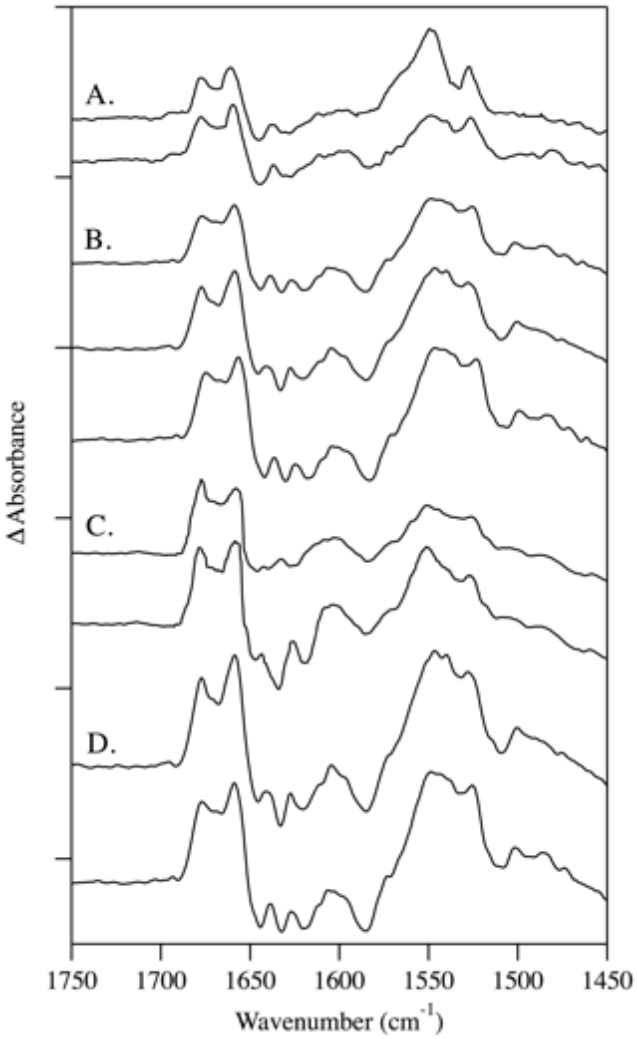

Figure 3.15 Individual α2β2 with ATP/CDP RIFT-IR spectra collected on the following date (A) 3/15/15 (B) 1/26/14 (C) 1/27/14 (D) 1/29/14 and were vertically offset for comparison. Tick marks for the spectra are 2 x 10^{-3} absorbance units.

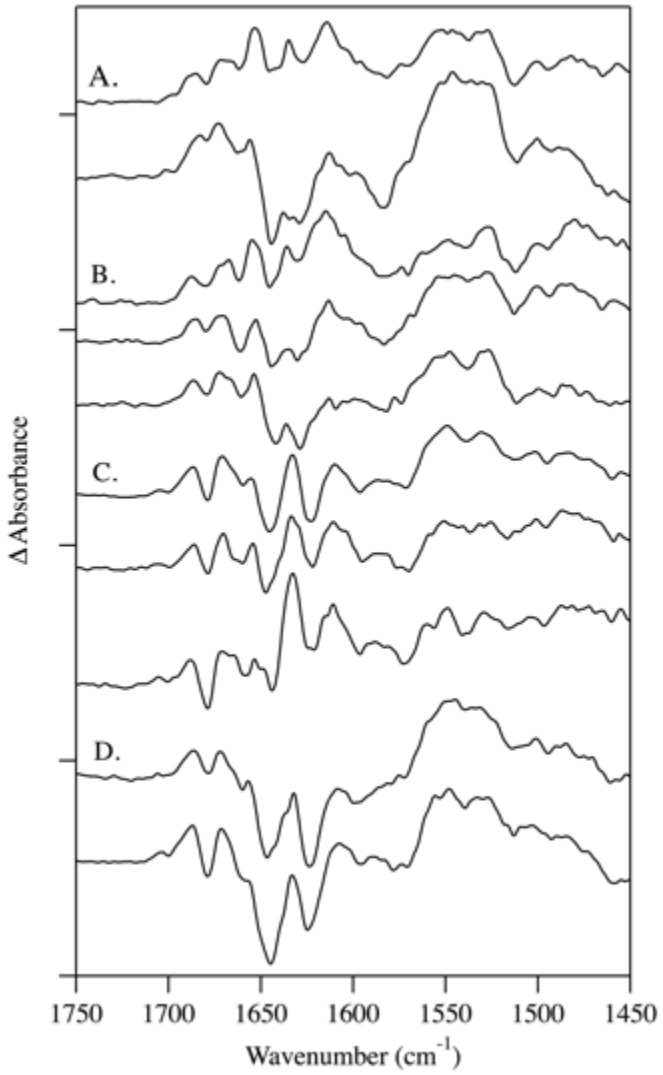

Figure 3.16 Individual α2β2 with ATP/CDP and HU RIFT-IR spectra collected on the following date (A) 3/15/15 (B) 1/26/14 (C) 1/27/14 (D) 1/29/14 and were vertically offset for comparison. Tick marks for the spectra are 2 x 10^{-3} absorbance units.

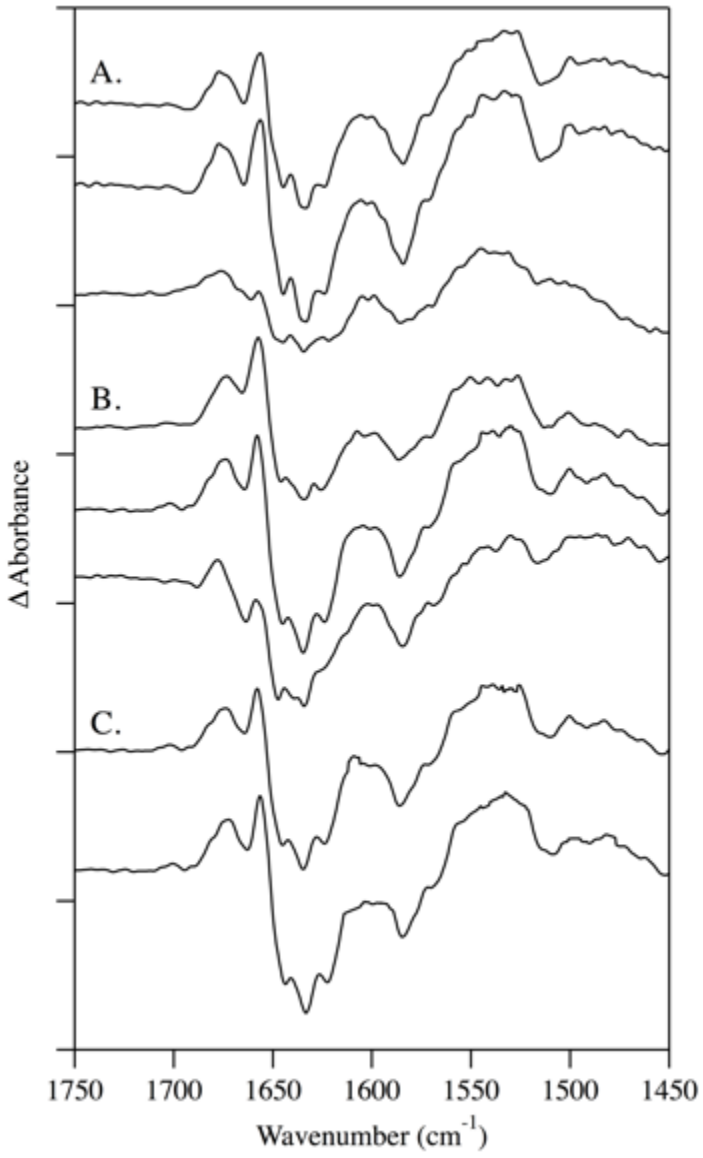

Figure 3.17 Individual α2β2 with ATP/CDP and Fe(II)-3AP RIFT-IR spectra collected on the following date (A) 2/24/16 (B) 2/25/16 (C) 3/08/16 and were vertically offset for comparison. Tick marks for the spectra are 2 x 10^{-3} absorbance units.

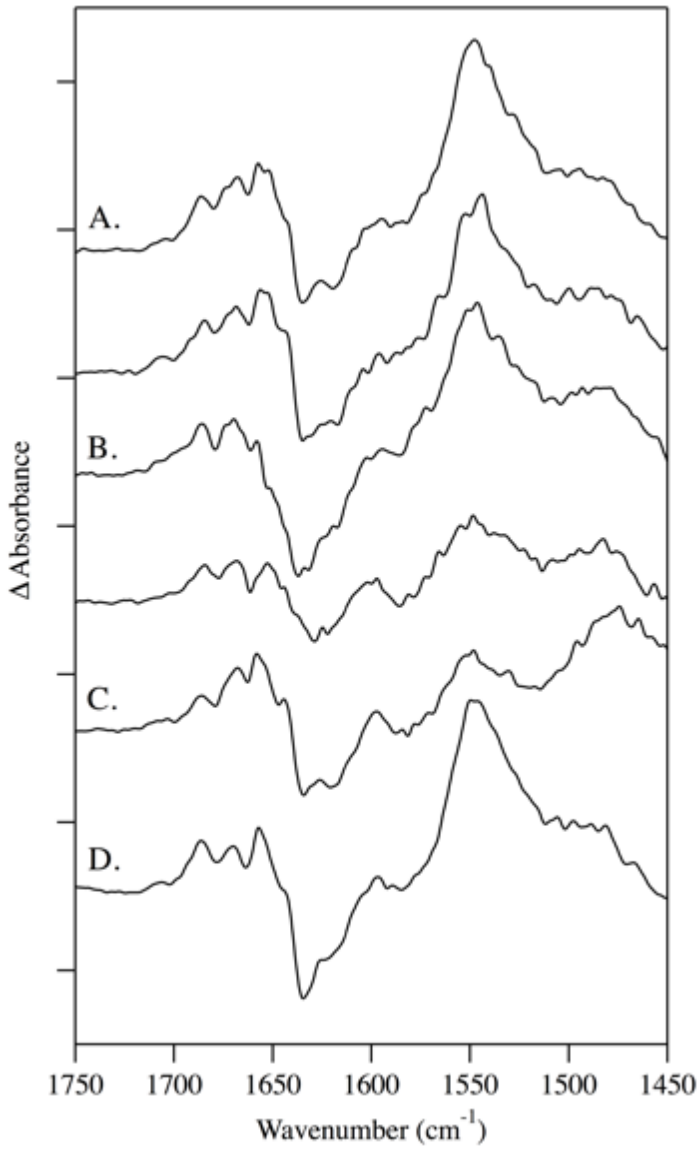

Figure 3.18 Individual α2β2 with TTP/UDP RIFT-IR spectra collected on the following date (A) 6/09/15 (B) 6/17/15 (C) 8/26/15 (D) 9/16/15 and were vertically offset for comparison. Tick marks for the spectra are 2 x 10^{-3} absorbance units.

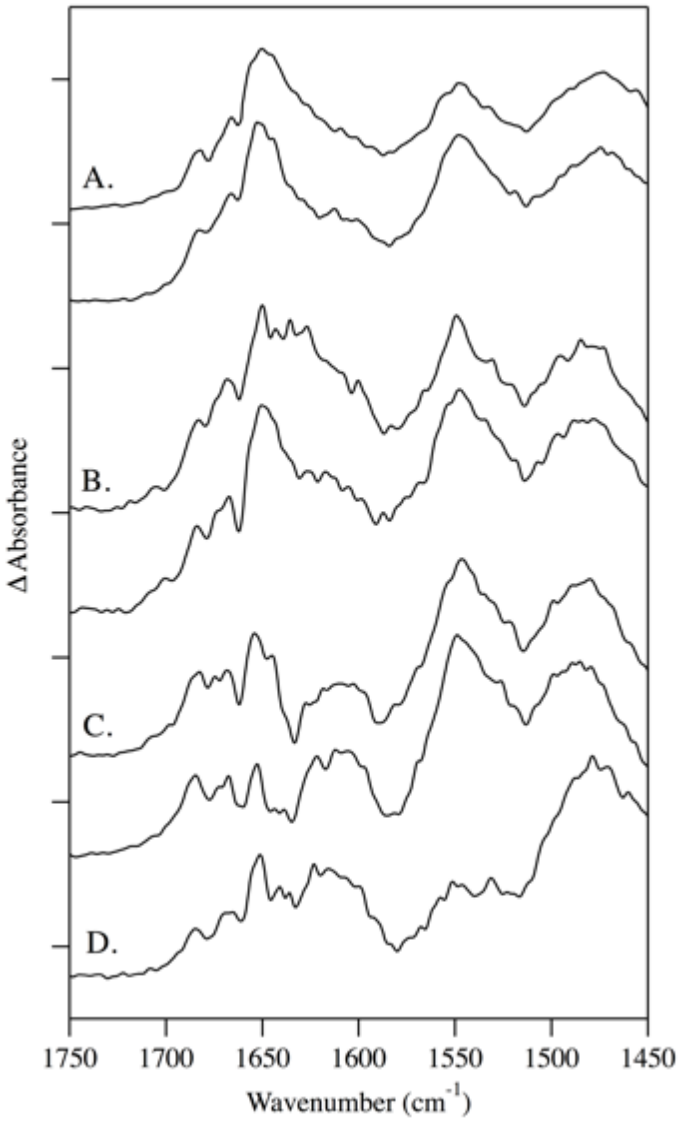

Figure 3.19 Individual α2β2 with TTP/UDP and HU RIFT-IR spectra collected on the following date (A) 6/09/15 (B) 6/17/15 (C) 8/26/15 (D) 9/16/15 and were vertically offset for comparison. Tick marks for the spectra are 2 x 10^{-3} absorbance units.

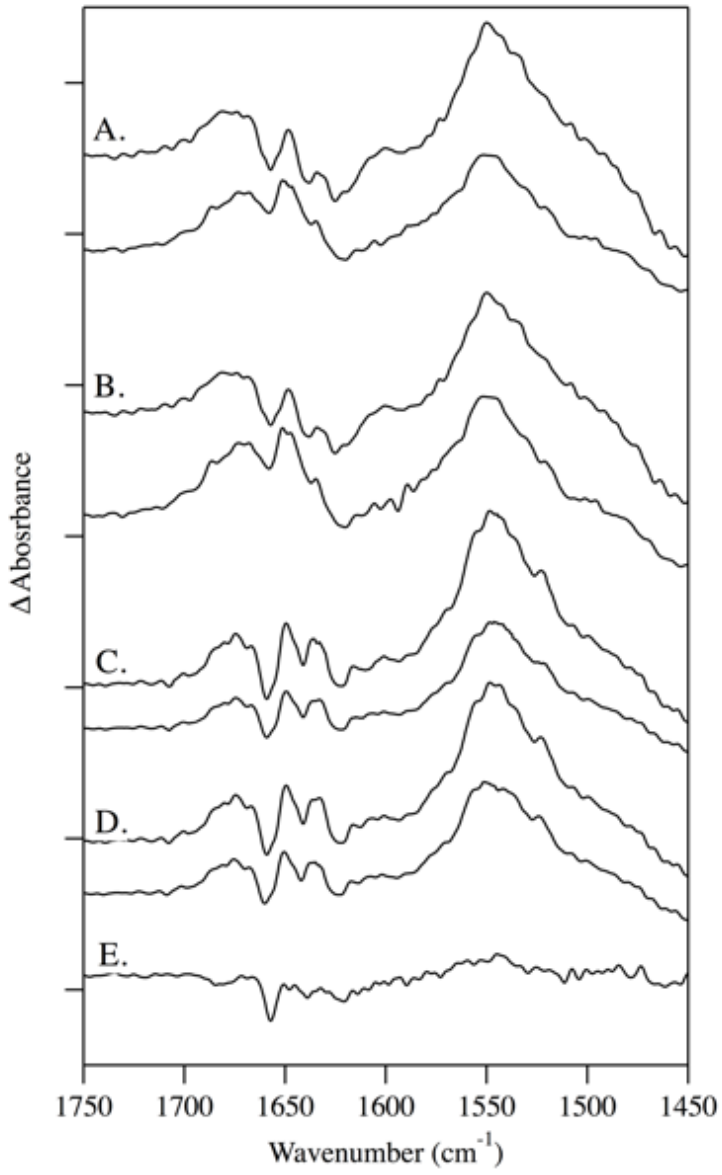

Figure 3.20 Individual α2β2 with TTP/AzUDP RIFT-IR spectra collected on the following date (A) 12/15/15 (B) 12/16/15 (C) 2/09/16 (D) 2/11/16 (E) 1/11/16 and were vertically offset for comparison. Tick marks for the spectra are 1 x 10^{-3} absorbance units.

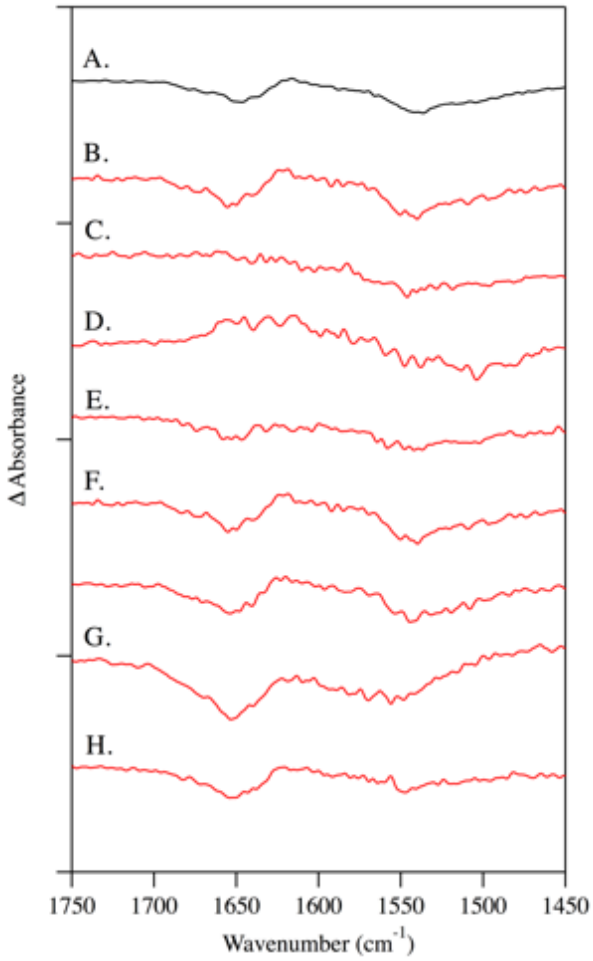

Figure 3.21 Isolated 100 µM β2 with no inhibitors present were vertically offset for comparison. (A) Average (shown in black) of individually collected spectra (B-H) Individual isolated β2 (shown in red). Dates that each sample was collected are as follows: (B) 3/15/13 (C) 7/05/13 (D) 7/09/13 (E) 7/10/13 (F) 11/08/13 (G) 1/25/13 (H) 12/15/14. Tick marks for the spectra are 1 x 10^{-3} absorbance units.

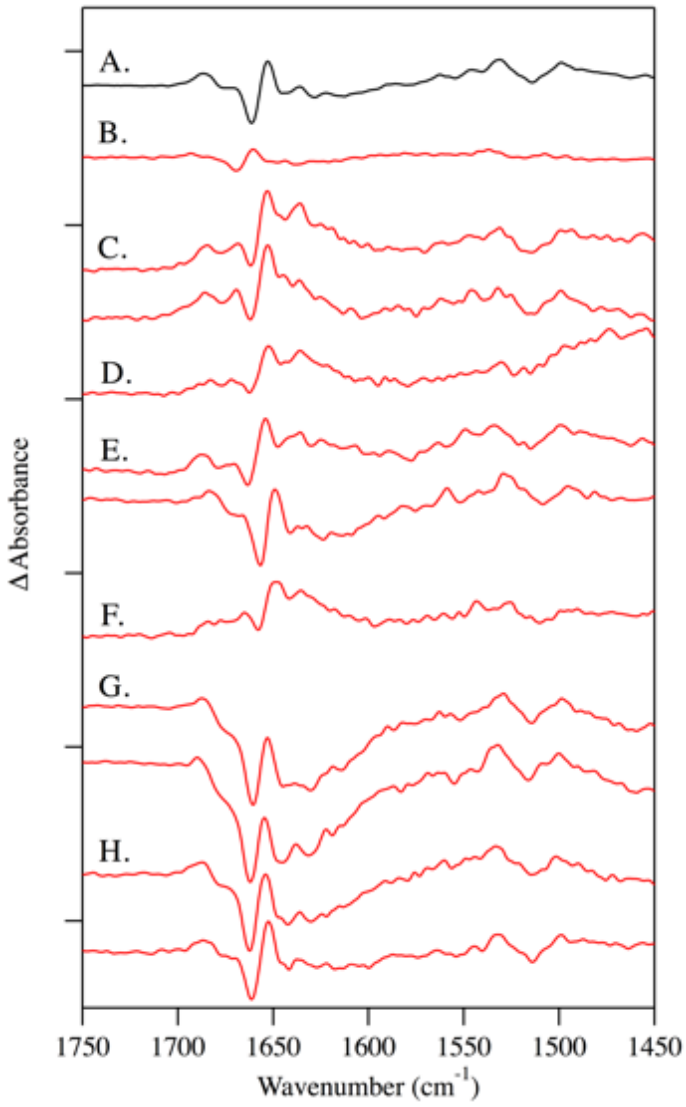

Figure 3.22 Isolated 100 µM β2 and 50 mM HU were vertically offset for comparison. Individual¬ spectra are shown in red. (A) Average (shown in black) of individually collected spectra (B-H) Individual isolated β2 (shown in red). Dates that each sample was collected are as follows: (B) 3/15/13 (C) 7/05/13 (D) 7/09/13 (E) 7/10/13 (F) 11/08/13 (G) 1/25/13 (H) 12/15/14. Tick marks for the spectra are 1 x 10^{-3} absorbance units.

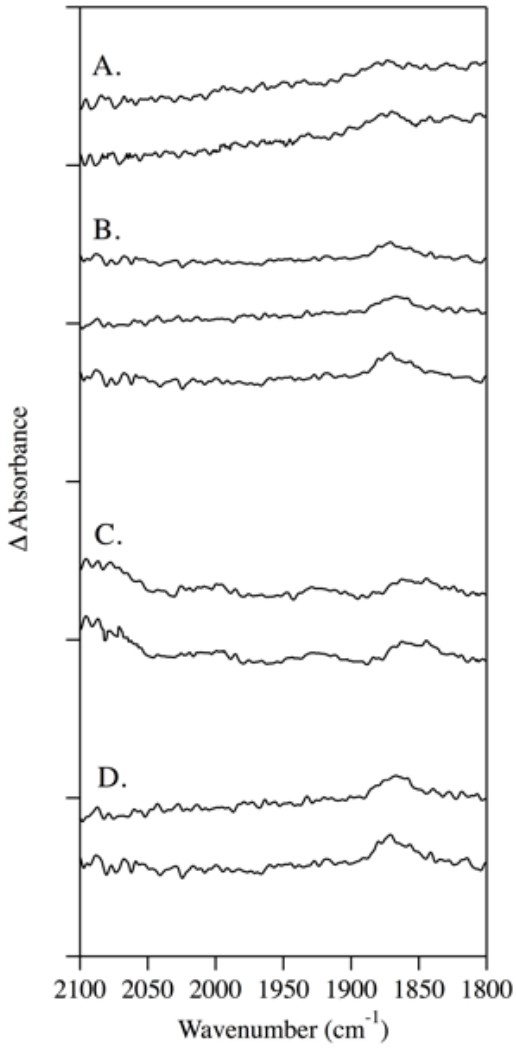

Figure 3.23 Individual α2β2 with ATP/CDP RIFT-IR spectra in the SD region were collected on the following date (A) 3/15/15 (B) 1/26/14 (C) 1/27/14 (D) 1/29/14 and were vertically offset for comparison. Tick marks for the spectra are 1 x 10^{-3} absorbance units.

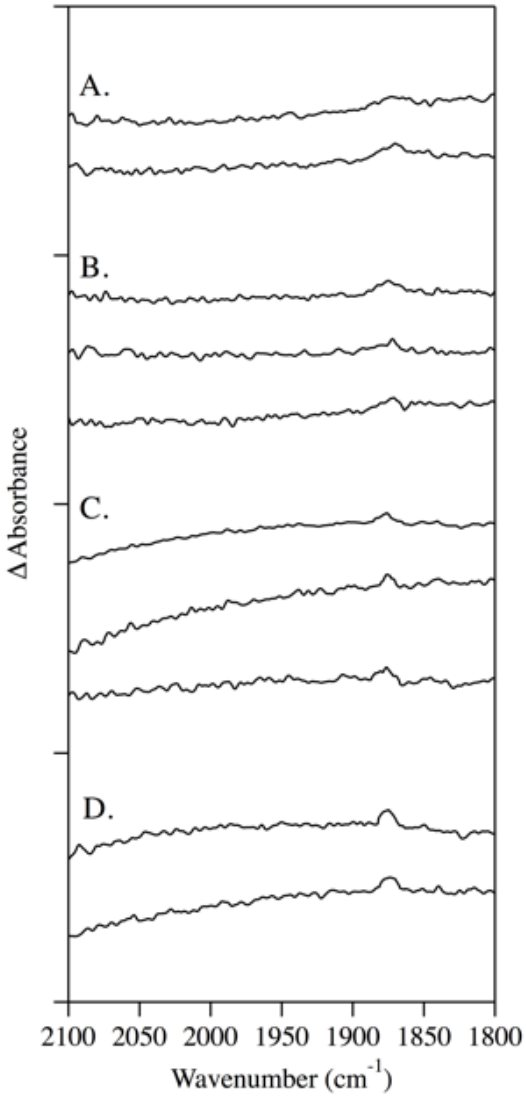

Figure 3.24 Individual α2β2 with ATP/CDP and HU RIFT-IR spectra in the SD region were collected on the following date (A) 3/15/15 (B) 1/26/14 (C) 1/27/14 (D) 1/29/14 and were vertically offset for comparison. Tick marks for the spectra are 1 x 10^{-3} absorbance units.

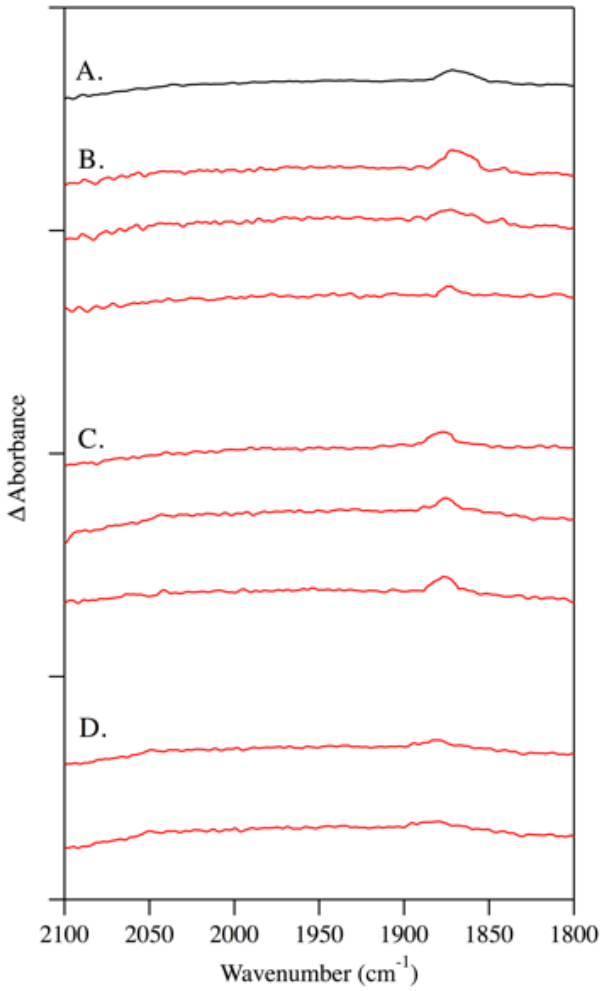

Figure 3.25 (A) Average α2β2 with ATP/CDP and Fe(II)-3AP RIFT-IR spectrum (black). Individual α2β2 with Fe(II)-3AP RIFT-IR spectra in the SD region (red) were collected on the following date (B) 2/24/16 (C) 2/25/16 (D) 3/08/16 and were vertically offset for comparison. Tick marks for the spectra are 1 x 10^{-3} absorbance units.

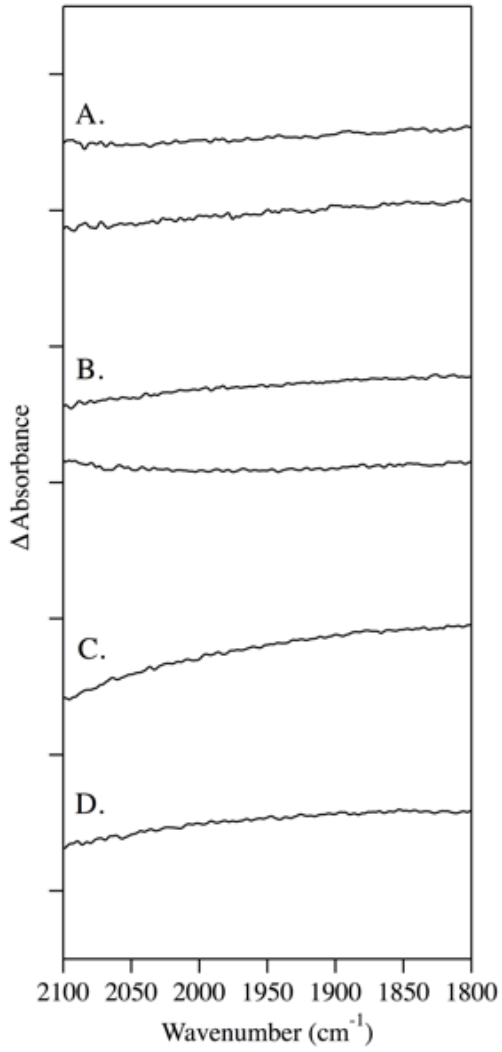

Figure 3.26 Individual α2β2 with TTP/UDP mixing spectra in the SD region were collected on the following date (A) 6/09/15 (B) 6/17/15 (C) 8/26/15 (D) 9/16/15. Tick marks for the spectra are 1 x 10^{-3} absorbance units.

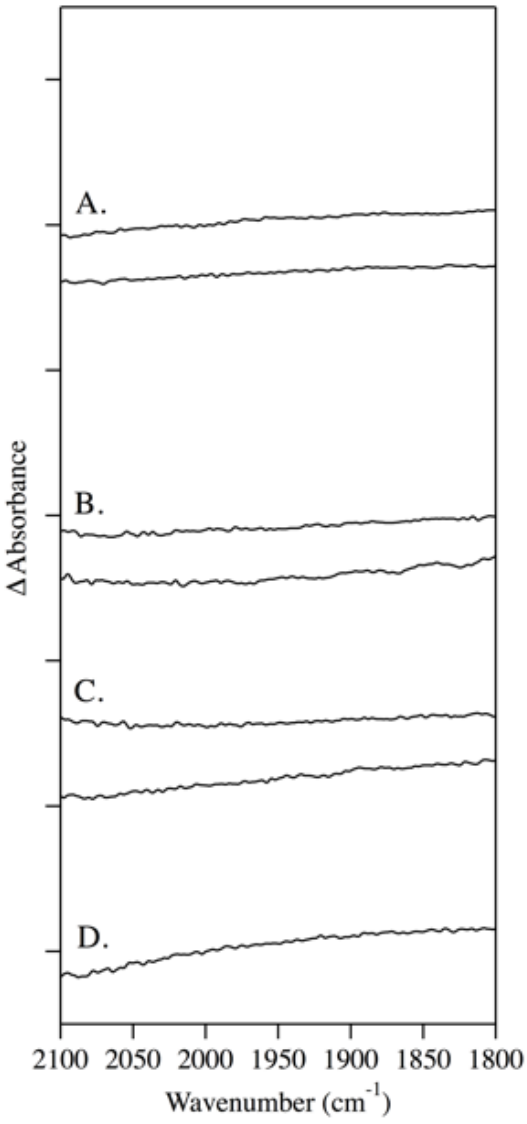

Figure 3.27 Individual α2β2 with TTP/UDP and HU mixing spectra in the SD region were collected on the following date (A) 6/09/15 (B) 6/17/15 (C) 8/26/15 (D) 9/16/15 and were vertically offset for comparison. Tick marks for the spectra are 1 x 10^{-3} absorbance units.

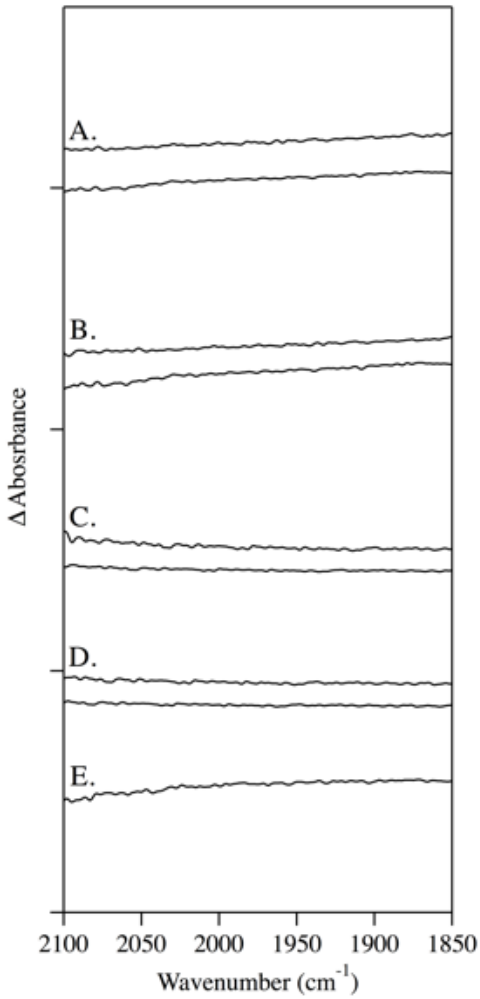

Figure 3.28 Individual α2β2 with TTP/AzUDP mixing spectra in the SD region were collected on the following date (A) 12/15/15 (B) 12/16/15 (C) 2/09/16 (D) 2/11/16 (E) 1/11/16 and were vertically offset for comparison. Tick marks for the spectra are 1 x 10^{-3} absorbance units.

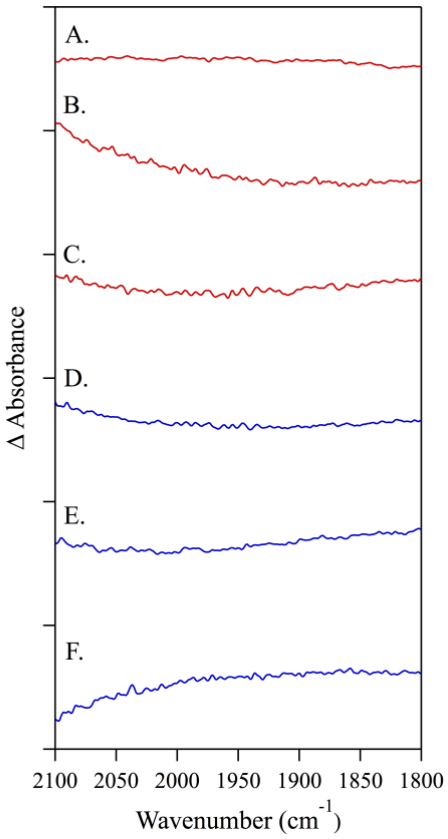

Figure 3.29 Isolated β2 controls were vertically offset for comparison: (A) 40 μM β2, 1 mM ATP, and 3 mM CDP (B) 40 μM β2, 1 mM ATP, 3 mM CDP, and 50 mM HU (C) 40 μM β2, 1 mM ATP, 3 mM CDP, and 40 μM Fe(II)-AP (D) 40 μM β2, 0.8 mM TTP, and 1 mM UDP (E) 40 μM β2, 0.8 mM TTP, 1 mM UDP, and 50mM HU (F) 40 μM β2, 0.8 mM TTP, and 1 mM AzUDP.

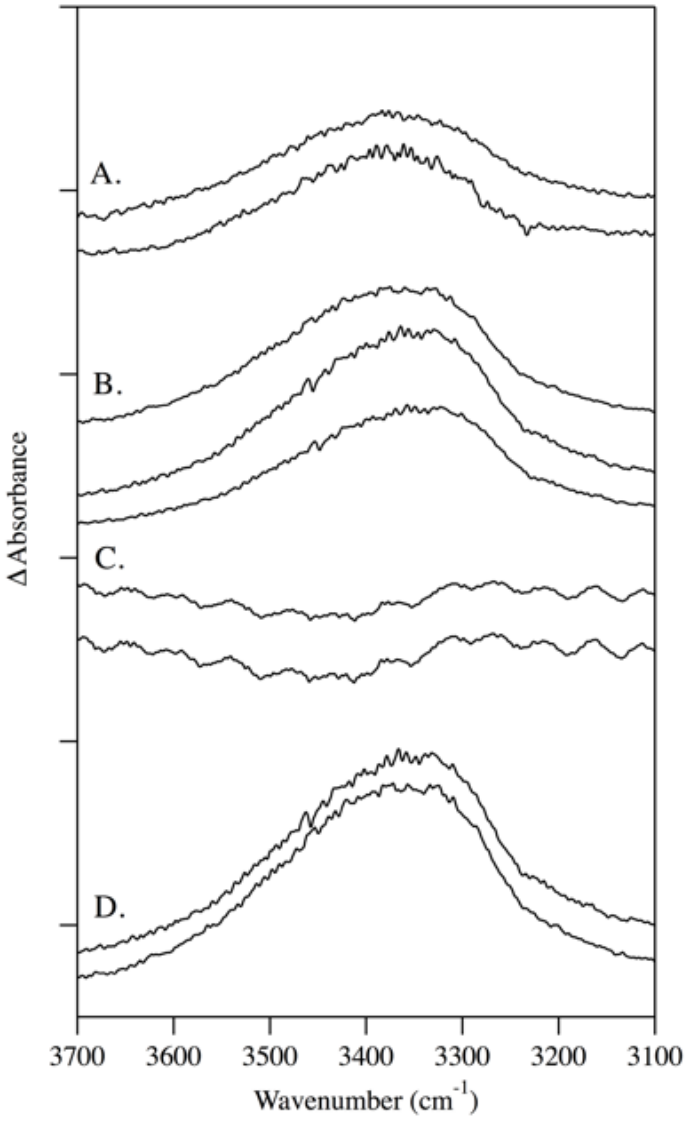

Figure 3.30 Individual α2β2 with ATP/CDP spectra in the water region were vertically offset and collected on the following date (A) 3/15/15 (B) 1/26/14 (C) 1/27/14 (D) 1/29/14. Tick marks for the spectra are 2 x 10^{-3} absorbance units.

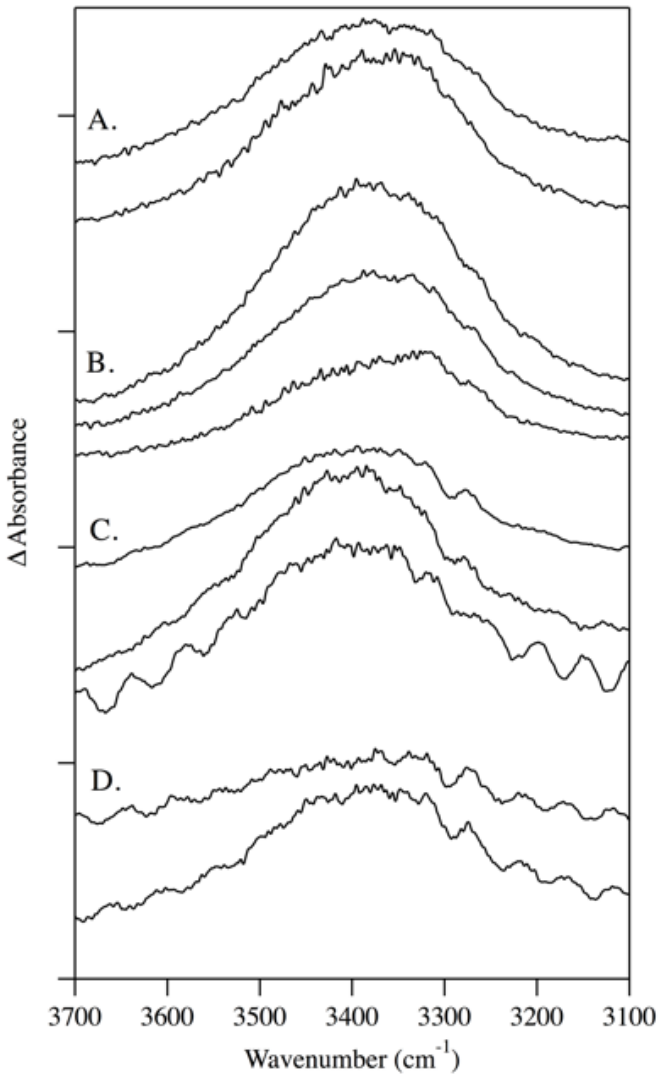

Figure 3.31 Individual α2β2 with ATP/CDP and HU spectra in the water region vertically offset and collected on the following date (A) 3/15/15 (B) 1/26/14 (C) 1/27/14 (D) 1/29/14. Tick marks for the spectra are 2 x 10^{-3} absorbance units.

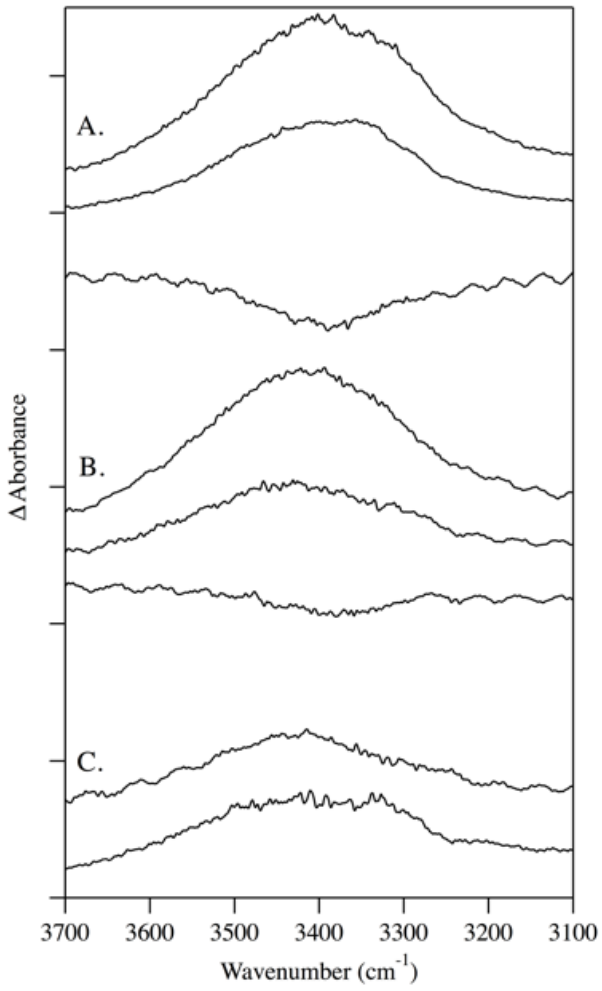

Figure 3.32 Individual α2β2 with ATP/CDP and Fe(II)-3AP spectra in the water region were vertically offset and collected on the following date (A) 2/24/16 (B) 2/25/16 (C) 3/08/16. Tick marks for the spectra are 2 x 10^{-3} absorbance units.

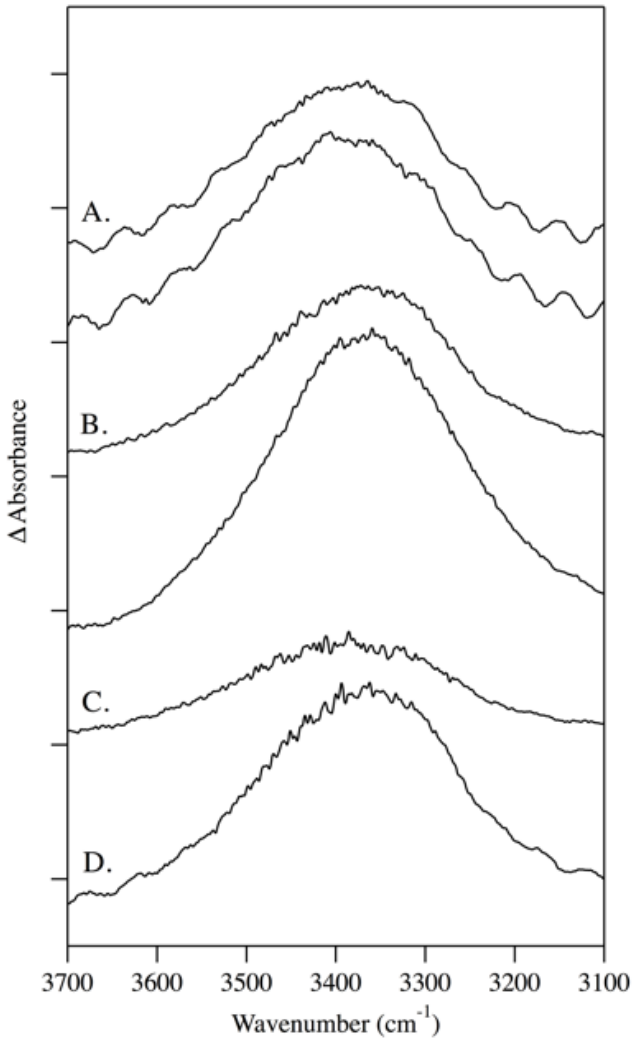

Figure 3.33 Individual α2β2 with TTP/UDP spectra in the water region vertically offset and collected on the following date (A) 6/09/15 (B) 6/17/15 (C) 8/26/15 (D) 9/16/15. Tick marks for the spectra are 2 x 10^{-3} absorbance units.

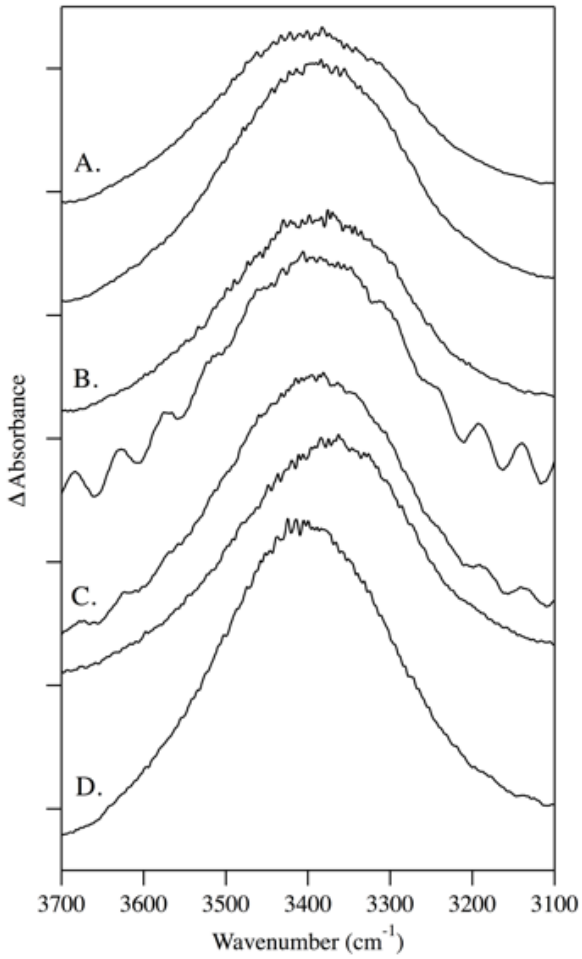

Figure 3.34 Individual α2β2 with TTP/UDP and HU RIFT-IR spectra in the water region vertically offset and collected on the following date (A) 6/09/15 (B) 6/17/15 (C) 8/26/15 (D) 9/16/15. The spectra were offset along the y-axis for comparison. Tick marks for the spectra are 2 x 10^{-3} absorbance units.

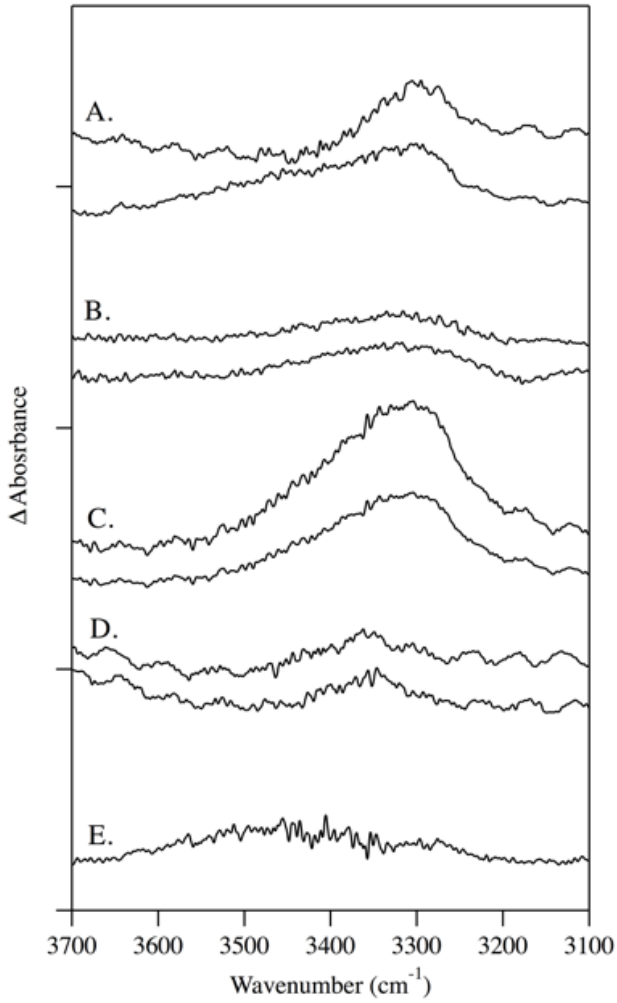

Figure 3.35 Individual α2β2 with TTP/AzUDP spectra of the water region vertically offset and collected on the following date (A) 12/15/15 (B) 12/16/15 (C) 2/09/16 (D) 2/11/16 (E) 1/11/16. Tick marks for the spectra are 2 x 10^{-3} absorbance units.

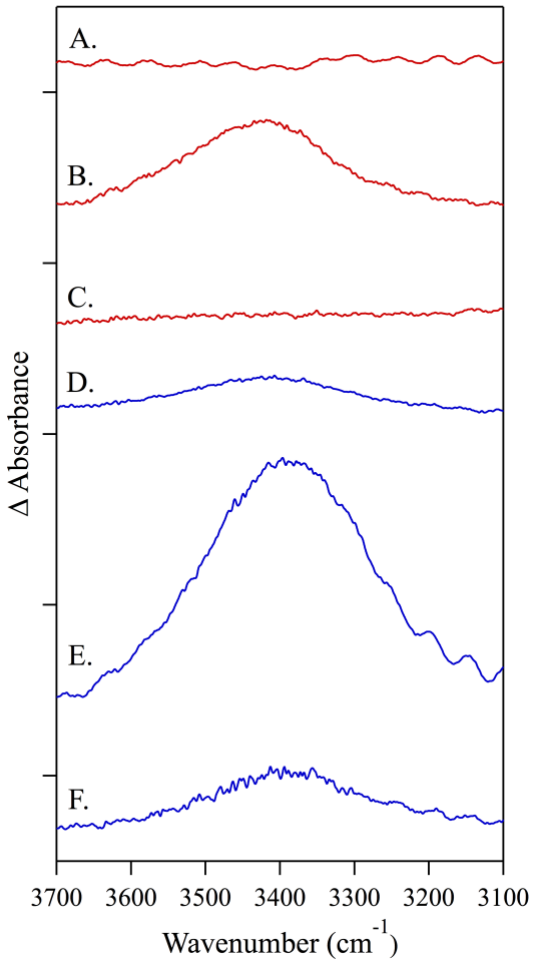

Figure 3.36 Individual isolated β2 controls in the water region were vertically offset for comparison: (A) 40 µM β2, 1 mM ATP, and 3 mM CDP (B) 40 µM β2, 1 mM ATP, 3 mM CDP, and 50 mM HU (C) 40 µM β2, 1 mM ATP, 3 mM CDP, and 40 µM Fe(II)-AP (D) 40 µM β2, 0.8 mM TTP, and 1 mM UDP (E) 40 µM β2, 0.8 mM TTP, 1 mM UDP, and 50mM HU (F) 40 µM β2, 0.8 mM TTP, and 1 mM AzUDP.

3.9 References

1. Huynh, M. H. V., Meyer, T. J. Proton-coupled electron transfer. *Chemical Reviews* **2007,** *107*, 5004-5064.
2. Minnihan, E. C., Nocera, D. G., Stubbe, J. Reversible, Long-range radical transfer in E. coli class Ia ribonucleotide reductase. *Accounts of Chemical Research* **2013,** *46*, 2524-2535.
3. Stubbe, J., Van der Donk, W. A. Protein radicals in enzyme catalysis. *Chemical Reviews* **1998,** *98*, 705-762.
4. Jordan, A., Reichard, P. Ribonucleotide Reductases. *Annual Review of Biochemistry* **1998,** *67*, 71-98.
5. Graf, E., Mahoney, J. R., Bryant, R. G., Eaton, J. W. Iron-catalyzed hydroxyl radical formation. Stringent requirement for free iron coordination site. *Journal of Biological Chemistry* **1984,** *259*, 3620-3624.
6. Mulliez, E., Fontecave, M., Gaillard, J., Reichard, P. An iron-sulfur center and a free radical in the active anaerobic ribonucleotide reductase of Escherichia coli. *Journal of Biological Chemistry* **1993,** *268*, 2296-2299.
7. Petersson, L., Gräslund, A., Ehrenberg, A., Sjöberg, B., Reichard, P. The iron center in ribonucleotide reductase from Escherichia coli. *Journal of Biological Chemistry* **1980,** *255*, 6706-6712.
8. Cukier, R. I., Nocera, D. G. Proton-coupled electron transfer. *Annual Review of Physical Chemistry* **1998,** *49*, 337-369.
9. Reece, S. Y., Hodgkiss, J. M., Stubbe, J., Nocera, D. G. Proton-coupled electron transfer: the mechanistic underpinning for radical transport and catalysis in biology. *Philosophical Transactions of the Royal Society B: Biological Sciences* **2006,** *361*, 1351-1364.
10. Stubbe, J., Nocera, D. G., Yee, C. S., Chang, M. C. Y. Radical initiation in the class I ribonucleotide reductase: Long-range proton-coupled electron transfer? *Chemical Reviews* **2003,** *103*, 2167-2202.
11. Offenbacher, A. R., Burns, L. A., Sherrill, C. D., Barry, B. A. Redox-linked conformational control of proton-coupled electron transfer: Y122 in the Ribonucleotide Rrductase β2 subunit. *The Journal of Physical Chemistry B* **2013,** *117*, 8457-8468.
12. Offenbacher, A. R., Minnihan, E. C., Stubbe, J., Barry, B. A.,Redox-linked changes to the hydrogen-bonding network of ribonucleotide reductase β2. *Journal of the American Chemical Society* **2013,** *135*, 6380-6383.
13. Guarino, E., Salguero, I., Kearsey, S. E. Cellular regulation of ribonucleotide reductase in eukaryotes. *Seminars in Cell & Developmental Biology* **2014,** *30*, 97-103.
14. Håkansson, P., Hofer, A., Thelander, L. Regulation of mammalian ribonucleotide reduction and dNTP pools after DNA damage and in resting cells. *Journal of Biological Chemistry* **2006,** *281*, 7834-7841.
15. Valko, M., Izakovic, M., Mazur, M., Rhodes, C. J., Telser, J. Role of oxygen radicals in DNA damage and cancer incidence. *Molecular and cellular biochemistry* **2004,** *266*, 37-56.
16. Mathews, C. K. DNA precursor metabolism and genomic stability. *The FASEB Journal* **2006,** *20*, 1300-1314.

17. Beckloff, G., Lerner, H., Frost, D., Russo-Alesi, F., Gitomer, S. Hydroxyurea (NSC-32065) in biologic fluids: dose-concentration relationship. *Cancer chemotherapy reports* **1965,** *48*, 57.
18. Eriksson, M., Uhlin, U., Ramaswamy, S., Ekberg, M., Regnström, K., Sjöberg, B.-M., Eklund, H. Binding of allosteric effectors to ribonucleotide reductase protein R1: reduction of active-site cysteines promotes substrate binding. *Structure* **1997,** *5*, 1077-1092.
19. Grinberg, I. R., Lundin, D., Hasan, M., Crona, M., Jonna, V. R., Loderer, C., Sahlin, M., Markova, N., Borovok, I., Berggren, G. Novel ATP-cone-driven allosteric regulation of ribonucleotide reductase via the radical-generating subunit. *Elife* **2018,** *7*, e31529.
20. Brignole, E. J., Tsai, K. L., Chittuluru, J., Li, H., Aye, Y., Penczek, P. A., Stubbe, J., Drennan, C. L., Asturias, F. 3.3-Å resolution cryo-EM structure of human ribonucleotide reductase with substrate and allosteric regulators bound. *eLife* **2018,** *7*, e31502.
21. Eriksson, S., Sjöberg, B. M., Jörnvall, H., Carlquist, M. A photoaffinity-labeled allosteric site in Escherichia coli ribonucleotide reductase. *Journal of Biological Chemistry* **1986,** *261*, 1878-1882.
22. Uhlin, U., Eklund, H. Structure of ribonucleotide reductase protein R1. *Nature* **1994,** *370*, 533.
23. Ando, N., Brignole, E. J., Zimanyi, C. M., Funk, M. A., Yokoyama, K., Asturias, F. J., Stubbe, J., Drennan, C. L. Structural interconversions modulate activity of Escherichia coli ribonucleotide reductase. *Proceedings of the National Academy of Sciences* **2011,** *108*, 21046-21051.
24. Rofougaran, R., Crona, M., Vodnala, M., Sjöberg, B.-M., Hofer, A. Oligomerization status directs overall activity regulation of the Escherichia coli class Ia ribonucleotide reductase. *Journal of Biological Chemistry* **2008,** *283*, 35310-35318.
25. Barry, B. A., Chen, J., Keough, J., Jenson, D., Offenbacher, A., Pagba, C. Proton-coupled electron transfer and redox-active tyrosines: Structure and function of the tyrosyl radicals in ribonucleotide reductase and photosystem II. *The Journal of Physical Chemistry Letters* **2012,** *3*, 543-554.
26. Nordlund, P., Reichard, P. Ribonucleotide Reductases. *Annual Review of Biochemistry* **2006,** *75*, 681-706.
27. Adams, J. D., Odunze, I. N. Oxygen free radicals and Parkinson's disease. *Free Radical Biology and Medicine* **1991,** *10*, 161-169.
28. Dreher, D., Junod, A. F. Role of oxygen free radicals in cancer development. *European Journal of Cancer* **1996,** *32*, 30-38.
29. Richardson, J. S. Free radicals in the genesis of Alzheimer's diseasea. *Annals of the New York Academy of Sciences* **1993,** *695*, 73-76.
30. Sjödin, B., Westing, Y. H., Apple, F. S. Biochemical mechanisms for oxygen free radical formation during exercise. *Sports Medicine* **1990,** *10*, 236-254.
31. Studer, A., Curran, D. P. Catalysis of radical reactions: A radical chemistry perspective. *Angewandte Chemie International Edition* **2016,** *55*, 58-102.
32. Gligorovski, S., Abbatt, J. P. An indoor chemical cocktail. *Science* **2018,** *359*, 632-633.

33. VanLoon, G. W., Duffy, S. J. Environmental chemistry: a global perspective. *Oxford university press* **2017.**
34. Halliwell, B., Gutteridge, J. M. Free radicals in biology and medicine. *Oxford University Press* **2015.**
35. Huyett, J. E., Doan, P. E., Gurbiel, R., Houseman, A. L., Sivaraja, M., Goodin, D. B., Hoffman, B. M. Compound ES of cytochrome c peroxidase contains a trp. pi cation radical: Characterization by continuous wave and pulsed Q-band external nuclear double resonance spectroscopy. *Journal of the American Chemical Society* **1995,** *117*, 9033-9041.
36. Stubbe, J., Van der Donk, W. Radicals with controlled lifestyles. *Chemical Communincation* **2003,** *2511*.
37. Seyedsayamdost, M. R., Chan, C. T. Y., Mugnaini, V., Stubbe, J., Bennati, M. PELDOR spectroscopy with DOPA-β2 and NH2Y-α2s: Distance measurements between residues involved in the radical propagation pathway of E. coli ribonucleotide reductase. *Journal of the American Chemical Society* **2007,** *129*, 15748-15749.
38. Argirević, T., Riplinger, C., Stubbe, J., Neese, F., Bennati, M. ENDOR spectroscopy and DFT calculations: evidence for the hydrogen-bond network within α2 in the PCET of E. coli ribonucleotide reductase. *Journal of the American Chemical Society* **2012,** *134*, 17661-17670.
39. Rhile, I. J., Markle, T. F., Nagao, H., DiPasquale, A. G., Lam, O. P., Lockwood, M. A., Rotter, K., Mayer, J. M. Concerted proton-electron transfer in the oxidation of hydrogen-bonded phenols. *Journal of the American Chemical Society* **2006,** *128*, 6075-6088.
40. Aberg, A., Hahne, S., Karlsson, M., Larsson, A., Ormö, M., Ahgren, A., Sjöberg, B. Evidence for two different classes of redox-active cysteines in ribonucleotide reductase of Escherichia coli. *Journal of Biological Chemistry* **1989,** *264*, 12249-12252.
41. Pizano, A. A., Olshansky, L., Holder, P. G., Stubbe, J., Nocera, D. G. Modulation of Y356 photooxidation in E. coli class Ia ribonucleotide reductase by Y731 across the α2: β2 interface. *Journal of the American Chemical Society* **2013,** *135*, 13250-13253.
42. Seyedsayamdost, M. R., Stubbe, J. Site-specific replacement of Y356 with 3,4-dihydroxyphenylalanine in the β2 subunit of E. coli ribonucleotide reductase. *Journal of the American Chemical Society* **2006,** *128*, 2522-2523.
43. Seyedsayamdost, M. R., Stubbe, J. Forward and reverse electron transfer with the Y356DOPA-β2 heterodimer of E. coli ribonucleotide reductase. *Journal of the American Chemical Society* **2007,** *129*, 2226-2227.
44. Seyedsayamdost, M. R., Xie, J., Chan, C. T., Schultz, P. G., Stubbe, J. Site-specific insertion of 3-aminotyrosine into subunit α2 of E. coli ribonucleotide reductase: direct evidence for involvement of Y730 and Y731 in radical propagation. *Journal of the American Chemical Society* **2007,** *129*, 15060-15071.
45. Seyedsayamdost, M. R., Yee, C. S., Reece, S. Y., Nocera, D. G., Stubbe, J. pH rate profiles of FnY356−R2s (n = 2, 3, 4) in Escherichia coli ribonucleotide reductase: Evidence that Y356 Is a redox-active amino acid along the radical propagation pathway. *Journal of the American Chemical Society* **2006,** *128*, 1562-1568.
46. Cordes, M., Köttgen, A., Jasper, C., Jacques, O., Boudebous, H., Giese, B. Influence of amino acid side chains on long-distance electron transfer in peptides:

Electron hopping via “stepping stones”. *Angewandte Chemie International Edition* **2008,** *47*, 3461-3463.
47. Yokoyama, K., Uhlin, U., Stubbe, J. A hot oxidant, 3-NO2Y122 radical, unmasks conformational gating in ribonucleotide reductase. *Journal of the American Chemical Society* **2010,** *132*, 15368-15379.
48. Olshansky, L., Pizano, A. A., Wei, Y., Stubbe, J., Nocera, D. G. Kinetics of hydrogen atom abstraction from substrate by an active site thiyl radical in ribonucleotide reductase. *Journal of the American Chemical Society* **2014,** *136*, 16210-16216.
49. Högbom, M., Galander, M., Andersson, M., Kolberg, M., Hofbauer, W., Lassmann, G., Nordlund, P., Lendzian, F. Displacement of the tyrosyl radical cofactor in ribonucleotide reductase obtained by single-crystal high-field EPR and 1.4-Å x-ray data. *Proceedings of the National Academy of Sciences* **2003,** *100*, 3209-3214.
50. Aye, Y., Li, M., Long, M. J. C., Weiss, R. S. Ribonucleotide reductase and cancer: biological mechanisms and targeted therapies. *Oncogene* **2014,** *34*, 2011.
51. Chitambar, C., Matthaeus, W., Antholine, W., Graff, K., O'Brien, W. Inhibition of leukemic HL60 cell growth by transferrin-gallium: effects on ribonucleotide reductase and demonstration of drug synergy with hydroxyurea. *Blood* **1988,** *72*, 1930-1936.
52. Elford, H. L. Effect of hydroxyurea on ribonucleotide reductase. *Biochemical and Biophysical Research Communications* **1968,** *33*, 129-135.
53. Aye, Y., Long, M. J. C., Stubbe, J. Mechanistic studies of semicarbazone Triapine targeting human ribonucleotide reductase *in vitro* and in mammalian cells: Tyrosyl radical quenching not involving radical oxygen species. *Journal of Biological Chemistry* **2012,** *287*, 35768-35778.
54. Popović-Bijelić, A., Kowol, C. R., Lind, M. E. S., Luo, J., Himo, F., Enyedy, É. A., Arion, V. B., Gräslund, A. Ribonucleotide reductase inhibition by metal complexes of Triapine (3-aminopyridine-2-carboxaldehyde thiosemicarbazone): A combined experimental and theoretical study. *Journal of Inorganic Biochemistry* **2011,** *105*, 1422-1431.
55. Salowe, S., Bollinger, J. M., Ator, M. A., Stubbe, J. Alternative model for mechanism-based inhibition of Escherichia coli ribonucleotide reductase by 2'-azido-2/-deoxyuridine S'-diphosphate1. *Biochemistry* **1993,** *32*, 12749-12760.
56. Van der Donk, W. A., Stubbe, J., Gerfen, G. J., Bellew, B. F., Griffin, R. G. EPR investigations of the inactivation of E. coli ribonucleotide reductase with 2’-azido-2’-deoxyuridine 5’-diphosphate: Evidence for the involvement of the thiyl radical of C225-R1. *Journal of the American Chemical Society* **1995,** *117*, 8908-8916.
57. Cerqueira, N. M., Fernandes, P. A., Ramos, M. J. Understanding ribonucleotide reductase inactivation by gemcitabine. *Chemistry–A European Journal* **2007,** *13*, 8507-8515.
58. Pereira, S., Fernandes, P. A., Ramos, M. J. Mechanism for ribonucleotide reductase inactivation by the anticancer drug gemcitabine. *Journal of computational chemistry* **2004,** *25*, 1286-1294.
59. Kameda, R., Ando, T., Kobayashi, S., Ueno, M., Ohkawa, S. A retrospective study of chemotherapy with cisplatin plus gemcitabine after the failure of gemcitabine monotherapy for biliary tract cancer. *Japanese Journal of Clinical Oncology* **2013,** *43*, 636-640.

60. S Gesto, D., MFSA Cerqueira, N., A Fernandes, P., J Ramos, M. Gemcitabine: a critical nucleoside for cancer therapy. *Current medicinal chemistry* **2012,** *19*, 1076-1087.
61. Lin, Z. P., Lee, Y., Lin, F., Belcourt, M. F., Li, P., Cory, J. G., Glazer, P. M., Sartorelli, A. C. Reduced level of ribonucleotide reductase R2 subunits increases dependence on homologous recombination repair of cisplatin-induced DNA damage. *Molecular pharmacology* **2011**, 94.
62. Kasanmascheff, M., Lee, W., Nick, T. U., Stubbe, J., Bennati, M. Radical transfer in E. coli ribonucleotide reductase: a NH 2 Y 731/R 411 A-α mutant unmasks a new conformation of the pathway residue 731. *Chemical science* **2016,** *7*, 2170-2178.
63. Krimm, S., Bandekar, J. Vibrational spectroscopy and conformation of peptides, polypeptides, and proteins. *Advances in protein chemistry* **1986,** 38, 181-364.
64. Chen, M. C., Zhou, B., Zhang, K., Yuan, Y. C., Un, F., Hu, S., Chou, C. M., Chen, C. H., Wu, J., Wang, Y. The novel ribonucleotide reductase inhibitor COH29 inhibits DNA repair in vitro. *Molecular pharmacology* **2015**, 94.
65. Liuzzi, M., Déziel, R., Moss, N., Beaulieu, P., Bonneau, A. M., Bousquet, C., Chafouleas, J. G., Garneau, M., Jaramillo, J., Krogsrud, R. L. A potent peptidomimetic inhibitor of HSV ribonucleotide reductase with antiviral activity in vivo. *Nature* **1994,** *372*, 695.
66. Cooper, C. E., Lynagh, G. R., Hoyes, K. P., Hider, R. C., Cammack, R., Porter, J. B. The relationship of intracellular iron chelation to the inhibition and regeneration of human ribonucleotide reductase. *Journal of Biological Chemistry* **1996,** *271*, 20291-20299.
67. Gautam, R., Akam, E., Astashkin, A., Loughrey, J., Tomat, E. Sirtuin inhibitor sirtinol is an intracellular iron chelator. *Chemical Communications* **2015,** *51*, 5104-5107.
68. Ator, M. A., Salowe, S., Stubbe, J. 2'-azido-2'-deoxynucleotide interaction with E . coli ribonucleotide reductase: Generation of a new radical species. *Journal of the American Chemical Society* **1984,** *106*, 1886-1887.
69. Kötting, C., Gerwert, K. Proteins in action monitored by time-resolved FTIR spectroscopy. *ChemPhysChem* **2005,** *6*, 881-888.
70. Siebert, F., Hildebrandt, P. Vibrational spectroscopy in life science, *Wiley* **2008.**
71. Vogel, R., Siebert, F. Vibrational spectroscopy as a tool for probing protein function. *Current Opinion in Chemical Biology* **2000,** *4*, 518-523.
72. Offenbacher, A. R., Watson, R. A., Pagba, C. V., Barry, B. A. Redox-dependent structural coupling between the α2 and β2 subunits in E. coli ribonucleotide reductase. *The Journal of Physical Chemistry B* **2014,** *118*, 2993-3004.
73. Offenbacher, A. R., Vassiliev, I. R., Seyedsayamdost, M. R., Stubbe, J., Barry, B. A. Redox-linked structural changes in ribonucleotide reductase. *Journal of the American Chemical Society* **2009,** *131*, 7496-7497.
74. Elledge, S. J., Zhou, Z., Allen, J. B. Ribonucleotide reductase: regulation, regulation, regulation. *Trends in Biochemical Sciences* **1992,** *17*, 119-123.
75. Reichard, P. Ribonucleotide reductases: Substrate specificity by allostery. *Biochemical and Biophysical Research Communications* **2010,** *396*, 19-23.
76. Zimanyi, Christina M., Ando, N., Brignole, Edward J., Asturias, Francisco J., Stubbe, J., Drennan, Catherine L. Tangled up in knots: Structures of inactivated forms of E. coli class Ia ribonucleotide reductase. *Structure* **2012,** *20*, 1374-1383.

77. Ge, J., Yu, G., Ator, M. A., Stubbe, J. Pre-steady-state and steady-state kinetic analysis of E. coli class I ribonucleotide reductase. *Biochemistry* **2003,** *42*, 10071-10083.
78. Shao, J., Zhou, B., Chu, B., Yen, Y. Ribonucleotide reductase inhibitors and future drug design. *Current Cancer Drug Targets* **2006,** *6*, 409-431.
79. Shao, J., Zhou, B., Di Bilio, A. J., Zhu, L., Wang, T., Qi, C., Shih, J., Yen, Y. A ferrous-triapine complex mediates formation of reactive oxygen species that inactivate human ribonucleotide reductase. *Molecular Cancer Therapeutics* **2006,** *5*, 586-592.
80. Boyd, A. S., Neldner, K. H. Hydroxyurea therapy. *Journal of the American Academy of Dermatology* **1991,** *25*, 518-524.
81. Finch, R. A., Liu, M. C., Cory, A. H., Cory, J. G., Sartorelli, A. C. Triapine (3-aminopyridine-2-carboxaldehyde thiosemicarbazone, 3-AP): an inhibitor of ribonucleotide reductase with antineoplastic activity. *Advances in enzyme regulation* **1999,** *39*, 3-12.
82. Finch, R. A., Liu, M. C., Grill, S. P., Rose, W. C., Loomis, R., Vasquez, K. M., Cheng, Y.-C., Sartorelli, A. C. Triapine (3-aminopyridine-2-carboxaldehyde-thiosemicarbazone): a potent inhibitor of ribonucleotide reductase activity with broad spectrum antitumor activity. *Biochemical pharmacology* **2000,** *59*, 983-991.
83. Graser-Loescher, G., Schoenhuber, A., Ciglenec, C., Eberl, S., Krupitza, G., Mader, R. M., Jadav, S. S., Jayaprakash, V., Fritzer-Szekeres, M., Szekeres, T. Thiosemicarbazone derivatives, thiazolyl hydrazones, effectively inhibit leukemic tumor cell growth: Down-regulation of ribonucleotide reductase activity and synergism with arabinofuranosylcytosine. *Food and Chemical Toxicology* **2017,** *108*, 53-62.
84. Miyazawa, T., Blout, E. The infrared spectra of polypeptides in various conformations: amide I and II bands. *Journal of the American Chemical Society* **1961,** *83*, 712-719.
85. Surewicz, W. K., Mantsch, H. H., Chapman, D. Determination of protein secondary structure by Fourier transform infrared spectroscopy: a critical assessment. *Biochemistry* **1993,** *32*, 389-394.
86. Fabian, H., Mäntele, W. Infrared spectroscopy of proteins. *Handbook of vibrational spectroscopy* **2002**.
87. Ingemarson, R., Thelander, L. A kinetic study on the influence of nucleoside triphosphate effectors on subunit interaction in mouse ribonucleotide reductase. *Biochemistry* **1996,** *35*, 8603-8609.
88. Parker, S. F. Assignment of the vibrational spectrum of L-cysteine. *Chemical Physics* **2013,** *424*, 75-79.
89. Ormö, M., Sjöberg, B. M. The Cys292→Ala substitution in protein R1 of class I ribonucleotide reductase from Escherichia coli has a global effect on nucleotide binding at the specificity-determining allosteric site. *European Journal of Biochemistry* **1996,** *241*, 363-367.
90. Ormö, M., Sjöberg, B. M. An ultrafiltration assay for nucleotide binding to ribonucleotide reductase. *Analytical Biochemistry* **1990,** *189*, 138-141.
91. Karlsson, M., Sahlin, M., Sjöberg, B. M. Escherichia coli ribonucleotide reductase. Radical susceptibility to hydroxyurea is dependent on the regulatory state of the enzyme. *Journal of Biological Chemistry* **1992,** *267*, 12622-6.
92. Krakoff, I. H., Brown, N. C., Reichard, P. Inhibition of ribonucleoside diphosphate reductase by hydroxyurea. *Cancer Research* **1968,** *28*, 1559-1565.

CHAPTER 4. SUMMARY

4.1 Summary and future directions

To summarize the work presented in this thesis, I have investigated the structure and utility of the active *E. coli* α2β2 complex upon binding of substrate and effectors. In addition to this, I have investigated the role that chemotherapeutics play in the isolated β2, where applicable, and the holoenzyme. Understanding the roles of these anti-cancer therapies and the conformational dynamics associated with their inhibition of the enzyme will aid in future drug design, to interact more specifically and be more potent, as well as elucidate the structural mechanisms surrounding RNR function. In Chapter 2, we optimized time-resolved RIFT-IR spectroscopy to examine the structural effects of α2β2 turnover with the effector ATP and the substrate CDP. Because RNR is such a high priority target for cancer therapies, the introduction of an inhibitor was used to observe quenching of the tyrosyl radical (Y122•→ Y122OH) by radical scavenger HU, which is a very widely study and characterized drug. The use of ^{13}C isotopic labels in the α and β subunits enabled us to clarify spectral features as resulting from a specific subunit in the QC. In Chapter 3, I expanded on this work by examining the structural repercussions, if any, of replacing the effector TTP and the substrate CDP versus ATP/CDP. Furthermore, expanding on our therapies investigation, we expanded our inhibitors to include an additional radical scavenger similar to HU, Triapine, and a radical trap that behaves as a substrate analog, AzidoUDP. By expanding the numbers of inhibitors, it allowed me to explore two questions when it comes to the study of RNR. Firstly, do two drugs that are believed to inhibit similarly, quenching the tyrosyl radical in the resting state of the enzyme, have the

same mechanism of inhibition when exposed to the enzyme under the same conditions. And secondly, will trapping the radical state in the active site of the α subunit reveal fundamental conformational dynamics associated with long-range proton-coupled electron transfer associated with radical transfer along the proposed hopping pathway.

In Chapter 2, we identified that the active complex could be observed in a physiological relevant turnover reaction. Not only could catalysis occur, but the production of dCDP could be observed by spectrophotometric assay. RIFT-IR spectra were acquired after mixing *E. coli* α2 and β2 with a substrate, CDP, and the allosteric effector, ATP. Isotopic chimeras, ^{13}Cα2β2 and α2^{13}Cβ2, were used to describe subunit-specific conformational modifications observed in the difference spectra as amide I (C=O) and II (CN/NH) bands, derived from either the α or β subunit. The addition of dATP resulted in a decreased contribution from amide I bands, attributable to beta strands and disordered structures. This result is expected as dATP has been shown to act as an inhibitor and been shown to be vital in forming the inactive complex, α4β4. Most notably, HU-mediated reduction of Y122O• was associated with structural changes in α2, as well as β2. Control experiments with isolated α2 have shown no interaction with HU. This suggests that α2 is conformational responsive to the tyrosyl radical being quenched in the β2 subunit and ultimately suggests that there is some form of communication channel between the subunits. Contributions of Y122O•/Y122OH in the quaternary complex were examined by $^{2}H_4$ labeling of β2 tyrosines and HU-editing. The bands of Y122O•, Y122OH, and D84, have been previously identified in isolated β2, were observed in the α2β2 complex. These spectra also provide evidence for a conformational rearrangement at an additional β2 tyrosine(s), Y_x, in the α2β2/CDP/ATP complex, the most likely explanation being Y356.

In Chapter 3, I used RIFT-IR spectroscopy to describe the conformational landscape of the α2 subunit when diverse substrates and allosteric effectors are bound to the catalytic and specificity sites. The mechanism of inhibition by hydroxyurea (HU) and Fe(II)-Triapine (Fe(II)-3AP), two radical scavengers that inhibit α2β2. While specific proton donors have been proposed along the PCET pathway, conformational gating within homodimeric subunits has remained unclear, but with the use of radical trap 2′-azido-2′-deoxyuridine 5′-diphosphate (AzUDP) conformational changes associated with the radical transition into the active site have been uncovered. RIFT-IR spectroscopy yielded amide I (C=O) and II (CN/NH) bands with catalytic and inhibitory conditions. The addition of the effector ATP/CDP, as opposed to TTP/UDP, resulted in the appearance of bands (+) 1872 and (–) 1040 cm^{-1}, likely due increased interactions between the conserved C292 in the specificity site, and, as a result, the enforced conformational response by loops 1 and 3. In the difference spectrum associated with the quenching of the tyrosyl radical by Fe(II)-3AP, the peak at (+) 1687 cm^{-1} previously assign to D84, a unidentate ligand to the differic cluster, is no longer present, but displays new negative features seen at (–) 1646, 1633, and 1624 cm^{-1}. AzUDP displays similarities at (+) 1685, 1674, and 1667 cm^{-1} with inhibition by HU, but also show bands at (+) 1657 and (–) 1649 cm^{-1} which have been assigned as contributions by D84 amide bond. I highlighted the utility by which reaction-induced FT-IR spectroscopy is able to detect conformational changes in complex enzymes previously seen in x-ray crystallography. I revealed HU and Fe(II)-3AP interact with isolated β2 similarly, but with the active complex in deviating processes to accomplish radical quenching. The distinctive inhibitor, AzUDP, reveals conformational changes accompanying long-range proton-coupled electron transfer (PCET) to demonstrate

backbone rearrangement associated with a redox-induced shift between Y122OH and D84 in a functional α2β2 complex.

There is still so much yet to learn about the mechanism of ribonucleotide reduction. The α2β2 enzyme displays distinct spectra when catalysis is occurring due to ATP and CDP versus when TTP and UDP are bound. Also, the method of inhibition by two radical quenchers and a radical trap in the active site of the α subunit exhibit discrete conformational responses during inactivation. To further clarify these newly discovered conformational changes, isotopic labeling of the α and β subunits would allow for specific assignment of these new spectral bands that have been observed in the α2β2 mixing experiments.

Isotopic labeling of the α subunit will identify fundamental subunit responses to substrate and effector binding to the active and allosteric regulation sites, as well as redox-linked physical changes in the α subunit. As described in chapter 3, there are two unique signals at (+) 1872 and (–) 1040 cm^{-1} that are observed when ATP and CDP are introduced to the α2 dimer and remain present regardless of under catalytic or inhibition conditions. Interestingly, these signals are no longer present when the substrate and effectors are changed to UDP and TTP, respectively. This band would be characteristic of an S–D band. By isotopically labeling the cysteine residue in the specificity site by an orthogonal tRNAse, and the unknown band is the proposed cysteine residue, the band would shift, which can be predicted by calculating the frequency based on the change in mass of the isotope compared to the natural abundance residue, the band would be identified. This experiment would inform the structural response by the α subunit when effectors are bound to the specificity site. If there is no shift by the band, the next likely explanation would be

the conserved cysteine residues in the active site. Another important isotopic labeling experiment would be labeling of Y730 and Y731. These two residues are conserved, and evidence has been provided to show that these residues are essential in the suggested radical hopping pathway. Previously, we have utilized global isotopic labeling residues of interest or the entire subunit as a whole. It was the unique environments of residues in the enzyme that allowed us to detect backbone residue shifts. Collaborators use an orthogonal tRNAse to specifically tag single amino acid residue. This technique would allow use to mark the individual tyrosine residues to observe conformational changes associated with long-range proton-coupled electron transfer. This experiment would provide much needed data about the α:β interface and the interactions between β-Y356 and α-Y31.

By isotopically labeling the β2 homodimer, it would inform the PCET pathway, and changes centered around the diiron cluster responsible for radical generation. Inhibition by Fe(II)-3AP proved to have a vastly altered FTIR spectrum compared to HU. The tyrosyl radical gives a unique signal in the FTIR spectra, so by global labeling tyrosine residues, precise modifications to Y122 can be observed. When Fe(II)-3AP quenches the tyrosyl radical, the process of interaction between inhibitor and enzyme will have a wider range of understanding. This includes further evidence of a second conformationally active tyrosine in β2. Additionally, comparisons can be drawn to HU to determine the similarities in the mechanisms between inhibition, if any. When AzUDP is introduced to the QC, these isotopic labels would provide further evidence of formation of hydrogen bonding interactions between Y122 and D84 due to radical reduction. We have previously shown that the iron bound ligand, D84, forms a hydrogen bond to Y122 after reduction of the radical. An interesting future direction for this project would be labeling of the glutamate

residues in the β2 protein. There are 3 iron bound glutamate residues. These residues are both unidentate and bidentate ligands. The conformational responses by the iron cluster to radical reduction in both isolated and α2β2 mixing experiments is vital. Particularly, those responses associated with AzUDP. This experiment would describe the metallo-cofactor during forward PCET, mimicking the natural biological system.

Class Ia RNR houses a tyrosyl radical, which was the first discovered biologically essential organic radical in any protein. To develop new drugs, information concerning the mechanism is critical. To obtain information, a more specific comprehension of the radical's complete cycle must be achieved. Fourier transform infrared spectroscopy allows for the detection of single amino acid changes that take place as a result of RNR due to catalysis and inhibition by radical quenching or substrate analog.

4.2 References

1. Elledge, S. J., Zhou, Z., Allen, J. B. Ribonucleotide reductase: regulation, regulation, regulation. *Trends in Biochemical Sciences* **1992,** *17*, 119-123.
2. Guarino, E., Salguero, I., Kearsey, S. E. Cellular regulation of ribonucleotide reductase in eukaryotes. *Seminars in Cell & Developmental Biology* **2014,** *30*, 97-103.
3. Håkansson, P., Hofer, A., Thelander, L., Regulation of mammalian ribonucleotide reduction and dNTP pools after DNA damage and in resting cells. *Journal of Biological Chemistry* **2006,** *281*, 7834-7841.
4. Ingemarson, R., Thelander, L. A kinetic study on the influence of nucleoside triphosphate effectors on subunit Interaction in mouse ribonucleotide reductase. *Biochemistry* **1996,** *35*, 8603-8609.
5. Åberg, A., Nordlund, P., Eklund, H. Unusual clustering of carboxyl side chains in the core of iron-free ribonucleotide reductase. *Nature* **1993,** *361*, 276.
6. Jackson, M., Mantsch, H. H. The use and misuse of FTIR spectroscopy in the determination of protein structure. *Critical reviews in biochemistry and molecular biology* **1995,** *30*, 95-120.
7. Jackson, M., Mantsch, H. H. Protein secondary structure from FT-IR spectroscopy: correlation with dihedral angles from three-dimensional Ramachandran plots. *Canadian journal of chemistry* **1991,** *69*, 1639-1642.
8. Kashlan, O. B., Scott, C. P., Lear, J. D., Cooperman, B. S. A comprehensive model for the allosteric regulation of mammalian ribonucleotide reductase. Functional consequences of ATP-and dATP-induced oligomerization of the large subunit. *Biochemistry* **2002,** *41*, 462-474.
9. Offenbacher, A. R., Burns, L. A., Sherrill, C. D., Barry, B. A. Redox-linked conformational control of proton-coupled electron transfer: Y122 in the ribonucleotide reductase β2 subunit. *The Journal of Physical Chemistry B* **2013,** *117*, 8457-8468.
10. Offenbacher, A. R., Minnihan, E. C., Stubbe, J., Barry, B. A. Redox-linked changes to the hydrogen-bonding network of ribonucleotide reductase β2. *Journal of the American Chemical Society* **2013,** *135*, 6380-6383.
11. Offenbacher, A. R., Vassiliev, I. R., Seyedsayamdost, M. R., Stubbe, J., Barry, B. A. Redox-linked structural changes in ribonucleotide reductase. *Journal of the American Chemical Society* **2009,** *131*, 7496-7497.
12. Nordlund, P., Eklund, H. Structure and function of the Escherichia coli ribonucleotide reductase protein R2. *Journal of molecular biology* **1993,** *232*, 123-164.
13. Nordlund, P., Sjöberg, B.-M., Eklund, H. Three-dimensional structure of the free radical protein of ribonucleotide reductase. *Nature* **1990,** *345*, 593.
14. Alvero, A. B., Chen, W., Sartorelli, A. C., Schwartz, P., Rutherford, T., Mor, G. Triapine (3-aninopyridine-2-carboxaldehyde thiosemicarbazone) induces apoptosis in ovarian cancer cells. *Journal of the Society for Gynecologic Investigation* **2006,** *13*, 145-152.
15. Beckloff, G., Lerner, H., Frost, D., Russo-Alesi, F., Gitomer, S. Hydroxyurea (NSC-32065) in biologic fluids: dose-concentration relationship. *Cancer chemotherapy reports* **1965,** *48*, 57.
16. Boyd, A. S., Neldner, K. H. Hydroxyurea therapy. *Journal of the American Academy of Dermatology* **1991,** *25*, 518-524.

17. Finch, R. A., Liu, M. C., Cory, A. H., Cory, J. G., Sartorelli, A. C. Triapine (3-aminopyridine-2-carboxaldehyde thiosemicarbazone, 3-AP): an inhibitor of ribonucleotide reductase with antineoplastic activity. *Advances in enzyme regulation* **1999,** *39*, 3-12.
18. Finch, R. A., Liu, M. C., Grill, S. P., Rose, W. C., Loomis, R., Vasquez, K. M., Cheng, Y.-C., Sartorelli, A. C. Triapine (3-aminopyridine-2-carboxaldehyde-thiosemicarbazone): a potent inhibitor of ribonucleotide reductase activity with broad spectrum antitumor activity. *Biochemical pharmacology* **2000,** *59*, 983-991.
19. Graser-Loescher, G., Schoenhuber, A., Ciglenec, C., Eberl, S., Krupitza, G., Mader, R. M., Jadav, S. S., Jayaprakash, V., Fritzer-Szekeres, M., Szekeres, T. Thiosemicarbazone derivatives, thiazolyl hydrazones, effectively inhibit leukemic tumor cell growth: Down-regulation of ribonucleotide reductase activity and synergism with arabinofuranosylcytosine. *Food and Chemical Toxicology* **2017,** *108*, 53-62.
20. Shao, J., Zhou, B., Chu, B., Yen, Y. Ribonucleotide Reductase Inhibitors and Future Drug Design. *Current Cancer Drug Targets* **2006,** *6*, 409-431.
21. Shao, J., Zhou, B., Di Bilio, A. J., Zhu, L., Wang, T., Qi, C., Shih, J., Yen, Y. A Ferrous-triapine complex mediates formation of reactive oxygen species that inactivate human ribonucleotide reductase. *Molecular Cancer Therapeutics* **2006,** *5*, 586-592.
22. Stearns, B., Losee, K. A., Bernstein, J., Hydroxyurea. A new type of potential antitumor agent1. *Journal of medicinal chemistry* **1963,** *6*, 201-201.
23. Stock, C., Clarke, D., Philips, F., Barclay, R. Cancer chemotherapy screening data. V. Sarcoma 180 screening data. *Cancer research* **1960,** *20*, 1.
24. Ator, M. A., Salowe, S., Stubbe, J. 2'-Azido-2'-deoxynucleotideInteraction with *E . coli* ribonucleotide reductase: generation of a new radical species. *Journal of the American Chemical Society* **1984,** *106*, 1886-1887.
25. Salowe, S., Bollinger, J. M., Ator, M. A., Stubbe, J. Alternative model for mechanism-based inhibition of *Escherichia coli* ribonucleotide reductase by 2'-Azido-2/-deoxyuridine S'-Diphosphate1. *Biochemistry* **1993,** *32*, 12749-12760.
26. Van der Donk, W. A., Stubbe, J., Gerfen, G. J., Bellew, B. F., Griffin, R. G. EPR investigations of the inactivation of *E. coli* ribonucleotide reductase with 2'-azido-2'-deoxyuridine 5'-diphosphate: evidence for the involvement of the thiyl radical of C225-R1. *Journal of the American Chemical Society* **1995,** *117*, 8908-8916.
27. Decornez, H., Hammes-Schiffer, S. Model proton-coupled electron transfer reactions in solution: predictions of rates, mechanisms, and kinetic isotope effects. *The Journal of Physical Chemistry A* **2000,** *104*, 9370-9384.
28. Reece, S. Y., Hodgkiss, J. M., Stubbe, J., Nocera, D. G. Proton-coupled electron transfer: the mechanistic underpinning for radical transport and catalysis in biology. *Philosophical Transactions of the Royal Society B: Biological Sciences* **2006,** *361*, 1351-1364.
29. Stubbe, J. Radicals with a controlled lifestyle. *Chemical Communication* **2003,** *20*, 2511-2513.
30. Stubbe, J., Van der Donk, W. A. Protein Radicals in Enzyme Catalysis. *Chemical Review* **1998,** *98*, 705-762.
31. Eriksson, M., Uhlin, U., Ramaswamy, S., Ekberg, M., Regnström, K., Sjöberg, B. M., Eklund, H. Binding of allosteric effectors to ribonucleotide reductase protein R1:

reduction of active-site cysteines promotes substrate binding. *Structure* **1997,** *5*, 1077-1092.
32. Parker, S. F. Assignment of the vibrational spectrum of L-cysteine. *Chemical Physics* **2013,** *424*, 75-79.
33. Seyedsayamdost, M. R., Xie, J., Chan, C. T., Schultz, P. G., Stubbe, J. Site-specific insertion of 3-aminotyrosine into subunit α2 of *E. coli* ribonucleotide reductase: direct evidence for involvement of Y730 and Y731 in radical propagation. *Journal of the American Chemical Society* **2007,** *129*, 15060-15071.
34. Yokoyama, K., Smith, A. A., Corzilius, B., Griffin, R. G., Stubbe, J. Equilibration of tyrosyl radicals (Y356•, Y731•, Y730•) in the radical propagation pathway of the *Escherichia coli* class Ia ribonucleotide reductase. *Journal of the American Chemical Society* **2011,** *133*, 18420-18432.
35. Offenbacher, A. R., Watson, R. A., Pagba, C. V., Barry, B. A. Redox-dependent structural coupling between the α2 and β2 subunits in *E. coli* ribonucleotide reductase. *The Journal of Physical Chemistry B* **2014,** *118*, 2993-3004.
36. Seyedsayamdost, M. R., Chan, C. T. Y., Mugnaini, V., Stubbe, J., Bennati, M. PELDOR spectroscopy with DOPA-β2 and NH2Y-α2s: distance measurements between residues involved in the radical propagation pathway of *E. coli* ribonucleotide reductase. *Journal of the American Chemical Society* **2007,** *129*, 15748-15749.
37. Seyedsayamdost, M. R., Stubbe, J. Site-specific replacement of Y356 with 3,4-dihydroxyphenylalanine in the β2 subunit of *E. coli* ribonucleotide reductase. *Journal of the American Chemical Society* **2006,** *128*, 2522-2523.
38. Seyedsayamdost, M. R., Yee, C. S., Reece, S. Y., Nocera, D. G., Stubbe, J., pH rate profiles of FnY356−R2s (n = 2, 3, 4) in *Escherichia coli* ribonucleotide reductase: evidence that Y356 is a redox-active amino acid along the radical propagation Pathway. *Journal of the American Chemical Society* **2006,** *128*, 1562-1568.
39. Yokoyama, K., Uhlin, U., Stubbe, J. A hot oxidant, 3-NO2Y122 radical, unmasks conformational gating in ribonucleotide reductase. *Journal of the American Chemical Society* **2010,** *132*, 15368-15379.